Review

Recent Advances on Hybrid Piezo-Triboelectric Bio-Nanogenerators: Materials, Architectures and Circuitry

Massimo Mariello

Laboratory for Processing of Advanced Composites (LPAC), École Polytechnique Fédérale de Lausanne (EPFL), 1015 Lausanne, Switzerland; massimo.mariello@epfl.ch or massimomariello@gmail.com

Abstract: Nanogenerators, based on piezoelectric or triboelectric materials, have emerged in the recent years as an attractive cost-effective technology for harvesting energy from renewable and clean energy sources, but also for human sensing and biomedical wearable/implantable applications. Advances in materials engineering have enlightened new opportunities for the creation and use of novel biocompatible soft materials as well as micro/nano-structured or chemically-functionalized interfaces. Hybridization is a key concept that can be used to enhance the performances of the single devices, by coupling more transducing mechanisms in a single-integrated micro-system. It has attracted plenty of research interest due to the promising effects of signal enhancement and simultaneous adaptability to different operating conditions. This review covers and classifies the main types of hybridization of piezo-triboelectric bio-nanogenerators and it also provides an overview of the most recent advances in terms of material synthesis, engineering applications, power-management circuits and technical issues for the development of reliable implantable devices. State-of-the-art applications in the fields of energy harvesting, in vitro/in vivo biomedical sensing, implantable bioelectronics are outlined and presented. The applicative perspectives and challenges are finally discussed, with the aim to suggest improvements in the design and implementation of next-generation hybrid bio-nanogenerators and biosensors.

Keywords: nanogenerators; piezoelectricity; triboelectricity; biosensors; hybridization

1. Introduction

Nanogenerators have emerged in the last years as a novel useful technology for several applications, i.e., for scavenging energy from the environments, for sensing human motion, for monitoring physiological parameters, for supplying self-powered sensor systems, for providing energy to miniaturized storage devices. The word nanogenerator refer to whichever micro-device that is able to convert energy from the available sources (mechanical, thermal, biochemical, etc.) into electrical energy, at the micro/nano scale [1]. These types of devices can act as power generators, sensors or actuators and represent a revolutionary alternative to standard bulky systems for energy generation or sensing [2–5].

The major issue addressed by the employment of nanogenerators is the global energy problem. A today's grand challenge is to exploit more massively natural resources of renewable and clean energy in order to reduce and avoid in the end the use of polluting and expensive fossil fuels [1,2,6–8]. Solar energy is the most widely present form of natural energy and research on solar/photovoltaic cells based on new materials and architecture (e.g., perovskites [9]) has received a remarkable boost in the recent years. Other energy sources include wind flows, ocean waves/currents, rainfalls, environmental vibrations, human body motions (voluntary movements, heartbeat, breathing, blood circulation, etc.).

These are more convenient to be exploited in places where solar energy is not really accessible because of unstable sunshine and weather conditions [10–12]: mechanical energy is ubiquitous, abundant and manifold [13] and scavenging this energy through distributed

networks of nanogenerators is a promising solution to pursue in parallel to standard current power plants [4,6,14,15].

The main purpose of harvesting energy is to overcome issues related to chemical batteries (limited lifetime, need of periodic recharging, environmental impact, unsuitability for positioning in unusual and hostile places [16–20]), thus to supply storage devices or to satisfy the increasing demand of highly efficient self-powered (battery-less) energy or sensing systems. These are often flexible, lightweight and wearable/implantable smart sensors based on nanogenerators, and they find application in diverse fields: real-time monitoring of life parameters [21–23], sensing of human motion [24–26], sports and athletics [27–29], smart grids, robotics [30–32] and prosthetics [33,34], biomedical active implants [22,35,36]. In the context of the Internet of Things (IoT) [37,38] and Internet of Bodies (IoB) [39], intelligent devices need to be adaptable to different operating conditions and places, even in remote locations, thus they require to be supplied with energy harvested locally [13]. Hence, nanogenerators are growingly based on cost-friendly, downscaling and widely-implementable flexible electronics with softness, conformability, biocompatibility and specific designs/architectures. Research and industry efforts have been moving towards the development of novel materials [14,40,41] and new environmental or biomedical applications [21–29,42–44].

The most widely employed nanogenerators are based on piezoelectricity and triboelectricity [4,40,45]. These two transducing mechanisms rely on charge generation due to mechanical deformations or contact friction and their practical realization is compatible with the required properties of advanced smart devices, such as flexibility, adaptability, multifunctionality, conformability and biocompatibility [4,46,47]. Their intrinsic capability of generating charges as well as their light mass and structural simplicity, make them advantageous with respect to other energy harvesting devices (e.g., electromagnetic, electrostatic, etc.). In terms of sensing properties, they are low-cost and affordable alternatives to wearable systems based on strain gauges [48], capacitive devices [49] or iontronics [50,51].

Additionally, their hybrid coupling has recently shown to obtain enhanced performances in terms of output power or sensitivity, beyond the linear summation of the single components [52]. The hybridization also allows to adapt the overall device to different operating conditions, without any constraints imposed by the single working mechanisms. Hybrid systems relying on the combination of piezoelectric and triboelectric devices, based on biocompatible materials and aimed for clean energy harvesting from the environment or for biomedical applications are hereafter called hybrid bio-nanogenerators (HBNGs). Figure 1 illustrates a qualitative comparison between HBNG, piezoelectric nanogenerators (PNGs) and triboelectric nanogenerators (TNGs), in terms of flexibility, output voltage, output current, output power density, lifetime and reliability, ease of miniaturization, low-frequency operation, high-frequency operation, biocompatibility. The most usual fields of applications for HBNGs are also displayed, i.e., energy harvesting, wearable bioelectronics and implantable bioelectronics, with some specific examples: tactile sensors, electronic skins, biosensors, biomedical implants, actuation, stimulation, robotics, human-machine interfaces, self-powered sensors and renewable energy sources.

In this review the main types of hybridization of piezo-triboelectric bio-nanogenerators are described and classified with a general overview of the most recent examples of HBNGs for energy harvesting, wearable or implantable bioelectronics. Section 2 provides a description of the working principles of piezoelectric and triboelectric nanogenerators, in terms of basic governing equations and most used materials. The different kinds of hybridization of the two mechanisms are presented in Section 3, where a classification is established according to the physical domains involved in the hybridization process, as well as the relative position of the piezoelectric and triboelectric components. State-of-the-art applications in the fields of energy harvesting, in vitro/in vivo biomedical sensing, implantable bioelectronics are outlined and presented in Section 4. A specific focus is reserved in Section 5 for the electronic interfaces of these devices and the power management circuits. In order to design and fabricate properly these circuitry, different issues

have to be addressed, including the attachment of electrical connections which must be suitable for the employed materials, and the analytical and equivalent-circuit models of each type of transducer. Finally, the applicative perspectives and future challenges are discussed, with the aim to suggest improvements in the design and implementation of next-generation hybrid bio-nanogenerators and biosensors. Hybrid devices able to sense, monitor, interact, recognize, learn or stimulate, represent the building blocks for all the low-cost and accessible technologies of the current fast-evolving IoT revolution.
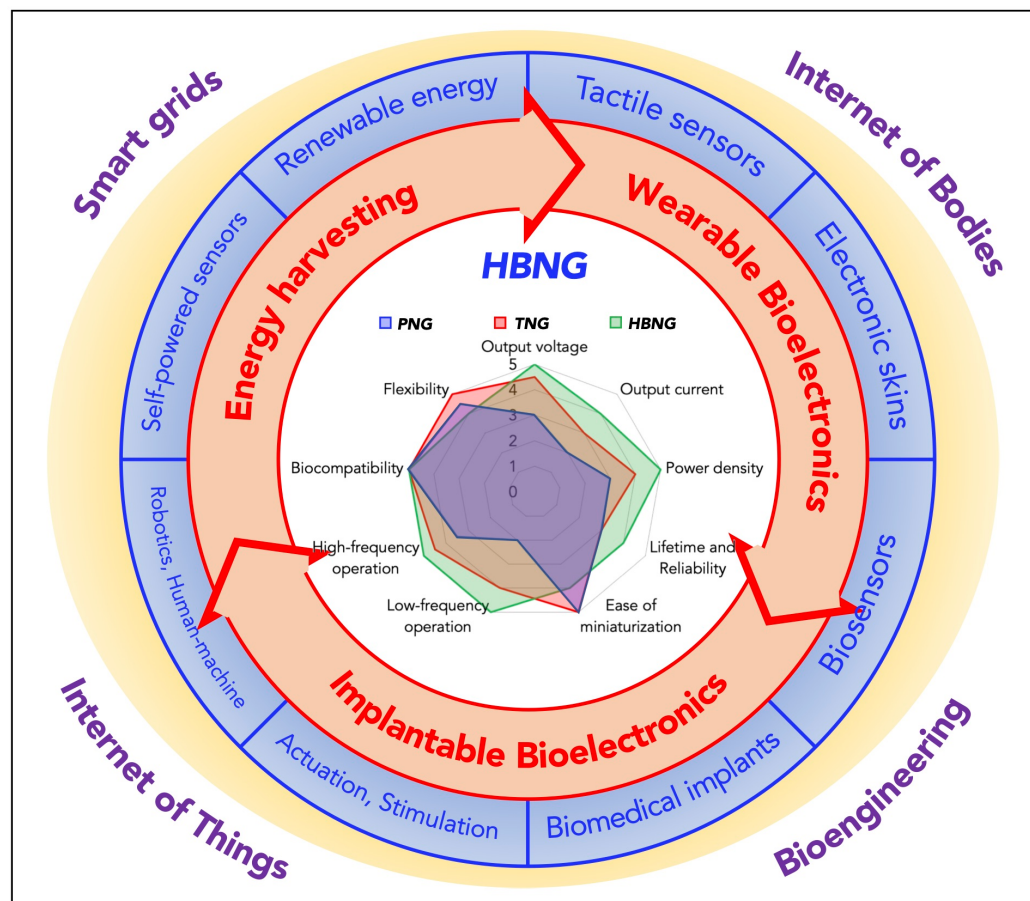
Figure 1. Illustrations of the potential applications of hybrid bio-nanogenerators (HBNGs). The radar chart in the center shows qualitatively the properties of piezoelectric nanogenerators (PNGs), tribo-electric nanogenerators (TNGs) and hybrid bio-nanogenerators (HBNGs): flexibility, output voltage, output current, output power density, lifetime and reliability, ease of miniaturization, low-frequency operation, high-frequency operation, biocompatibility. The surrounding scheme shows the most usual fields of applications for HBNGs, i.e., energy harvesting, wearable bioelectronics and implantable bioelectronics, with some specific examples: tactile sensors, electronic skins, biosensors, biomedical implants, actuation, stimulation, robotics, human-machine interfaces, self-powered sensors and renewable energy sources. The words outside the circle indicate the main technological contexts for the aforementioned applications: smart grids and cities, Internet of Things (IoT), Internet of Bodies (IoB) and Bioengineering.

2. Piezo-Triboelectric Transducing Mechanisms

In this section the governing equations of the analytical model for piezoelectric and triboelectric nanogenerators are outlined because they can be used as useful guidelines for the study and analysis of HBNGs. The main features of the materials usually adopted for exploiting piezoelectricity and triboelectricity are also briefly described.

2.1. Piezoelectric Materials and Mechanisms

Piezoelectric materials directly convert applied strain energy into electrical energy and exhibit high output power densities [46,53,54]: they are generally used in the form of nanostructured materials [55–57] or as thin films in layered structures [58–62]. The common feature is the non-centrosymmetric microstructure [63] which is responsible of the intrinsic capability of converting even ultra-weak mechanical stimuli into electrical energy, without external powering [64] (see Figure 2a). There are several choices among piezoelectric materials: they include piezo-ceramics or polymers [63,64] and they can be deposited on soft substrates through low-cost techniques for the fabrication of flexible and bendable piezoelectric nanogenerators and sensors [47]. In addition to lead zirconate titanate (PbZr$_{1-x}$Ti$_x$O$_3$, PZT) and its derivatives, which are highly performing but also less environmentally friendly, other valuable ceramic lead-free alternatives are barium titanate (BaTiO$_3$) [65], potassium sodium niobite (KNN) [66], lithium niobite (LiNbO$_3$) [67], zinc oxide (ZnO) [58,68] or aluminum nitride (AlN) [69,70]. AlN [5,71–74] has emerged as a promising material in the form of transparent µm-thick films deposited on flexible substrates [13,69,75–77] and with high-temperature and humidity resistance [78], mechanical and chemical stability [79,80], and biocompatibility [47,59]. LiNbO$_3$ is another cheap and easily accessible epitaxially grown piezoelectric material exploited for acoustic and optical devices [81]. It is chemically inert, heat-resistant, with lower dielectric constant than other piezo-ceramics [82], and its processability as thin films has been investigated and demonstrated [67]. Poly(vinylidene fluoride) (PVDF) and its co-polymers [83,84] are widely used for flexible polymeric biocompatible piezoelectric devices. Although it has a high dissipation factor, high dielectric constants, poor heat resistance, damped and worse performances than inorganic piezo-materials [85], it is very lightweight, soft and suitable for being employed in fluid flows or for wearable/implantable patches [84,86,87].

A piezoelectric nanogenerator (PNG) basically consists of a piezoelectric element sandwiched between two electrodes, which is subjected to a given mechanical load, depending on the specific application, thus generating electric power (Figure 2a(I,II)). In order to have a unified model of a PNG, in the context of mechanical vibrations and harmonic excitations, it may be considered as an oscillator vibrating along some directions, in the simplest case only one (therefore with a single degree of freedom, sDOF (Figure 2b(I)). This model can be used for rigid beams and as an approximated model for flexible oscillating beams. The dynamic behaviour of a piezoelectric beam/cantilever is generally described by the equations of mechanical motion:

$$\frac{\partial^2 \mathcal{M}(s,t)}{\partial s^2} + c_s \mathcal{I} \frac{\partial^5 w(s,t)}{\partial s^4 \partial t} + c_a \frac{\partial w(s,t)}{\partial t} + m \frac{\partial^2 w(s,t)}{\partial t^2} = -m \frac{\partial^2 w_b(s,t)}{\partial t^2} \tag{1}$$

where m is the equivalent mass per unit length; s is the longitudinal spatial coordinate; t is time; $\mathcal{M}(s,t)$ is the internal bending moment; c_s, c_a are the strain rate damping coefficient and viscous air damping coefficient, respectively; $\mathcal{I}$ is the moment of inertia of the cross section; $w(s,t)$ is the relative displacement, related to the base displacement $w_b(s,t)$ by the expression $\mathcal{W}(s,t) = w(s,t) + w_b(s,t)$, with $\mathcal{W}(s,t)$ the absolute displacement.

To explicit (1) for piezoelectric materials, the e-form piezoelectric constitutive equations may be applied:

$$\begin{cases} T_i = \sum_{j=1}^{6} c_{ij}^E S_j - \sum_{\kappa=1}^{3} e_{\kappa i} E_\kappa, & i = 1, \ldots, 6 \\ D_i = \sum_{j=1}^{6} e_{ij} S_j + \sum_{\kappa=1}^{3} \epsilon_{\kappa\kappa}^S E_\kappa, & i = 1, \ldots, 3 \end{cases} \tag{2}$$

where T_i, S_i are the stress and strain components along direction "i"; c_{ij}^E are the elastic stiffness matrix components at constant electric field; D_i, E_i are the electric displacement and electric field along direction "i"; e_{ij} are the piezoelectric coefficients; ϵ_{ii}^S are the electric permittivities at constant strain.

Using a simplified notation, the piezoelectric polarization charge density ρ_P and the electric potential can be deduced from the following expressions:

$$\rho_P = d_P T, \quad \nabla E = -\frac{\rho_P}{\epsilon} \tag{3}$$

where d_P is the piezoelectric coefficient, T is the applied stress and ∇E is the divergence of the electric field. Equations (2) and (3) hold true for any type of piezoelectric material: although most of them are dielectrics, piezoelectric semiconductors have been also synthesised and studied such as ZnO or GaN fibers, nanotubes, belts and films. In this case, the basic behaviour of these materials with semiconductive properties relies on the equations of linear piezoelectricity and the conservation of charge for electron and holes, electrostatic equations, current-density equations and continuity equations [88–94], which are developed in the theories of piezotronics and piezo-phototronics [95–99].
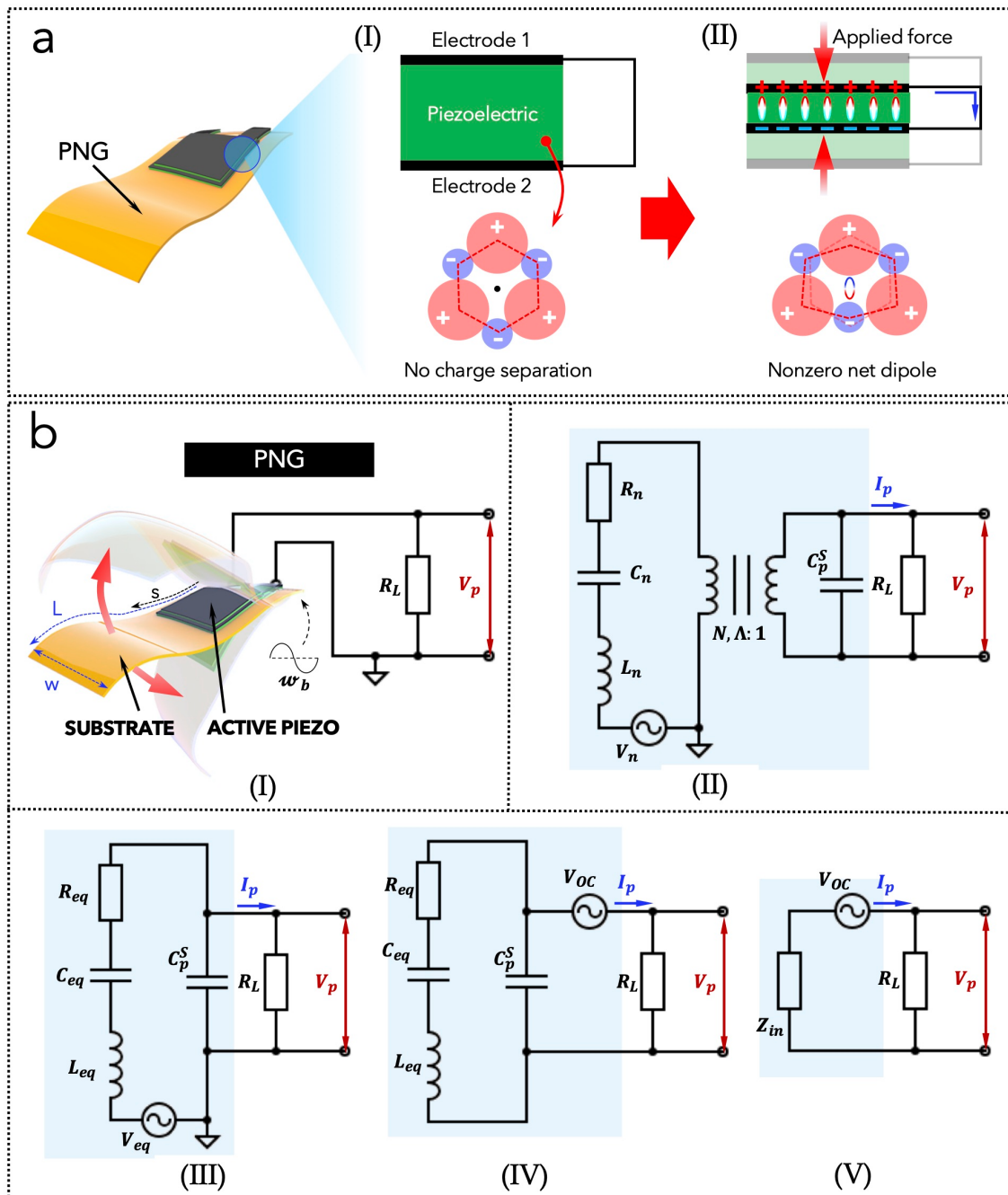
Figure 2. (**a**) Piezoelectric mechanism: (**I**) unloaded state and no charge separation; (**II**) loaded state with an applied force or strain and a non-zero net electrical dipole. (**b**(**I**–**V**)) Equivalent circuit model of a PNG. (**I**) PNG connected to a resistive load (R_L) and subjected to a base excitation (w_b). (**II**–**IV**) Full equivalent circuit model and simplified versions. (**V**) Final equivalent circuit model of a PNG, consisting of an internal impedance (Z_{in}) and an alternate voltage source (V_{OC}).

For a sDOF PNG, the following assumptions hold true: (i) Euler-Bernoulli beam hypothesis; (ii) negligible external excitation from air damping; (iii) strain rate damping and viscous air damping are proportional to the bending stiffness and mass per length of the beam; (iv) uniform electric field over the piezoelectric thickness; (v) small deformations of the PNG [100]. It is worth noticing that these assumptions do not account for non-linear structural behaviour or for very large deformations (e.g., very flexible PNG in turbulent flows).

Therefore, as discussed in [100–103], the piezoelectric constitutive equations can be simplified and together with Equation (1) yield:

$$
\begin{cases}
Y\mathcal{I}\frac{\partial^4 w}{\partial s^4} + c_s\mathcal{I}\frac{\partial^5 w}{\partial s^4 \partial t} + c_a\frac{\partial w}{\partial t} + m\frac{\partial^2 w}{\partial t^2} + KV_p(t)\left[\frac{d\delta(s)}{ds} - \frac{d\delta(s-L)}{ds}\right] = -m\frac{\partial^2 w_b}{\partial t^2} \\
\frac{V_p(t)}{R_L} + C_p^S\frac{dV(t)}{dt} + \int_0^L e_{31}h_{pn}w\frac{\partial^3 w}{\partial^2 s \partial t}ds = 0
\end{cases} \tag{4}
$$

where $Y\mathcal{I}$ is the average bending stiffness; L, w are the length and width of the beam; K is the electromechanical coupling coefficient; $\delta(s)$ is the Dirac delta function; $V_p(t)$ is the output voltage; R_L is a generic resistive load connected to the PNG; h_{pn} is the distance of the center of the piezoelectric layer from the beam's neutral axis.

The mechanical motion of a sDOF PNG subjected to harmonic vibrations, fluid/pressure-induced oscillations may be represented as $w(s,t) = \sum_n \lambda_n(s)u_n(t)$, where $\lambda_n(s)$ and $u_n(t)$ are, respectively, the mass normalized eigenfunction and the modal coordinate for the nth mode of the beam harmonic motion.

Hence, the modal electromechanical equations for the PNG are:

$$
\begin{cases}
\ddot{u}_n + 2\xi_n\omega_n\,\dot{u}_n + \omega_n^2 u + \Lambda_n V_p = -f_n\ddot{u}_b \\
I_p + C_p^S\dot{V}_p - \sum_n \Lambda_n\,\dot{u}_n = 0
\end{cases} \tag{5}
$$

where $I_p(t) = V_p(t)/R_L$ is the output current; $\omega_n, \xi_n, \Lambda_n, f_n$ are the natural frequency, the damping ratio, the modal electromechanical coupling coefficient (or force-voltage factor) and the modal mechanical forcing function for the n-th mode, respectively, with $\Lambda_n = \int_0^L K\frac{d^2\lambda_n(s)}{ds^2}ds$ and $f_n = \int_0^L m\lambda_n(s)ds$.

The analytical model takes into account only a resistive load connected to the PNG and the maximum output power consumption on the load is yielded by the optimal load resistance [101]. Accordingly, a load resistor is usually taken into account for during the transducer design and optimisation stage. However, this approach is not exhaustive, in fact, the circuit downstream of the PNG is often more complex in order to transfer efficiently the power to an energy storage, as discussed in [104]. On the other hand, the approach of electromechanical analogy, i.e., between electrical and mechanical domains, is a useful tool for solving this issue. Each element in the mechanical motion of the PNG may be translated to a homologous electric counterpart, therefore the PNG can be replaced by its equivalent circuit model (ECM) [100–102].

For the *n*th mode, the base excitation $-f_n\ddot{u}_b$ is equivalent to an AC voltage source V_n; the electromechanical coupling may be considered as a force-voltage ideal transformer with ratio $N_n = \Lambda_n$; the mass m (per unit length), the compliance $1/\omega_n^2$ and the mechanical damping $2\xi_n\omega_n$ correspond, respectively, to an inductance L_n, a capacitance C_n and a resistance R_n. The electrical counterparts of the modal coordinate and velocity are the generated charge q_n and flowing current I_n. Figure 2b(II–IV) reports the variations of the ECM for a PNG, based on the electromechanical analogy and circuital simplifications. In the simplest case a PNG may be replaced by a current source connected in parallel or a voltage source connected in series to the free capacitor of the piezoelectric material (Figure 2b(V)). The RC matching method asserts that the optimal resistance is the impedance of the free capacitor [105]. However, other ECMs based on lumped parameters have been proposed [106–108], which are useful for designing the power management circuits and for accurately account for the power output across the whole frequency range [102,109,110]. In particular, a pure resistive load that matches the internal impedance of the transducer

only takes into account the case of an existing zero-phase impedance matching, which yields a power peak in the power/resistance curve [108,111].

2.2. Triboelectric Materials and Mechanisms

Triboelectricity is a phenomenon through which the relative contact between two dissimilar materials induces the generation of superficial charges [112–114]. Electrostatic induction is responsible of the redistribution of charges from these materials to some conductive or metal electrodes which collect and transfer them to an external circuit to generate electrical power [115–117]. Surface charge density is a key parameter and it is determined by the surface triboelectric polarities of materials, i.e., the capability of attaining electrons or positive charges on the surface. Triboelectric series list most of materials in terms of their triboelectric capability, depending on the electron affinity and the work function [115,118,119]. The charge transfer during contact electrification is basically a surface process so it can be favored or enhanced by different nanostructuring/patterning techniques, by acting on the surface roughness, the porosity and the wettability properties to increase the effective friction area [120–128].

Triboelectric nanogenerators (TNGs) present several advantages against other electromagnetic generators, e.g., light mass, low density, cost-effectiveness, higher scalability and no need of bulky coils and magnets [14,24,113,129–134]. Flexible devices rely on soft substrates and polymers as triboelectric layers, due to their flexibility and deformability. Common examples are polytetrafluoroethylene (PTFE), Polyimide (PI), polyethyleneterephtalate (PET), polydimethyl siloxane (PDMS), etc. Parylene C (poly(para-xylylene)) is also another promising material for TNG because of several attractive properties [135,136], e.g., chemical inertness, conformality, FDA-approved biocompatibility, barrier properties, anticorrosive/antibiofouling behavior and high flexibility [137–142]. It can be easily deposited through an efficient, room-temperature, controlled process (Gorham route) [143] and it can also be variously surface-treated, e.g., under oxygen plasma, ozonized UV, or by wet and dry etching processes [5,76,137,144,145].

A TNG can be basically regarded as a pair of materials separated by a gap, which come into contact owing to an external mechanical load, generating an electrical potential and a current in an external circuit that serve to re-establish the electrostatic equilibrium broken by the contact electrification (Figure 3a(I–III)). Several operating modes are possible for a TNG (vertical contact-separation mode, sliding mode, free-standing mode, single-electrode mode) [5], but the theoretical foundation of the triboelectrification phenomenon is the Maxwell's displacement current, given by:

$$J_D = \frac{\partial D}{\partial t} = \epsilon \frac{\partial E}{\partial t} + \frac{\partial P_S}{\partial t} \tag{6}$$

where D is the displacement field, E is the electric field and P_S is the polarization due to the presence of surface polarization charges.

The triboelectric potential and the triboelectric current may be defined by the following equations [146]:

$$\Delta V = -\frac{\rho_T d}{\epsilon}, \quad I = C_T \frac{\partial \Delta V}{\partial t} + \Delta V \frac{\partial C_T}{\partial t} \tag{7}$$

where ρ_T is the generated triboelectric charge density, d is the gap distance between the materials, C_T is the capacitance of the overall system.

The analytical model of a TNG can be derived from a Lagrangian formulation, as reported in [147]. In particular, for a sDOF generic dual dielectric contact-mode triboelectric generator, the electromechanical equations of motions can be written as:

$$\begin{cases} m\ddot{x} + c_{eq}\dot{x} + k_{eq}x - \frac{S}{2\epsilon_2}\left(\sigma_2 + \frac{q}{S}\right)^2 = f + mg \\ R\dot{q} + \frac{q}{A}\left(\frac{d_1}{\epsilon_1} + \frac{d_2}{\epsilon_2} + \frac{d_3}{\epsilon_3} - \frac{x}{\epsilon_2}\right) + \frac{\sigma_2}{\epsilon_2}(d_2 - x) + \frac{d_1}{\epsilon_1}(\sigma_1 + \sigma_2) = 0 \end{cases} \tag{8}$$

where x is the displacement of the top electrode, q is the electrical displacement of the bottom dielectric, k_{eq} is the equivalent stiffness of the system, S is the surface active area, c_{eq} is the equivalent damping coefficient of the system; d_1, d_2, d_3 are the thicknesses of the

upper dielectric, the air gap and the bottom dielectric; σ_1, σ_2 are the surface charge density on the top and bottom dielectrics; f is a mechanical load; m is the mass of the system.
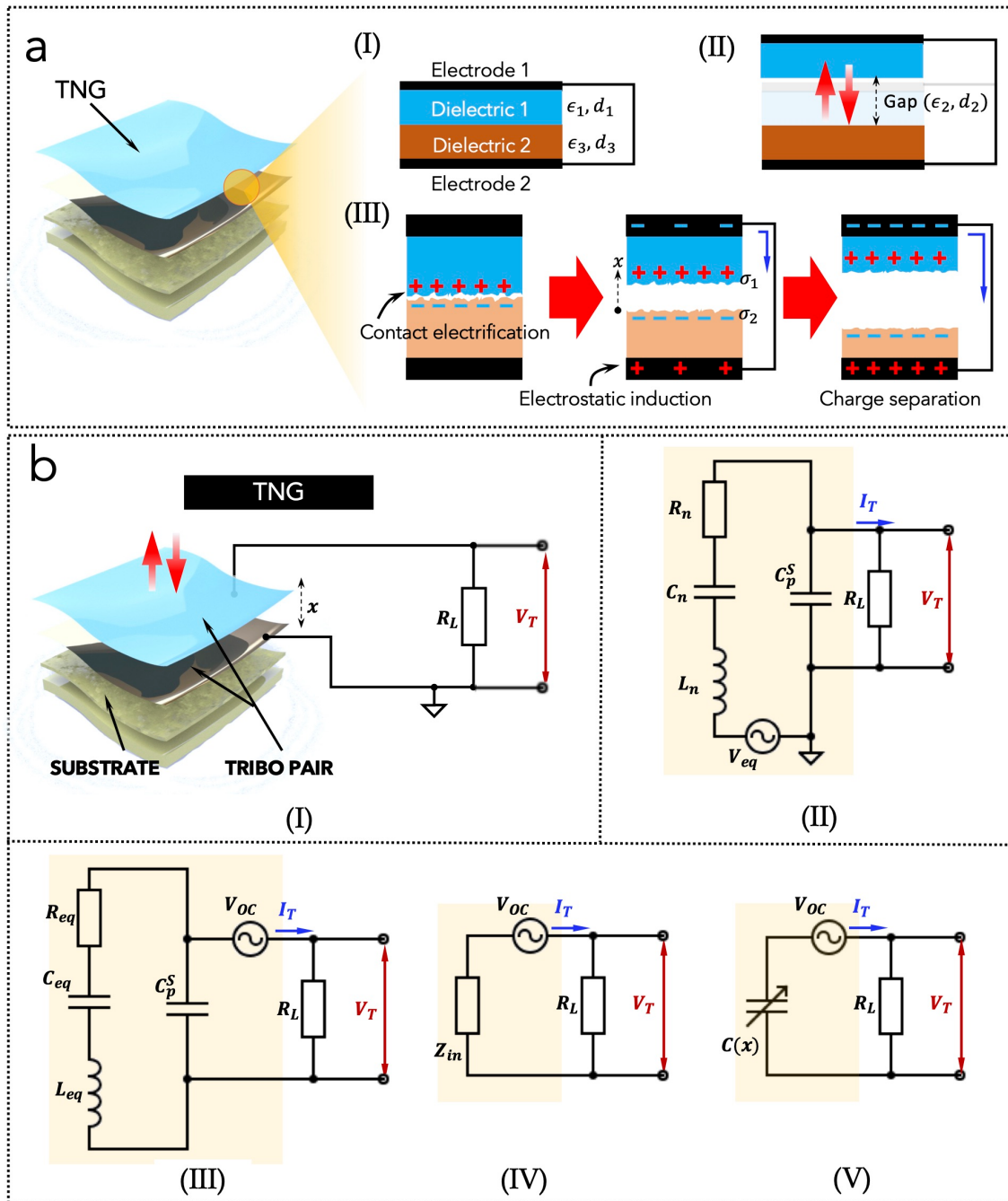
Figure 3. (**a**) Pressed state of a TNG with two dielectrics in contact. (**I**) Released state of the TNG. (**II**,**III**) Contact electrification and process of triboelectric charge separation. (**b**) Equivalent circuit model of a TNG. (**I**) Schematic of a TNG connected to a resistive load (R_L) and subjected to a periodic vertical contact-separation motion (x). (**II–IV**) Full equivalent circuit model and simplified versions. (**V**) Final equivalent circuit model of a TNG, made of an internal variable capacitance ($C_{(x)}$) and an alternate voltage source (V_{OC}).

In the assumption of small oscillations, the equations of motions may be simplified into the following:

$$\begin{cases} \ddot{x} + 2\xi\omega_n \dot{x} + \omega_n^2 x - \frac{\alpha}{m}q - \frac{\beta}{m}q^2 = \frac{f}{m} \\ \dot{q} + \frac{1}{C(x)R}q - \frac{\alpha}{R}x = 0 \end{cases} \tag{9}$$

where $C(x)$ is the variable equivalent capacitance; $\xi = c_{eq}/2\sqrt{mk_{eq}}$ is the damping ratio, $\omega_n = \sqrt{k_{eq}/m}$ is the natural frequency; R is a load resistance; α and β are two lumped parameters defined as $\alpha = 1/\epsilon_2 \cdot (\sigma_2 + Q_0/S)$ and $\beta = 1/2\epsilon_2 S$, with Q_0 the initial total charge on the dielectrics.

As for the PNGs, from the electromechanical equations it is possible to deduce the electromechanical analogy and pass from the mechanical to the electrical domain. The applied force is equivalent to an alternating voltage source V_n; the mass m, the compliance $1/\omega_n^2$ and the mechanical damping $2\xi\omega_n$ correspond, respectively, to an inductance L_n, a capacitance C_n and a resistance R_n [148].

Figure 3b(I–V) reports the variations of the ECM for a TNG, based on the electromechanical analogy and circuital simplifications. The simplest ECM of a TNG can be represented as an alternating voltage source in series with a capacitor with varying capacitance [148,149], and according to the RC matching method, the optimal resistance is the impedance of this capacitor [105].

3. Piezo-Triboelectric Hybridization

Hybrid bio-nanogenerators (HBNGs) are aimed at constituting sustainable power systems that integrate different kinds of transducing mechanisms, e.g., mechanical, photovoltaic, thermal, exploiting electromagnetic induction, triboelectrification, piezoelectricity, solar light, temperature gradients [52]. The objective of this innovative systems is to enhance the performances of the single components, to harness simultaneously several renewable energy sources and to improve the sensitivity range of the devices.

In fact, PNGs and TNGs often require specific operating conditions and present some disadvantages. In particular, the type of output voltages and currents originating from the piezoelectric and triboelectric effects are different: the piezoelectric signal is very effective with impulsive loads and rapid mechanical deformations, the triboelectric signal is more perceptible with continuous slow friction. Additionally, their impedances are different implying that the output voltage/current is lower/higher for piezoelectrics and higher/lower for triboelectrics. Therefore, the hybridization of the two mechanisms allows to overcome these constraints, to integrate their functionalities in the same device, enhancing the overall sensitivity and widening the measurement ranges [120,150–154].

HBNGs can be considered multi-source, multi-function and multi-mechanism devices. In this section, the hybridization of PNGs and TNGs is taken into consideration. Depending on the way these two components are connected and coupled, different structural schemes can be distinguished, and the circuit model and the power management circuits necessary to extract signals are different.

The first classification regards the physical domains involved in the energy conversion process: if they belong to the same species and are ruled by the same physical processes, then the hybridization is called "*intra-domain*". This holds true in most cases for piezoelectric-triboelectric devices because the common domain is the mechanical one. In all the other cases, when solar, thermal or biochemical energy is involved for energy/signal generation, the hybridization is called "*inter-domain*".

The second classification is related to the way the materials of the piezoelectric or triboelectric components are physically coupled. If they are not permanently in contact with each other and belong to distinct single devices, then the hybridization occurs "*with physical separation*". On the other hand, if there is a physical connection or interpenetration between the active materials responsible for the two transducing mechanisms, then the hybridization is "*with physical integration*". This difference is also crucial for the number and positioning of the electrodes within the hybrid device.

The third classification concerns the number of mechanisms coupled together in the same hybrid device. A "coupling number" (CN) can be defined in this respect as the number of processes separately responsible for charge generation. For instance, most of piezo-triboelectric hybrid devices have a CN equal to 2, a piezo-triboelectric-electromagnetic hybridized device has a CN equal to 3. In case of wearable patches, the triboelectrification

due to the contact with human skin can generate further charges [76] and this would count as an additional process, increasing the CN. Hence, the CN is correlated with the structural complexity of the whole system. A higher CN implies more electrodes, connections and processes involved in the transduction mechanism.

Han et al. [155] have investigated and compared (theoretically and experimentally) different piezoelectric-triboelectric nanogenerators, taking into account the number of terminals and contacted materials, the polarization direction and electrode connection (Figure 4a). They classified six different configurations (three in conductor-to-dielectric mode and three in dielectric-to-dielectric mode), as well as one, three and nine possible configurations for two-terminal, three-terminal and four-terminal devices, respectively. Additionally, for each configuration, two possibilities can be distinguished with forward or reverse polarization of the piezoelectric material. Thus, 52 configurations have been considered in total. In general, if *n* is the number of terminals, the following formula can be proposed for the number of possible configurations:

$$
\begin{cases}
4 \cdot \prod_{\substack{k=0 \\ k \le \frac{n}{2}-1}} \begin{pmatrix} n-2k \\ 2 \end{pmatrix}, & n \le 3 \\
4 \cdot \prod_{\substack{k=0 \\ k \le \frac{n}{2}-1}} \begin{pmatrix} n-2k \\ 2 \end{pmatrix} \cdot \frac{3}{2}, & n > 3
\end{cases}
\tag{10}
$$

where the factor 4 accounts for the two conductor/dielectric modes and for the two forward/reverse polarization modes, whereas the factor 3/2 is for avoiding repetitions.

The structure, polarization direction and electrode connection strongly affect the output performance of the overall hybrid device. In particular, it can be enhanced or reduced almost to zero just modifying the electrode connection: this can be an advantage because with the same polarization direction and configuration, the performances can be tuned to maximize the output power (in case of an energy harvester) or to minimize the electrostatic charges (in case of preventing charging in electronic devices).

Another key point is that with the same parameters and configurations, the performances can be modulated by acting on the mechanical design, regardless the piezoelectric coefficients or the triboelectric surface charge densities. In this respect, the piezoelectric component can be designed to obtain specific required stress variations during the contact-separation cycle of the triboelectric component, so that there is a simultaneous coupling of the two mechanisms.

The combination of piezoelectric and triboelectric effects for a specific configuration can be correlated with an output state characterized by different multi-level electric outputs, depending on the electrode connections. This can be exploited for logic communication devices, SC/OC detection systems or active impedance-based sensors [155].

For an HBNG, deriving and applying the electromechanical equations is very complex, especially when the motions of the two components are closely related. A general system of equations that govern an HBNG is given by the combinations of the piezoelectric and triboelectric equations: in particular, the Maxwell's law of displacement current, i.e., (6 [156], holds true but it is diversified within the piezoelectric or triboelectric domain, thus the analytical model can be represented in general as follows (assuming a polarization and a contact-separation cycle along the *z*-axis, and no external applied electric field):

$$
\begin{cases}
J_D^{piezo}\Big|_x = \frac{\partial D_x}{\partial t} = \frac{\partial P_x}{\partial t} = (e)_{ij}\left(\frac{\partial S}{\partial t}\right)_j\Big|_x = \frac{\partial \sigma_P(x)}{\partial t} \\
J_D^{tribo}\Big|_x = \frac{\partial D_x}{\partial t} = \frac{\partial \sigma_I(x,t)}{\partial x} = \sigma_c \frac{dx}{dt} \frac{d_1\epsilon_0/\epsilon_1 + d_2\epsilon_0/\epsilon_2}{[d_1\epsilon_0/\epsilon_1 + d_2\epsilon_0/\epsilon_2 + x]^2} \\
\mathcal{F}\left(\Delta V_{piezo}, \Delta V_{tribo}, J_D^{piezo}, J_D^{tribo}\right) = 0.
\end{cases}
\tag{11}
$$

where x is the separation distance between the triboelectric layers or the distance inside the piezoelectric material; $\sigma_P(x)$ is the surface polarization charge density on the piezoelectric material; $\sigma_I(x,t)$ is the surface density of free electrons accumulated in the electrodes of the triboelectric material; d_i, ϵ_i are the thicknesses and dielectric constants of two dielectrics of

the triboelectric pair; $\Delta V_{piezo}, \Delta V_{tribo}$ are the output voltage downstream of the piezoelectric and the triboelectric device; $\mathscr{F}$ is a function that involves the output voltages and currents of the piezoelectric and triboelectric components and which depends on the specific configuration and electrode connections.
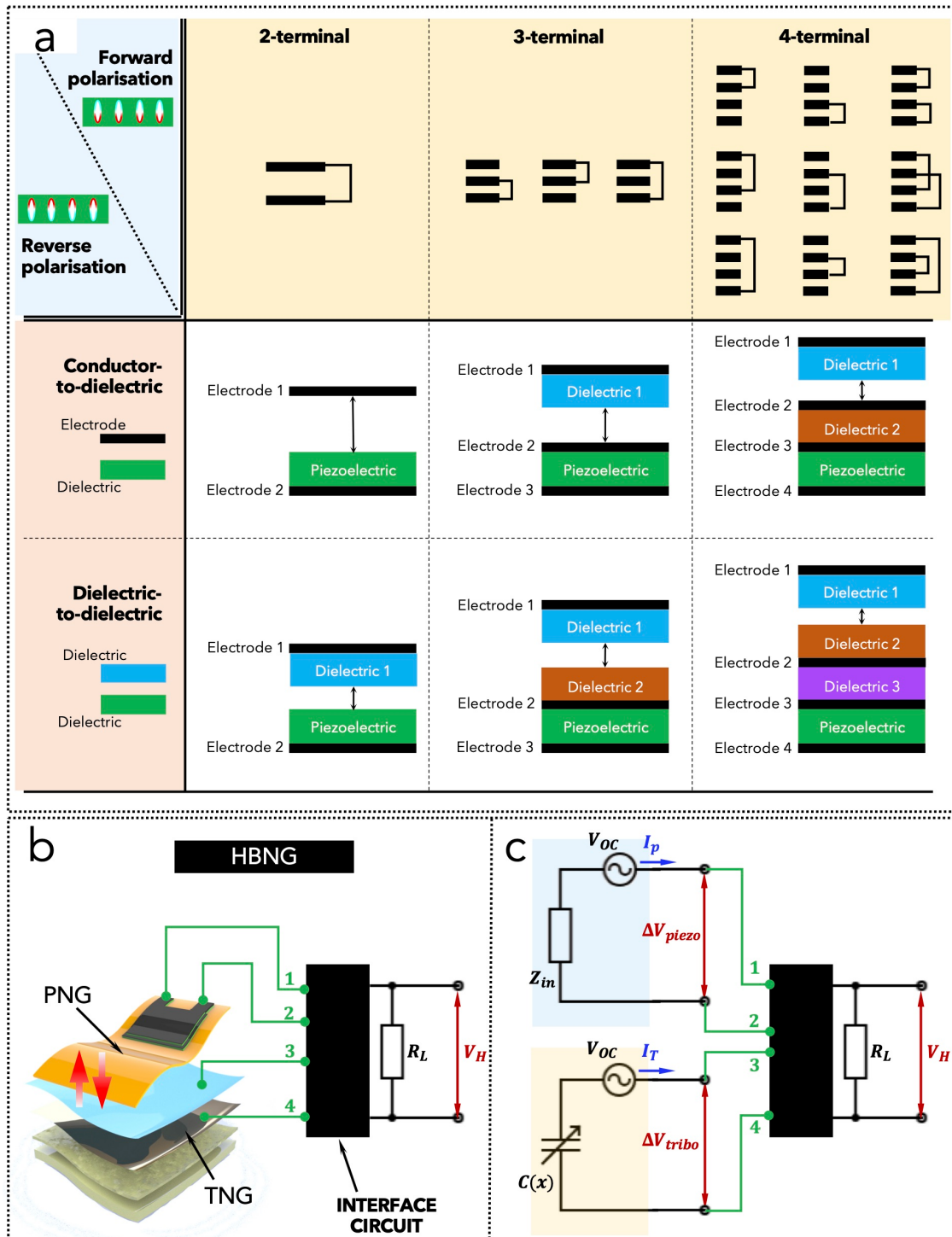
Figure 4. (**a**) Classification of the HBNGs with respect to the number of electrodes, the contact mode (conductor-to-dielectric or dielectric-to-dielectric) and the polarization direction of the piezoelectric material. (**b**,**c**) Equivalent circuit model of a HBNG. (**b**) Schematic of a HBNG connected to a resistive load (R_L) and subjected to a periodic vertical contact-separation motion. (**c**) Simplified equivalent circuit model of a HBNG.

Chen et al. [157] proposed a first example of theoretical analysis of the contact-mode hybrid piezoelectric-triboelectric nanogenerator, describing the relationships among transfer charges, voltage, current and average output power in terms of material properties and operating conditions. This model can be used for a general 3-electrode HBNG with a single-electrode TNG: assuming that the triboelectric charges are distributed uniformly on the triboelectric layer with a small decay, the contact area is much larger than the gap and only vertical components of the electric fields exist in the air gap, the charge balance holds true:

$$\sigma_1 + \sigma_2 + \sigma_3 - \sigma = 0 \tag{12}$$

where σ is the triboelectric charge density and $\sigma_1, \sigma_2, \sigma_3$ the surface charge densities on the electrodes. The electric fields of the piezoelectric, triboelectric and air gap. Then, for a closed loop in a circuit, it is possible to write:

$$V_a + V_T + V_1(t) = 0, \quad V_P + V_2(t) = 0 \tag{13}$$

where V_a, V_T, V_P are the voltages across the air gap, the triboelectric layer and the piezoelectric layer; V_1, V_2 are the voltages across two external resistors connected to the PNG and TNG. Combining the previous equations with the V-Q-x relationship for the TNG unit and the charge transfer equation for the PNG unit, it is possible to obtain the current and voltage expressions for the full hybrid device [157].

Therefore, since it is challenging to predict theoretically the function $\mathscr{F}$, the ECM is necessary in this case for determining the electromechanical behaviour of the device (Figure 4b). Here a simple ECM is proposed for a piezoelectric and triboelectric HBNG based on contact-mode (Figure 4c). The HBNG can be considered as a set of two separate ECMs for the PNG and TNG, respectively, and then their distinct outputs ($\Delta V_{piezo}, \Delta V_{tribo}$) are used as inputs of an interface circuit that provides the output voltage (V_H) of the HBNG, as a two-terminal device. The electrodes deriving from the PNG and TNG are in total four but they can vary depending on the configuration.

The next sections describe the main types of hybridization that can occur between PNGs and TNGs, and examples of HBNGs from previous works are comprehensively summarized in Table 1.

3.1. Intra-Domain Hybridization with Physical Separation

This category includes the devices where piezoelectric and triboelectric nanogenerators are coupled separately (Figure 5a). This means there are at least two electrodes for the PNG and one electrode for the TNG. The 3-terminal and 4-terminal configurations illustrated in Figure 5a are included in this group. The physical separation between the two devices allows to extract separately the signal generated by each component and perform an additive sum through rectifying circuits downstream of the hybrid device. Thus, the hybridization occurs mostly within the electronic interface according to the combination of output voltages and currents: it can be considered an *"external hybridization"*. A slight contribution is only provided by the materials interaction because the two devices work as if they were alone: this is especially true for a PNG and a two-electrode TNG (four-terminal HBNG). When the TNG has only one single electrode (three-terminal HBNG), although it is still separated from the PNG, the contact electrification occurs between the triboelectric layer and one of the layers of the PNG (Figure 5b): in this case the interaction between the two devices plays a role in the hybridization [13]. In particular, the piezoelectric polarization direction and the triboelectric charge polarity on the common electrode is determining for the enhancement or reduction of the hybrid signal [13].

Table 1. Hybrid bio-nanogenerators (HBNGs) classified in terms of hybridization approach, materials, performances and applicative context. The green, yellow, blue and pink colors are, respectively, for: 2-mechanism hybrid piezo-triboelectric, 2-mechanism hybrid with piezoelectric or with triboelectric, intra-domain 3-mechanism hybrid with piezo-triboelectric, 2/3-mechanism inter-domain hybrid. The coupling number (CN) represents the total number of transducing mechanisms present in the device.

Ref.	Coupled Mechanisms	CN	Hybridization Type	Materials	Thickness /Size	Output Performances	Application Field
Chen et al. [158]	Piezo-Tribo	2	intraD-PI	PVDF NMFs, Cu-PCB	~500 µm	15 V; 0.0783 µW/cm^2	MEH
Chen et al. [159]	Piezo-Tribo	2	intraD-PI	P(VDF-TrFE) NFs, Kapton, Cu, PET/ITO, PDMS	-	96 V; 0.887 µW/cm^2(piezo) 8 V; 1.14 µW/cm^2(tribo1) 16 V; 17.6 µW/cm^2 (tribo2)	MEH
Zhao et al. [160]	Piezo-Tribo	2	intraD-PS	P(VDF-TrFE), Au, PET, Al, PTFE	650 µm	210 V; 6040 µW/cm^2	MEH
Xia et al. [161]	Piezo-Tribo	2	intraD-PI	PVDF, Al, PDMS	~600 µm	5.36 V; 1 µW/cm^2 (Piezo) 5.84; 1.68 µW/cm^2 (Tribo)	MEH
Suo et al. [162]	Piezo-Tribo	2	intraD-PI	PET/ITO, BTO/PDMS, Cu	200 µm	3.3 V	MEH
Singh et al. [68]	Piezo-Tribo	2	intraD-PS	Au, ZnO/PVDF, PTFE, Al	~245 µm	~97 V; 24.5 µW/cm^2	MEH
Guo et al. [163]	Piezo-Tribo	2	intraD-PI	Conductive mat, Silk FBs, PVDF FBs	145.3 µm	~500 V; 310 µW/cm^2	MEH, WBS
Wang et al. [164]	Piezo-Tribo	2	intraD-PI	Al, ZnO, P(VDF-TrFE), PDMS	~200 µm	751.1 mW/m^2	MEH, WBS
Huang et al. [165]	Piezo-Tribo	2	intraD-PI	PVDF FBs, conductive mat	-	210 V; 70 µW/cm^2	MEH
Chen et al. [166]	Piezo-Tribo	2	intraD-PS	P(VDF-TrFE), PDMS, PU/CNTs/AgNWs	-	57.1 V; 0.11 µW/cm^2 (Piezo) 183 V; 84 µW/cm^2 (Tribo)	MEH, WBS
Wang et al. [150]	Piezo-Tribo	2	intraD-PS	Al, ZnO, P(VDF-TrFE), PDMS/MWCNTs, Al	130 µm	2.5 V; 0.689 mW/cm^3 (Piezo) 25 V; 1.98 mW/cm^3 (Tribo)	MEH
Mariello et al. [13,76]	Piezo-Tribo	2	intraD-PS	Mo, AlN/Kapton, pC, Ti/Au, PDMS/Ecoflex	~86 µm	16 V; 0.8 W/m^2	MEH, WBS
Jung et al. [167]	Piezo-Tribo	2	intraD-PS	Polyimide, Al, PVDF, PTFE, Au	~200 µm	370 V, 12 µA/cm^2, 4.44 mW/cm^2	MEH
Li et al. [168]	Piezo-Tribo	2	intraD-PS	Nylon, ZnO, PDMS, Cu	3 mm	10.2 mW/m^2 (piezo) 42.6 mW/m^2 (tribo)	MEH
Mariello et al. [84]	Piezo-Tribo	2	intraD-PI	PVDF NFs, Cardanol, PDMS, Kapton	~120 µm	~0.5 V; ~0.85 10^{-2} µW/cm^2	MEH, WBS
Zhu et al. [169]	Piezo-Tribo	2	intraD-PS	PDMS, skin, PVDF-TrFE NFs	~500 µm	25.8 V. 6.15 µW/g (6 mm amplitude)	WBS
Wang et al. [170]	Piezo-Tribo	2	intraD-PS	Ecoflex, nickel fabric, PZT	2.9 cm	15 V/g (0–1.5 g) (g: gravity acc.)	MEH, IoT
Yu et al. [153]	Piezo-Tribo	2	intraD-PI	PDMS, PZT-PVDF-TrFE NFs	~200 µm	15.43 V/kPa (0–100 kPa) 18.96 V/kPa (100–800 kPa)	WBS
Yang et al. [171]	Piezo-Tribo	2	intraD-PS	Acrylic, PVDF-TiO2, PDMS-GQD, ITO, PET, Al, Cu	-	88 V, 19.5 µA343.5 µW (Tribo), 43.2 µW (Piezo)	MEH

Table 1. *Cont.*

Ref.	Coupled Mechanisms	CN	Hybridization Type	Materials	Thickness /Size	Output Performances	Application Field
Wang et al. [172]	Tribo-ElectroM	2	intraD-PS	PTFE, Kapton, Cu, Magnet	2 cm	8.8 mW/g (Tribo) 0.3 mW/g (ElectroM)	MEH
Yang et al. [173]	Tribo-ElectroM	2	intraD-PS	PTFE, PDMS, NaNbO3, acrylic	mm-cm	15.5 V/cm^2; 0.08 mW/cm^2	MEH
Wang et al. [174]	Tribo-ElectroM	2	intraD-PS	Acrylic, Polymer films, Cu, Magnet	4 cm	65 V; 438.9 mW/kg (Tribo) 7 V; 181 mW/kg (ElectroM)	MEH
Hu et al. [175]	Tribo-ElectroM	2	intraD-PS	Acrylic, Kapton, Cu	-	7.7 mW (Tribo) 1.9 mW (ElectroM)	MEH
Quan et al. [176]	Tribo-ElectroM	2	intraD-PS	Acrylic, Kapton, PVB/PDMS, Cu	3 cm	0.1 mW (Tribo); 2.8 mW (ElectroM)	MEH
Zhang et al. [177]	Tribo-ElectroM	2	intraD-PS	Acrylic, PTFE, Al, magnet	-	17.5 mW, 55.7 W/m^3	MEH
Ran et al. [178]	Tribo-ElectroM	2	intraD-PS	PLA, FEP, Cu, magnet	~10 cm	48 V, 1 mA, 13 mW	MEH
Zhao et al. [179]	Piezo-ElectroM	2	intraD-PS	PZT, metal, Copper, Magnet	mm-cm	11 μW/cm^2 (@11 m/s)	MEH
Hamid and Yuce [180]	Piezo-ElectroM	2	intraD-PS	PZT, magnets, coils	37 mm	1.8 V, 3.3 V; 0.550 mW	MEH, WBS
Fan et al. [181]	Piezo-ElectroM	2	intraD-PS	PMMA, Nd-Fe-B-N35, Phosphor bronze Brass, PZT	14 mm	0.13 mW (Piezo); 2.94 mW (ElectroM)	MEH
Toyabur et al. [182]	Piezo-ElectroM	2	intraD-PS	Acrylate, Copper, NdFeB magnet, PZT, Al	mm-cm	250.23 μW (Piezo) 244.17 μW (ElectroM)	MEH
Gong et al. [182]	Piezo-ElectroS	2	intraD-PI	PLLA, PLA, Au	~500 μm	0.31 mW; 35 V, 1 μA	MEH, WBS
Lagomarsini et al. [182]	Piezo-ElectroS	2	intraD-PS	VHB, PZT, PVDF	500 μm	85 V, 17 μJ (PZT); 15 V, 0.45 μJ (PVDF)	MEH, WBS
He et al. [183]	Piezo-Tribo-ElectroM	3	intraD-PS	Acrylic, PVDF, Cu, PVS, Steel, Magnet	37 mm	12.6 V; 41.0 μW (Piezo) 362.1 mV; 66.5 μW (ElectroM) 13.3 V; 4.6 μW (Tribo)	MEH
Rodrigues et al. [184]	Piezo-Tribo-ElectroM	3	intraD-PS	Au, ZnO, PMMA, ITO, PET, Magnet, Copper, Nylon, Kapton, PTFE	0.1 mm	34 V (430 N)	MEH
He et al. [152]	Piezo-Tribo-ElectroM	3	intraD-PS	Silicone, CNT, Copper, PZT, Magnet, ABS	2.6 cm	78.4 μW (Tribo) 36 mW, 38.4 mW (ElectroM) 122 mW, 105 mW (Piezo)	MEH
Singh et al. [185]	Piezo-Tribo-ElectroM	3	intraD-PS	Acrylic, Copper, Gold, PTFE, ZnO-PVDF	6 cm	192 V, 2.78 mA	MEH
Wang et al. [186]	Piezo-Tribo-Pyro	3	interD	Kapton, Al, Cu, PVDF, PTFE	~200 μm	5.12 μW (Piezo-Tribo) 6.05 μW (Pyro)	MEH, TEH

Table 1. *Cont.*

Ref.	Coupled Mechanisms	CN	Hybridization Type	Materials	Thickness /Size	Output Performances	Application Field
Zheng et al. [187]	Piezo-Tribo-Pyro	3	interD	FEP, PVDF, Kapton, Cu	156 μm	350 V; 4.74 mW (Tribo) 20 V; 184.32 μW (Piezo-Pyro)	MEH, TEH
Xu et al. [188]	Piezo-Solar	2	interD	GaN, Si, ZnO	~500 μm	0.424 V; 4.5 μA/cm^2; 1.908 μW/cm^2	MEH, SEH
Xu et al. [189]	Piezo-Solar	2	interD	GaN, Glass, ZnO NWs	~10 μm	0.433 V; 252 μA/cm^2; 34.5 μW/cm^2	MEH, SEH
Yoon et al. [190]	Piezo-Solar	2	interD	PEN, Glass, ZnO, P3HT:PC$_{60}$BM	~50 μm	0.71 V; 10.17 mA/cm^2	MEH, SEH
Liu et al. [191]	Piezo-Solar	2	interD	PEN, Si, ZnO NWs	~126 μm	3V; 280 μA	MEH, SEH
Yang et al. [192]	Piezo-Pyro-Solar	3	interD	PET, PVDF, ZnO-P3HT	~500 nm	~5 V, 50 nA (Piezo-Pyro) 0.41 V, 31 μA/cm^2 (Solar)	MEH, SEH, TEH
Pan et al. [193]	Piezo-Biofuel	2	interD	ZnO, Au, CNT	~10 μm	3.1 V, 300 nA	MEH, BEH
Hansen et al. [194]	Piezo-Biofuel	2	interD	Kapton, PVDF, PBS	530 μm	50–95 mV	MEH, BEH
Wu et al. [195]	Tribo-Solar-Chemical	3	interD	Acrylic, PTFE, Al, Si, NaCl	3 mm	60 V, 500 μA	MEH, SHE, BEH
Li et al. [196]	Tribo-Solar	2	interD	PET, PTFE, Si	~600 μm	30 V, 4.2 mA/cm^2 (tribo) 0.6 V; 350 A/m^2 (solar)	MEH, SEH
Yang et al. [197]	Tribo-Solar	2	interD	PET, Al, PDMS, ITO, Si	>300μm	12 V; 17.4 mA	MEH, SEH
Dudem et al. [198]	Tribo-Solar	2	interD	PET, Glass, PDMS, ZnO NWs, Dye, TiO$_2$	0.6–2 μm	2–10 V	MEH, SEH
Wang et al. [199]	Tribo-Solar	2	interD	Acrylic, FEP, Cu	~12.5 mm	12 mA	MEH, SEH
Wang et al. [200]	Tribo-Thermal-ElectroM	3	interD	Acrylic, PTFE, Polyamide, magnet	~2–3 cm	5 V, 160 mA	MEH, TEH
Kim et al. [201]	Tribo-Thermal	2	interD	Buffer, PTFE, Al	3.4 mm	14.98 mW/cm^2	MEH, TEH
Mariello et al. [74]	Piezo-Optical	2	interD	SiO$_2$ optical fiber, AlN	~220 μm	~35 mV (buckling tests)	IBE

intraD-PS: intra-domain hybridization with physical separation; intraD-PI: intra-domain with physical integration; interD: inter-domain hybridization. Piezo: piezoelectric; Tribo: tribo-electric; ElectroM: electromagnetic. ElectroS: electrostatic, electret. MEH: mechanical energy harvesting; SEH: solar energy harvesting; BEH: biochemical energy harvesting; TEH: thermal energy harvesting; WBS: wearable biosensing; IBE: implantable bioelectronics, IoT: Internet of Things.
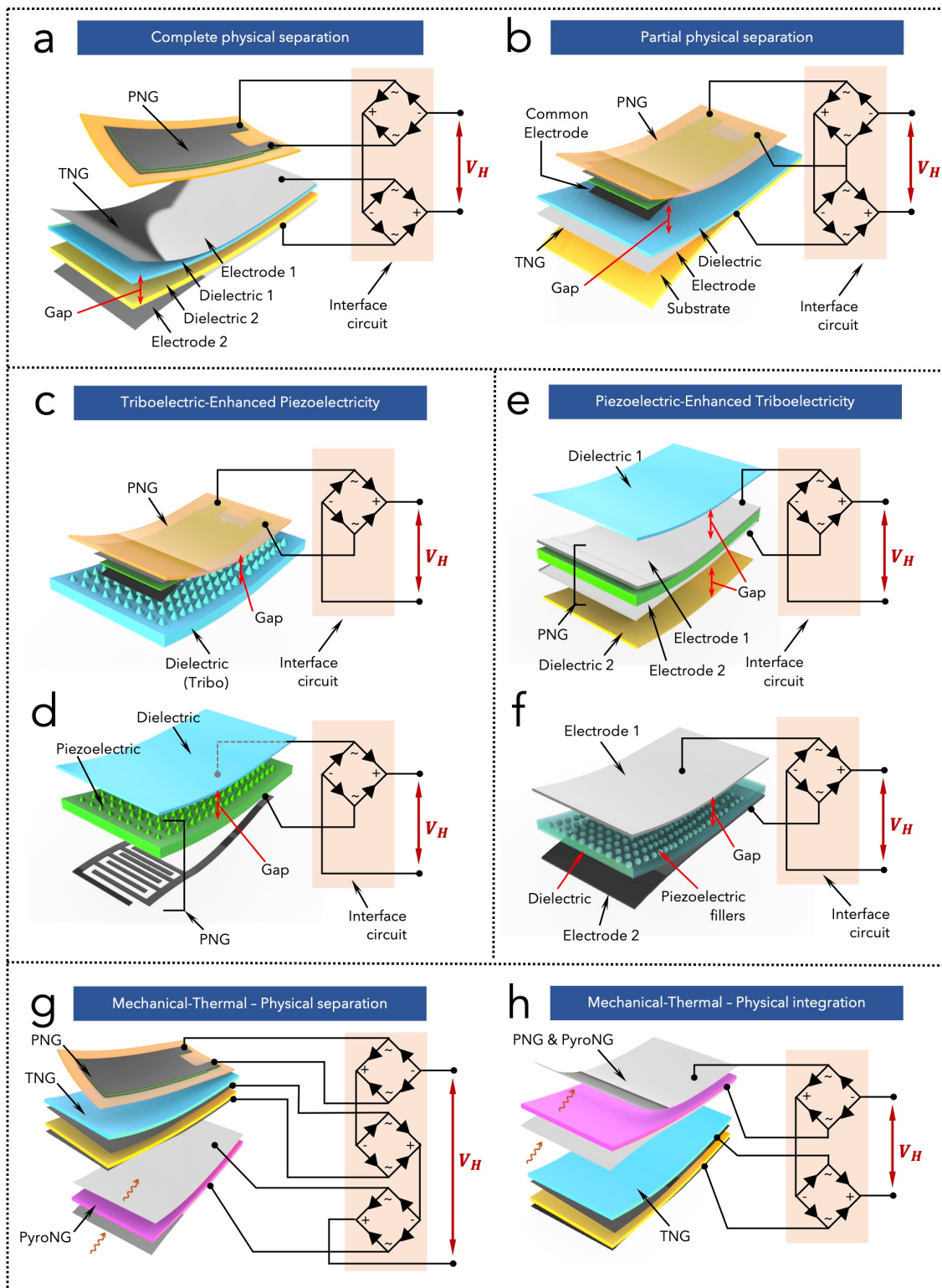
Figure 5. (**a**,**b**) Classification of intra-domain hybridization with complete (**a**) or partial (**b**) physical separation. (**b**–**f**) Classification of intra-domain hybridization with physical integration, as Triboelectric Enhanced Piezoelectricity, TeP (**c**,**d**) and Piezoelectric-Enhanced Triboelectricity, PeT, (**e**,**f**). The classification is based on the surface micro-/nano-patterning of the triboelectric (**c**) or piezoelectric (**d**) layer, on the interposition of piezoelectric between triboelectric layers (**e**), or on the incorporation of piezoelectric fillers into a triboelectric layer. (**g**,**h**) Classification of inter-domain hybridization with (**g**) physical separation or (**h**) physical integration, using as example a piezoelectric-triboelectric-pyroelectric nanogenerator.

3.2. Intra-Domain Hybridization with Physical Integration

In HBNGs based on physical integration, the hybridization occurs before the signal extraction through the electronic interface. This happens when the materials used for the PNG and TNG are not physically separated thus the same deformation or friction induces simultaneously the piezoelectric and triboelectric effects: this can be considered an *"internal hybridization"* (Figure 5c–f). The physical integration can be performed by incorporating piezoelectric nanofillers into polymeric matrices, such as lead-free inorganic compounds ($BaTiO_3$, KNN, etc.), or non-piezoelectric nanofillers into piezoelectric polymers, such as metallic particles, carbon nanofillers or ionic salts. These nanofillers are effective nucleating fillers to induce polar electroactive phases, with no need of electrical poling [202–208]. In addition, they play a role in the triboelectrification because they enhance the stretchability, flexibility, robustness, charge transport and breakdown fields [209]. Common strategies to enhance the performances consist of aligning conductive fillers along the perpendicular direction of the electric field, or of electrically poling the whole matrix to orient properly the nanofillers with the right electroactive phase. Hence, these fillers embedded in a polymer matrix represent a source for the enhancement of the piezo-triboelectric hybridization, which occurs before the actual extraction of electronic signals through the terminals into an external circuit [210,211]. Thus, the physical integration can provide two types of hybridization modes: the piezoelectric-enhanced triboelectricity (PeT, Figure 5c,d) and the triboelectric-enhanced piezoelectricity (TeP, Figure 5e,f). The key point is that the main transducing mechanism is enhanced by the other mechanism owing to the physical integration and without adding more electrodes to the overall system. Figure 5c shows a PeT-HBNG based on a PNG (two-electrodes) faced on a micro-patterned dielectric layer which acts as an additional source of charges through triboelectrification, whenever this layer comes into contact with the PNG. Figure 5d shows that it would be possible to micro-pattern the surface of the piezoelectric material and use it for amplify the piezoelectric charge generation through the contact with another dielectric layer; in this case the PNG includes planar electrodes, e.g., interdigital electrodes. Figure 5e illustrates a PNG interposed between two dielectric layers: in this case the triboelectric charge transfer is enhanced by the piezoelectric charge separation during the contact, but there are still two electrodes for the signal extraction. Figure 5f corresponds to the embedding of piezoelectric fillers into a dielectric layer: the presence of additional piezoelectric materials enhances the triboelectric generation [212].

3.3. Inter-Domain Hybridization

This category of HBNGs includes the combination of piezo-triboelectric devices with systems belonging to a non-mechanical physical domain. This can be a solar/photovoltaic cell (light domain), a biofuel cell (biochemical domain), a thermoelectric/pyroelectric nanogenerator (thermal domain), etc. For instance, Figure 5g,h show the integration of a piezo-triboelectric device with a pyroelectric device to exploit simultaneously the mechanical and thermal domain. The inter-domain hybridization requires the presence of more than one energy source, thus it is suitable or necessary for more complex operating conditions. It can occur at the electronic interface where the signals of the two coupled devices are added through some rectifying circuits (Figure 5g), or in the devices themselves, in case one of the active materials is used for both systems (Figure 5h). In the latter case, a multifunctional material is generally deployed: ferroelectric materials, for instance, can be used to exploit simultaneously the piezoelectric, pyroelectric and photoelectric effects [213]. This internal hybridization reduced the total number of electrodes in the coupled hybrid device and allows to magnify the charge quantity and electric power from various energy resources, making the HBNG useful when they are available either individually or simultaneously [214]. A side type of inter-domain internal hybridization regards the use of one domain as trigger source and the other domain as a detecting source. Piezoelectric photoacoustic probes are an example: the light injected through the optical component induces a photoelastic effect in the targeted tissue, resulting in

thermo-mechanical vibrations that can be detected by a piezoelectric transducer [215–217]. The hybridization occurs when the optical stimulator and the electromechanical transducers are integrated in the same device [74,218].

4. Hybrid Piezo-Triboelectric Bio-Nanogenerators (HBNGs)

4.1. HBNGs for Energy Harvesting

The most investigated application field of HBNGs is energy harvesting, especially from mechanical energy sources [5], such as wind flows, water waves, raindrops, environmental vibrations. In most cases, the HBNG is manufactured into the shape of a flapping-foil device, for instance for wind energy harvesting. As a renewable energy source, wind and water have a strong potential to meet the growing global energy demand: onshore wind is considered the cheapest form of new power generation in Europe, covering 15% of Europe's electricity demand in 2019 [5,219]. 320 GW of wind energy capacity is expected to be installed in the EU by 2030, 254 GW of onshore wind and 66 GW of offshore wind, with a resulting production of 778 TWh of electricity (24.4% of the EU's electricity demand) [219]. Water also represents another promising choice: it is plentiful and widely accessible in different forms, e.g., precipitations, slow flows, buoying waves and ocean currents. The blue energy is that conveyed by water, typically in five forms, i.e., wave energy, current energy, thermal energy, tidal energy and osmotic energy. Wave energy, in particular, represents the most widely exploitable and is estimated to be more than 2 TW globally, around the coast [220,221].

HBNGs represent a complementary solution to the bulky standard technologies for wind/water energy harvesting, based on turbines and power plants [2–4].

Wind energy harvesting through HBNGs is based on flow-induced structural vibrations and deflections of an oscillating element that is generally made of piezoelectric material and during the flapping it touches double frames at each side triggering the triboelectric effect [5]. Since wind is intermittently available due to highly variable weather and working conditions [222–229], the performances of HBNGs are often increased by applying concurrent vibration sources [224,225] or by optimizing the aerodynamic shape to exploit fluid vortexes [225,230–234]. Piezo-triboelectric nanogenerators are most commonly combined in a hybrid unit [150,158–160,235–237] and their charge generation mechanisms do not overlap [162]. In order to exploit efficiently vortex-induced vibrations (VIV), nonlinear restoring forces, e.g., magnetic or external axial loading forces, can be introduced and integrated in the device to widen the range of possible resonant frequencies and thus increase the efficiency [4,238–241]. These restoring forces can be used also to exploit buckling instability of the piezoelectric cantilevers, enhancing the performance level of harvested power [242]. For instance, Yang et al. [240] demonstrated a magnet-induced nonlinearity for a double-beam harvester made of two piezoelectric beams with two magnets attached which allow the reduce the critical wind speed needed to activate the galloping vibrations up to about 42%. Huang et al. [243] presented a hybrid magnetic-assisted noncontact TNG combined with a magnetic responsive composite (PDMS with magnetic Fe-Co-Ni powder): the key mechanism is that the wind forces are converted into the contact-separation action for the triboelectricity, enhanced by the magnetic forces.

Jung et al. [167] presented a HBNG based on PVDF and poly(tetrafluoroethylene) (PTFE) and demonstrated the interaction between piezoelectricity and triboelectricity (Figure 6a(I,II)). At the full-contact state, in fact, the piezoelectric material generates a potential between the electrodes due to the application of an external force and the triboelectric charge transfer is maximum, achieving rectified peak output voltage, current density and power density of 370 V, 12 μAcm^{-2} and 4400 μWcm^{-2}, respectively. Xia et al. [161] demonstrated a HBNG based on a flapping-leaf mechanism using two PVDF leaves-shape cantilevers symmetrically assembled on top and bottom of micro-patterned PDMS films. Driven by the wind flow, the cantilevers undergo bending, generating piezoelectric charges, and become in intermittent contact with the PDMS frame, triggering the triboelectrification. This HBNG can generate, at 4.5 m/s speed, peak voltages and peak powers of 5.36 V, 5.84 V

and 1 μWcm^{-2}, 1.68 μWcm^{-2}) for the piezoelectric and triboelectric parts, respectively. Chen et al. [158] proposed a HBNG based on piezoelectric PVDF nano-/micro-fibers and a triboelectric nano-textured Cu–PCB, which can obtain an output voltage of 15 V and a peak power density of 0.0783 μWcm^{-2}, at 3.4–15 m/s wind speed. Zhao et al. [160] demonstrated a HBNG by integrating a bimorph-based PNG into a one-end fixed TNG: exploiting a rotor-stator mechanism the device can achieve output voltage, output current and power density of 150 V, 150 μA, 6040 μWcm^{-2}, at 14 m/s wind speed (Figure 6b(I,II)). Chen et al. [159] adopted electrospinning to prepare flexible piezoelectric P(VDF-TrFE) nanofiber film and they interposed the PNG between two TNGs based on double-side metallized Kapton film. The device exhibits an enhancement of the performances due to the piezoelectric-triboelectric interaction, of 49.7%, 10% an 4.4% with respect to the PNG, the upper and lower TNG, respectively. Singh and Khare [68] fabricated a hybrid energy harvester with power density of 24.5 $\mu W/cm2$, for mechanical vibrations in which the piezoelectric film (ZnO nanorods-embedded PVDF) is also one triboelectric layer paired with PTFE (Figure 6c(I,II)).

Water energy harvesting can be similarly based on flow-induced oscillations but several other designs and structures can be exploited, as reviewed by Wang et al. [221]: rolling ball structure, multilayer structure, grating structure, pendulum structure, mass-spring structure, spacing structure, water-solid contact structure. Most of these structures harness one or more TNGs, but HBNGs have recently been explored as well. Su et al. [244] presented a hybrid TNG for water wave energy harvesting, composed of an interfacial electrification enabled TNG and an impact-TNG. This is an example of "broad-sense" hybrid device because it is based on two transducers with the same working mechanism (triboelectricity). The first component is made of FEP with electrodes to scavenge electrostatic energy at water-solid interface; the second one is made of nanostructured PTFE to scavenge impact energy of water waves. The device is able to produce, at wave-propagation speed of 0.5 m/s, short-circuit currents of 5.1 μA and 4.3 μA for the first and second components, respectively. Mariello et al. [13] reported on the fabrication of a multifunctional flexible, biocompatible low-thickness (~86 μm) HBNG for water energy harvesting (Figure 6d(I–VIII)). The PNG is based on a 1 μm-thick piezoelectric AlN sandwiched between Molybdenum (Mo) thin electrodes, all sputter-deposited on a flexible substrate. The TNG is instead composed of a Ti/Au metallized porous elastomeric patch. The hybrid device exploits the piezoelectricity and triboelectricity to harvest water-conveyed energy from different mechanical sources, i.e., impacts/breakwaters, raindrops and sea waves, achieving power densities of 0.8 W/m^2, 9 mW/m^2, 3.2 mW/m^2, respectively.

TNGs are often integrated with electromagnetic generators (EMGs) to increase the current generation, thus many examples of hybrid TNG-EMG devices have been proposed for wind or water energy harvesting [245–251]. Wang et al. [172] proposed a electromagnetic−triboelectric nanogenerator to scavenge airflow kinetic energy, based on two TNGs and two EMGs, able to generate 1.8 mW and 3.5 mW at 18 m/s wind speed, respectively. Wang et al. [174] demonstrated another similar hybrid system with a rotary-blade TNG and a rotary EMG, for harvesting rotation energy: under a wind speed of 5.7 m/s, the device can generate 438.9 mW/kg and 181 mW/kg for the TNG and EMG, respectively. Three-mechanism HBNGs have been also proposed, based on the hybridization between piezoelectricity, triboelectricity and another transducing mechanism. In the context of mechanical energy, the EMG is often used as a third component, exhibiting important advantages, i.e., superior output performances in terms of power density and current. He et al. [183] described, for instance, a PNG-TNG-EMG device with four PVDF L-shaped vibrating beams with NdFeB permanent magnets and four beams with patterned PDMS and PET. The PNG, TNG and EMG units can generate 12.6 V (41.0 μW), 13.3 V (4.6 μW) and 362.1 mV (66.5 μW) at ~20 Hz and an acceleration of 0.5 g.
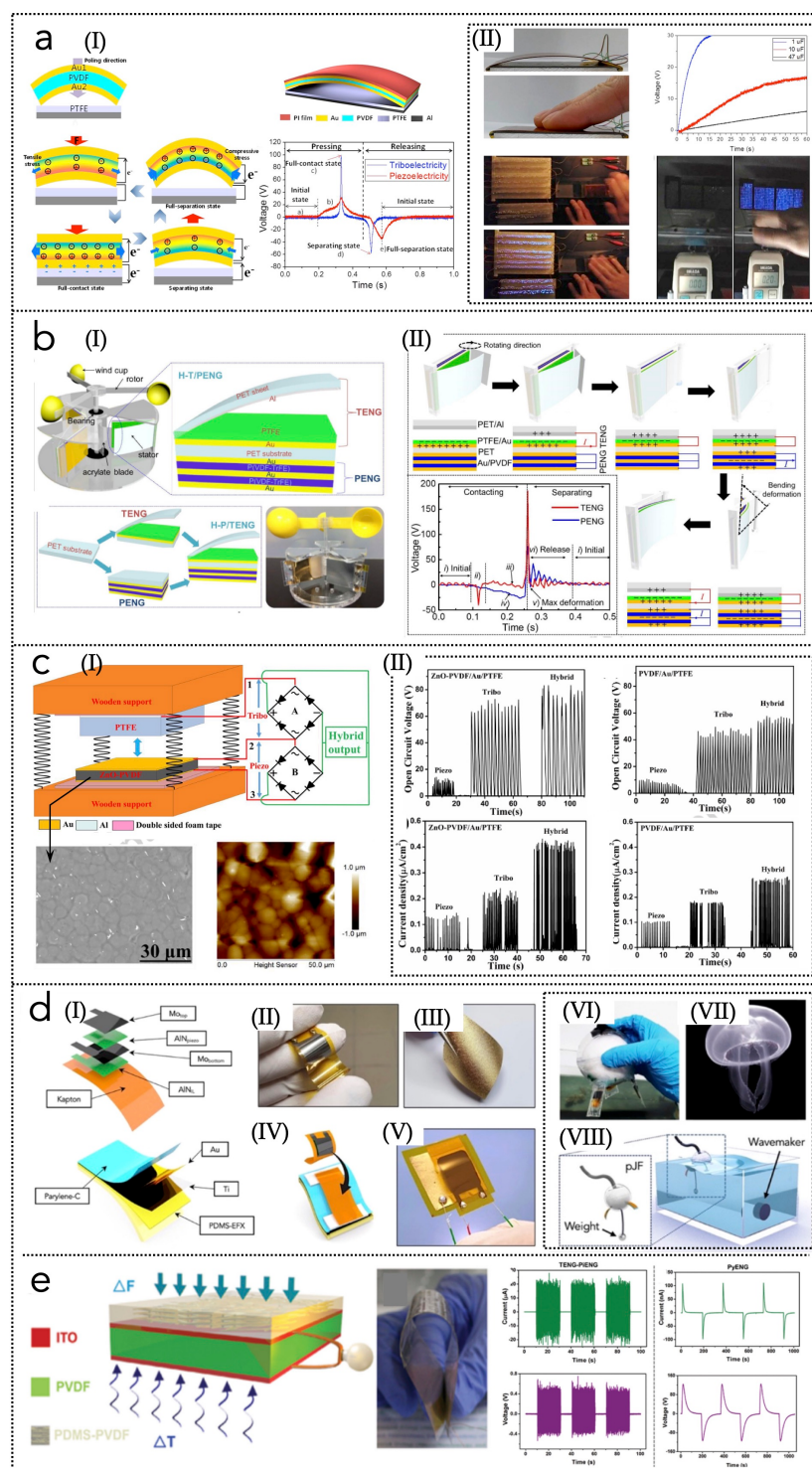
Figure 6. HBNGs for energy harvesting. (**a**(**I,II**)) High-output HBNG based on PVDF and PTFE. Reprinted with permission from ref. [167], 2015, Copyright Springer Nature. (**b**(**I,II**)) HBNG for efficient and stable rotation energy harvesting. Reprinted with permission from ref. [160], 2018, Copyright Elsevier. (**c**(**I,II**)) Flexible ZnO-PVDF/PTFE HBNG for energy harvesting. The incorporation of ZnO enhances the piezoelectric and triboelectric properties of PVDF. Reprinted with permission from ref. [68], 2018, Copyright Elsevier. (**d**(**I–V**)) HBNG based on AlN and PDMS-parylene for water wave energy harvesting. The system piezoJellyFish (pJF) is designed to have three devices connected simultaneously for scavenging energy from buoying waves (**VI–VIII**). Reprinted with permission from ref. [13], 2021, Copyright Elsevier. (**e**) Piezoelectric-Triboelectric-Pyroelectric HBNG for harvesting mechanical and thermal energy. Reprinted with permission from ref. [187], 2016, Copyright Wiley-VCH Verlag GmbH and Co. KGaA.

The inter-domain hybridization has been often used for combining mechanical and thermal energy, exploiting the piezo-triboelectric and the pyroelectric effects [213]. Wang et al. [186] characterized a TNG-PNG-PyroNG device based on PVDF nanowires-PDMS composite film as a triboelectric layer and a polarized PVDF film, sandwiched between ITO electrodes, as piezoelectric/pyroelectric layer. The device can produce 5.12 µW and 6.05 µW with the PNG-TNG and PyroNG mechanisms, respectively, and it is suitable for harvesting energy from wind and temperature variations simultaneously. Zheng et al. [187] presented a wind-driven TNG-PNG-PyroNG system based on fluorinated ethylene propylene (FEP) and PVDF films as triboelectric and piezoelectric layers, on a Kapton substrate (Figure 6e). The outputs of this device are 184.32 µW and 4.74 mW at 18 m/s wind speed, for the PNG-PyroNG and the TNG, respectively.

Hence, HBNGs have been demonstrated as suitable tools to harvest mechanical (kinetic) energy (rotational or oscillatory) from different sources, e.g., wind and water waves. The contribution of the HBNGs to the energy harvesting field must be ascribed to two aspects. First, the use of them as renewable energy sources employed in complementary way with the large energy platforms (power plants, wind turbines, hydraulic turbines, hydrovoltaic systems, etc.), in order to mitigate the energy crisis. Second, the deployment of these devices for supplying energy to small self-powered IoT sensors used for healthcare, sport, medicine, automotive, robotics, etc. The use of energy harvesting HBNG devices as wearable or implantable systems is discussed in the next sections.

4.2. HBNGs for Wearable Bioelectronics

Wearable bioelectronics (WBE) includes all the systems that can be applied on the human body and that can be employed for applications in health monitoring, robotics, sports, rehabilitation. The main requirements for WBE are flexibility, conformality, shape-adaptability, lightweight and high sensitivity. PNGs and TNGs have been widely used as wearable sensors [27,125,252–256] and their integration in a single hybrid device allows to increase the measurement range and the sensitivity. The hybridization can occur by coupling separately the two devices, or by using the same flexible ferroelectric material as piezoelectric and triboelectric layer (e.g., PVDF or inorganic perovskites such as BeFiO$_3$ [85]). PNGs and TNGs can thus be coupled and applied to monitor cardiovascular, respiratory or neurological disorders [257].

Yu et al. [153] reported on a tactile PeT-HBNG based on a PZT-PDMS composite film (Figure 7a), demonstrating enhancements in terms of sensitivity, good skin-conformality, good linearity, fast response and high stability. To avoid the use of PZT, a similar PeT-HBNG was presented by Guo et al. [163]: the device is based on electrospun silk fibroin and PVDF nanofibers, exhibiting high energy harvesting capability, good air permeability, possibility of identifying various types of body motion. Figure 7b(I,II) shows the structure and materials of the HBNG, its working principle and the simulated/experimental piezo-triboelectric interaction effects in accordant and opposite state (depending on the piezoelectric polarization). Wang et al. [150] proposed a flexible wearable HBNG made of P(VDF-TrFE) electrospun nanofibers and multiwall carbon nanotubes (MWCNT)-doped PDMS composite membrane (Figure 7c). The device exhibits, as a power source, a peak-to-peak voltage and power density, respectively, of 25 V, 1.98 mW/cm^3 for PNG, and 2.5 V, 0.689 mW/cm^3 for TNG. Electrospinning is a useful technology to produce films of piezoelectric materials without the need of electrical poling, even though the process parameters are characterized by a wide variability.

Tang et al. [258] described a self-powered HBNG used for the simultaneous detection of multi-parameter sensory information of finger mechanical operations, for applications in human-machine interfaces. The TNG is made of a PTFE friction layer, two PET films, a nylon grid, whereas the PNG is composed of an Al-sandwiched PVDF. Chen et al. [166] reported on a conformable HBNG for harvesting touch energies and real-time monitoring human physiological signals. The PNG is made of a P(VDF-TrFE) nanofiber mat sandwiched between two electrospun PU films coated with CNTs and AgNWs; the TNG is

a single-electrode device based on micro-patterned PDMS. Suo et al. [162] developed a HBNG based on BaTiO$_3$ NPs/PDMS composite film, demonstrating the mutual enhancing effect of piezoelectricity and triboelectricity in a single material component (hybridization with physical integration). Mariello et al. [76] proposed a flexible, ultra-thin biocompatible HBNG as wearable conformal sensor on the human body. The PNG is based on thin-film AlN sputter deposited on a polyimide and sandwiched between thin-film Mo electrodes, and the TNG is made of an ultra-soft PDMS-Ecoflex patch encapsulated in a parylene C friction film, surface-treated with UV/ozone and oxygen plasma. The HBNG is an inorganic/elastomeric 3-electrode device for multi-site and multifunctional conformal sensing: it works as a skin-adaptable sensor for gait walking, gestures recognition and monitoring of joints movements, yielding repeatable and real-time rectified signals. The architecture of the device is based on a bridge configuration, i.e., only the ends of the device are attached on the skin, so that an additional triboelectric mechanism is exploited between the skin and the bottom triboelectric layer (skin-contact actuation), besides the piezo-tribo hybrid contact (Figure 7d(I,II)). This allows to widen the measurement range for tiny and irregular human motions, combining together the impulsiveness of piezoelectricity and the slowness and sensitivity of friction-based triboelectricity.

Definitely, the main practical issues related to wearable HBNGs are: high thicknesses, poor layer adhesion and delamination, non-optimal deformability and conformability, complex design, unproper choice of materials [76].
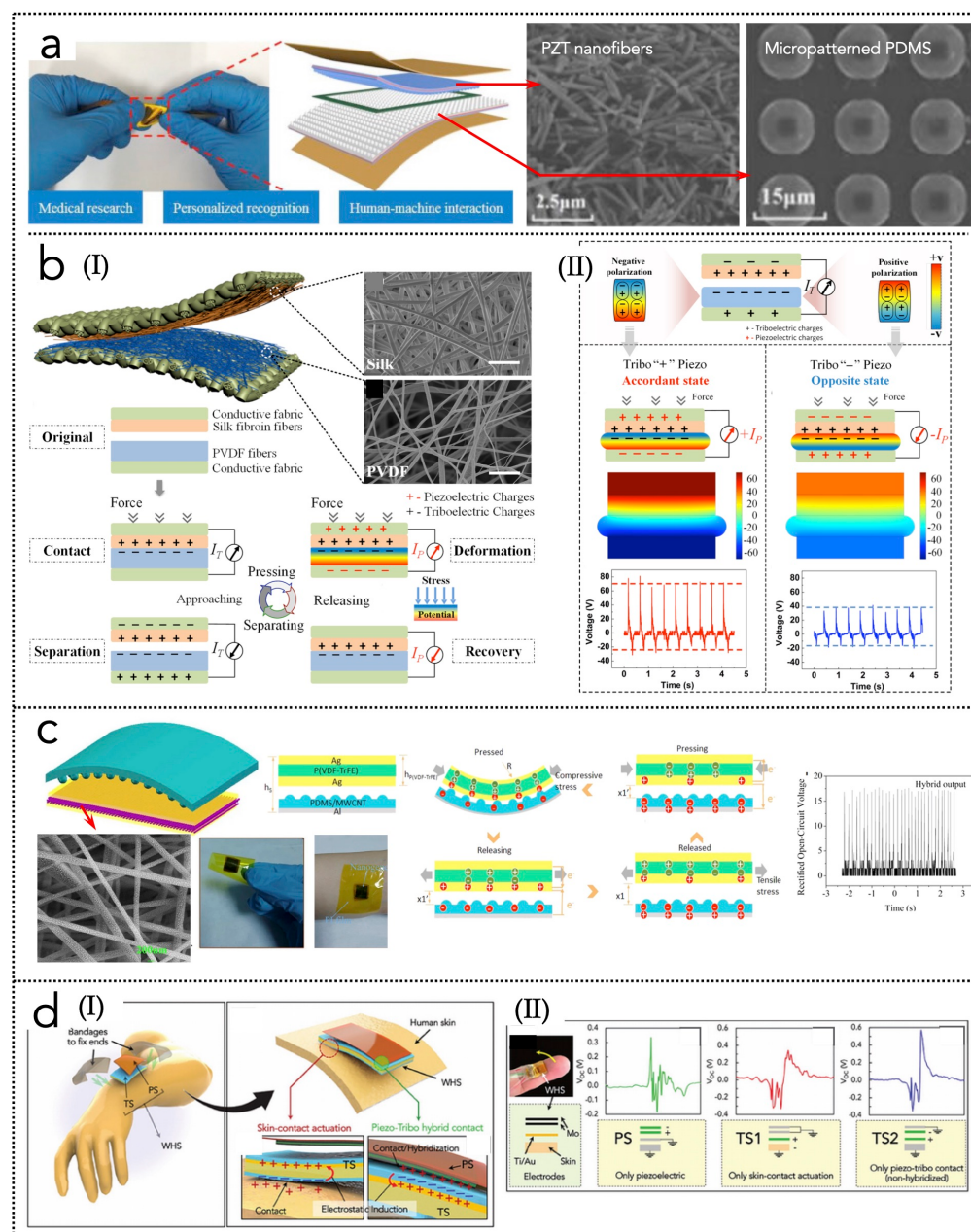
4.3. HBNGs for Implantable Bioelectronics

Implantable systems need more stringent requirements in terms of materials, design, mechanical response and reliability, since they have to be employed inside the human body or of the selected animal models, and they must be in direct contact with tissues, organic and biofluids. This implies the need of flexibility, stretchability, conformality and durability. These devices often require barrier encapsulations to avoid water permeation inside the electronic components, and the barriers are usually made of ultrathin coatings deposited from the vapor phase (e.g., SiO$_2$ [259,260], SiN$_x$ [261], Al$_2$O$_3$ [262], TiSi$_2$ [263], SnO$_2$ [264], etc.).

HBNGs are still not massively adopted for implantable applications but the use of PNGs and TNGs as implants has been recently explored [265–269]. However, the friction effects with the surrounding tissues are always present due to the sliding movements of the devices, thus the resulting signal produced by the system can be a combination with triboelectric signals, therefore an internal hybridization is possible to occur. Dagdeviren et al. [270] reported on biocompatible, flexible PZT-based energy harvesters monolithically integrated with rectifiers and millimeter-scale batteries for simultaneous power generation and storage, including high-power, multilayer designs. The devices are evaluated in live animal models, on various locations/orientations on different internal organs (heart, lung, diaphragm), as well as inside the body of a bovine model through thoracotomy experiments. Output voltages of ~4 V, ~4 V, and ~2 V, respectively, can be generated from contraction and relaxation of the right ventriculus, lung, and diaphragm, whereas a stack of five devices can harvest 1.2 μW/cm^2 power density. The same authors [271] presented ultrathin, stretchable networks of mechanical actuators (seven) and sensors (six) constructed with PZT nanoribbons, that allows for in vivo measurements of viscoelasticity in the near-surface regions of the epidermis as well as on ex vivo freshly explanted, unpreserved bovine organs (heart and lung). Zhang et al. [272] fabricated a PNG based on 200 μm-thick Al/PVDF wrapped around the ascending aorta of a pig, for harvesting energy from the variations in diameter of the carotid artery between the systolic and diastolic states (Figure 8a(I,II)). The resulting peak output voltage is 1.5 V at a heart rate and blood pressure of 120 bpm and 160/105 mmHg, respectively.

Yang et al. [273] demonstrated a single-wire PNG consisting of a ZnO nanowire affixed laterally at its two ends on a flexible substrate, for scavenging biomechanical energy (e.g., the movement of a human finger and the body motion of a live hamster) into electrical

power (Figure 8b(I,II)). Four series-connected devices located on the back of a running hamster yield an output voltage of ~0.1–0.15 V. With the same principle, Li et al. [274] investigated the use of a single-wire PNG for energy harvesting under in vivo conditions, in a live rate, generating ~1 mV and 3 V output voltages from breathing (diaphragm) and heart beating, respectively (Figure 8c). Hwang et al. [275] presented a thin-film PMN-PT PNG to harvest energy from the motion of a rat's heart (with an output voltage of 8.2 V at a 0.36% strain and 2.3%/s strain rate) and also to act as an artificial heart stimulator.

Figure 7. HBNGs for wearable bioelectronics. (**a**) Tactile PeT-HBNG based on a PZT-PDMS composite film. Reprinted with permission from ref. [153], 2019, Copyright Elsevier. (**b(I,II)**) PeT-HBNG based on electrospun silk fibroin and PVDF nanofibers. Reprinted with permission from ref. [163], 2018, Copyright, Elsevier. (**c**) Flexible wearable HBNG made of P(VDF-TrFE) electrospun nanofibers and multiwall carbon nanotubes (MWCNT)-doped PDMS composite membrane. Reprinted with permission from ref. [150], 2016, Copyright, Springer Nature. (**d(I,II)**) Inorganic/elastomeric 3-electrode skin-contact-actuation HBNG for multi-site and multifunctional conformal sensing. Reprinted from ref. [76], 2021, Copyright Wiley-VCH GmbH, Creative Commons CC-BY.
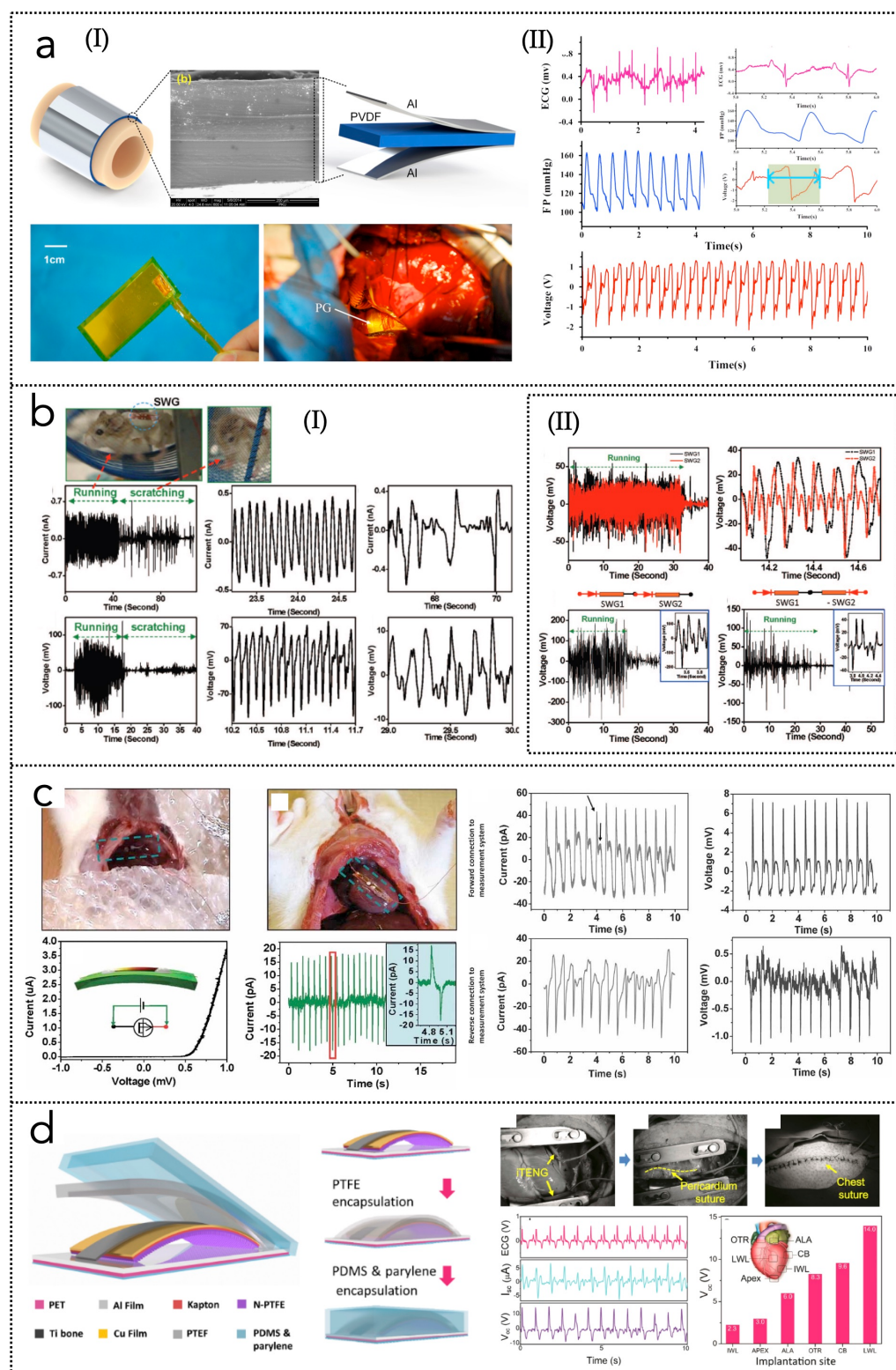
Figure 8. HBNGs for implantable bioelectronics. (**a**(**I,II**)) PNG based on 200 μm-thick Al/PVDF wrapped around the ascending aorta of a pig. Reprinted with permission from ref. [272], 2015, Copyright Elsevier. (**b**(**I,II**)) Single-wire PNG for scavenging biomechanical energy from a live hamster. Reprinted with permission from ref. [273], 2009, Copyright American Chemical Society. (**c**) Single-wire PNG for energy harvesting from breathing and heartbeat in a live rate. Reprinted with permission from ref. [274], 2010, Copyright Wiley-VCH Verlag GmbH and Co. KGaA. (**d**) Implantable TNG for in vivo biomechanical energy harvesting from the heartbeat of adult swine. Reprinted with permission from ref. [22], 2016, Copyright American Chemical Society.

Many examples of implantable TNGs can be found in literature [276–279]. Ryu et al. [280] reported on a commercial coin battery-sized high-performance inertia-driven TNG based on body motion and gravity, able to produce 4.9 µW/cm^3. The TNG has been also integrated with a cardiac pacemaker, demonstrating the successful operation mode of a self-rechargeable pacemaker system. Zheng et al. [22,281] proposed an innovative implantable TNG for in vivo biomechanical energy harvesting from the heartbeat of adult swine (Figure 8d). The structure is designed properly to achieve a leak-proof performance in vivo and it is composed of a multilayered core/shell/shell structure ("keel structure"), with nanostructured PTFE as triboelectric layer on Au-metallized Kapton as flexible substrate. A highly resilient titanium strip is introduced as the keel structure to strengthen the overall mechanical property and guarantee the contact-separation in vivo. The device can also be integrated in a self-powered wireless transmission system for real-time wireless cardiac monitoring.

The existing approaches that have been demonstrated for energy harvesting from the bodies of living subjects (animals and humans) for self-powered electronics are summarized in a review by Dagdeviren et al. [282] who described the material choices, device layouts and working principles (especially biofuel cells, thermoelectricity, triboelectricity and piezoelectricity) with a specific focus on in vivo applications, with future perspectives in disease diagnostics, treatment and prevention. Zheng et al. [209] and Zhang et al. [209] also reviewed the recent progresses of piezo-triboelectric flexible sensors and energy harvesters, providing examples of in vivo energy harvesting and direct stimulation of living cells, tissues and organs.

Energy harvesting, wearable and implantable bioelectronics represent the main application fields of HBNGs and while the first one has been widely explored, the others are promising in terms of scientific and commercial perspectives. Additionally, cutting-edge applications such as HBNGs for tissue engineering and nanomedicine may require in the future new research efforts.

5. Electronic Interfaces and Power Management Circuits for HBNGs

Interface electronics allows to transfer the output electrical signal generated by a transducer to a supplier or an energy storage downstream of the device. Generally speaking, integrated circuits (ICs) and discrete components are often used, and the demand of higher performances in terms of speed, low power, reduced parasitic capacitances, low noise-to-signal ratio and low cost is progressively increasing [283]. The recent needs of high multi-functionality, adaptability and diversification of transducers, especially with the introduction of hybridized systems, require in many cases the combination of interface electronics with high-performance packaging or their monolithic integration in the same system. In this context, the approaches of system-on-chip (SoC) and System-in-package (SiP) [284] with on-board systems for signal-processing and wireless communication [283,285] represent the most adopted methods for the fabrication of novel micro-systems, but are challenging when dealing with flexible and soft materials and devices. In fact, stretchable and conformal substrates and patches for flexible electronics require a multidisciplinary approach for the connection and integration with interface electronics, i.e., including fields of electrical circuits, material science, nanotechnology and packaging. This is further a more complex issue when the systems must be employed in contact with the human body or for the fabrication of implantable biomedical devices (IBDs): in this case requirements of conformability, biocompatibility and even biodegradability are essential, as well as durability of materials and reliability of electrical connections [286,287]. Moreover, the implementation of interface electronics strongly depends on the type of transducer and the ensemble of characteristics of the final micro-system, in terms of response, accuracy, cost and power consumption, is unavoidably determined by both the device and the connected electronics [283,284]. For instance, mechanical transducers, especially used for energy harvesting, require different types of power management circuits depending on the applied mechanical loads, exciting frequency and working mechanism: low-frequency mechanical

source, such as water waves or weak breezes, require very low-threshold rectifying circuits or high-yield amplification [13,14,212].

In addition, PNGs and TNGs made of soft and flexible materials present different characteristics in terms of internal impedance, output power generation capability, frequency range of utilization and working principles, therefore they need specific circuits to convey the harvested power or sensory signals [100,115]. Since their outputs are usually composed of noncontinuous pulses with irregular magnitude, they cannot directly drive electronic devices that need a constant DC voltage, so to act as a battery, the PNG/TNG needs a self-charging power unit (SCPU) with at least an energy storage device. Therefore, the circuit attached to a nanogenerator is more complicated than a resistor for current regulation and power management, thus the challenge remains to establish a more general modelling approach to account for both complex operating conditions and practical energy harvesting circuit. This is further complicated when the two components are coupled to make HBNGs because signal rectification is necessary when they are out-of-phase. Additionally, their employment in harsh environments such as water, the human body, strong airflows or heavy gases, is a further issue to be addressed for the design and package of circuitry.

5.1. Circuits for Piezoelectricity

The simplest method to extract signal from a PNG is to connect it to a load resistance and detect the corresponding voltage. However, especially in the field of energy harvesting, this is not enough to power portable electronic devices and the AC signal must be converted into a DC signal. The most common approach is the rectification which can be implemented according to different models. The first is the Direct Energy Transfer (DET) approach which relies on a direct connection of the PNG with a bridge rectifier, a DC-DC converter and a storage capacitor (Figure 9a). The main issue of this approach is the risk that the energy stored in the capacitor flows back to the PNG when its instantaneous power is negative (energy return phenomenon [288]). Additionally, there is a problem of impedance matching with the internal resistance and capacitance of the PNG. A traditional interface used to match the PNG output impedance is described by Li et al. [289] and it is based on two coils with the same resonance frequency (i.e., a transformer, Figure 9b) which, however, needs a high value of inductance to have a proper impedance matching. A development of this interface consists of using a frequency up-conversion technique to shift the working operational frequency to higher values [290] (Figure 9c).

The second approach is based on resonant rectifiers (RR), i.e., the PNG is intermittently connected to the resonant electronic interface for very short time intervals and switched magnetic components (inductors or transformers, directly connected to the PNG or after a rectification stage) are responsible of the resonant effect (Figure 9d). This way, the impedance matching can be obtained whenever the RR is connected to the PNG, behaving similar to an LC oscillator, with a resulting enhancement of the maximum generated voltage with respect to an open-circuit condition [291,292]. Several RR have been introduced in previous works and they are comprehensively reviewed by Dicken et al. [293] and Dell'Anna et al. [294]: (1) series-synchronized switch harvesting on inductor (S-SSHI) [295] (Figure 9e); (2) parallel-synchronized switch harvesting on inductor (P-SSHI) [296] (Figure 9f); (3) synchronized switching and discharging to a storage capacitor through an inductor (SSDCI) [297] (Figure 9g); (4) synchronous electric charge extraction (SECE) [298] (Figure 9h); (5) phase shift synchronous electric charge extraction (PS-SECE) [299]; (6) synchronized switch harvesting on inductor magnetic rectifier (MR-SSHI) [300] (Figure 9i); (7) Hybrid MR/P-SSHI (Figure 9l); (8) Double synchronized switch harvesting (DSSH) [301] (Figure 9m); (9) enhanced synchronized switch harvesting (ESSH) [302]; (10) adaptive synchronized switch harvesting (ASSH) [302]; (11) energy injection technique [303] (Figure 9n). All the SSHI approaches depend strongly on the load, thus an additional DC-DC converter is usually required in practical implementations. The other methods (SECE, DSSH, ESSH) are more independent on the connected load, but they are affected by a linear decrease of the rectified voltage. The SSDCI approach allows a constant

power extraction at certain loads and the EI technique provides higher output power peak performances. Another rectification approach relies on employing Maximum Power Point Tracking (MPPT) algorithms to control the impedance seen by the PNG, coupled with full-bridge (FB), half-bridge (HB) rectifiers or voltage/charge doublers (VD, CD) [304].
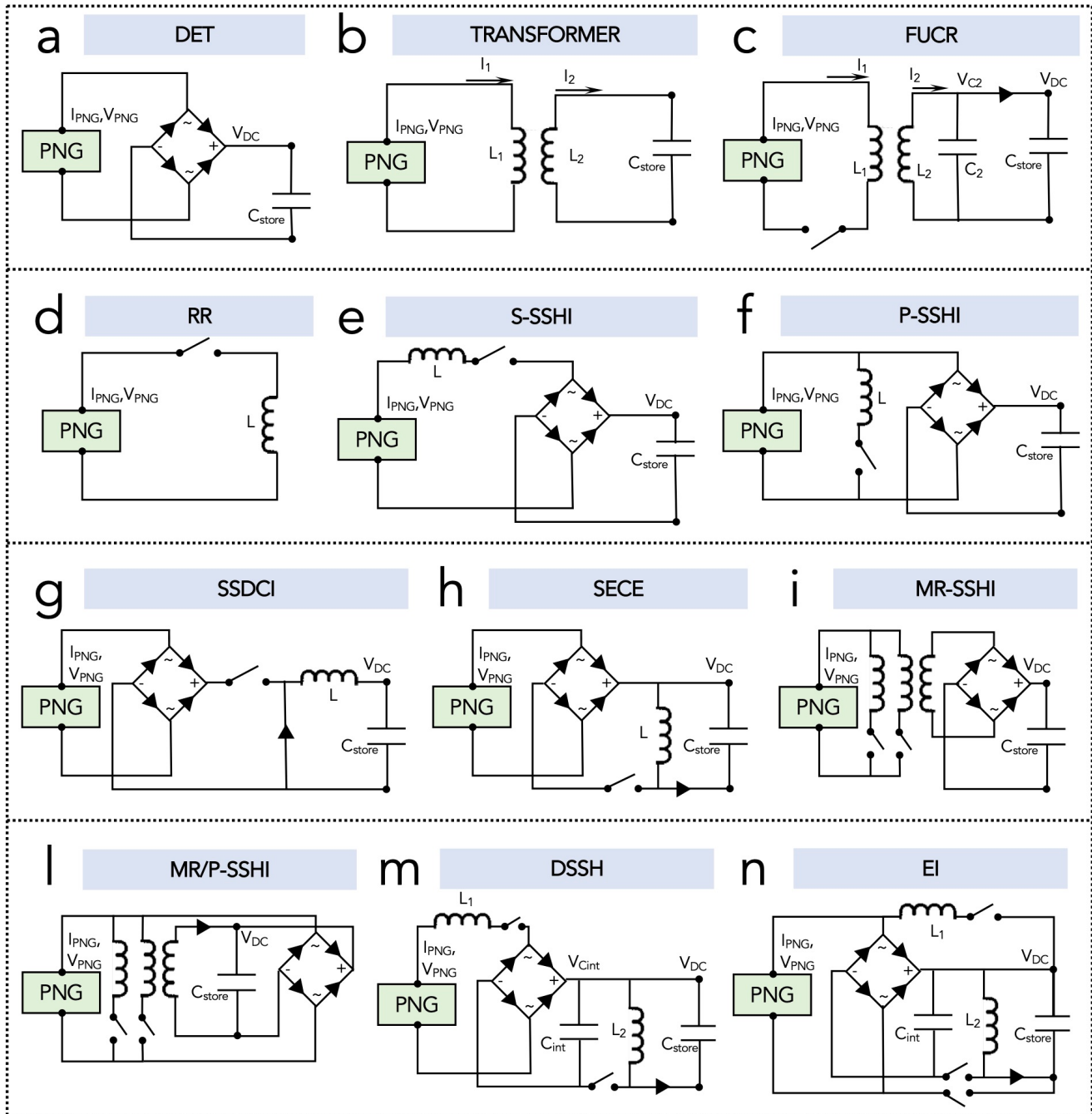
Figure 9. Electronic interfaces and power management circuits for PNGs. (**a**) Direct energy transfer (DET) approach. (**b**) Transformer-based approach. (**c**) Frequency up-conversion rectifier (FUCR). (**d**) Resonant rectifier (RR). (**e**) Series-Synchronized Switch Harvesting on Inductor (S-SSHI). (**f**) Parallel-Synchronized Switch Harvesting on Inductor (P-SSHI). (**g**) Synchronized Switching and Discharging to a storage Capacitor through an Inductor (SSDCI). (**h**) Synchronous Electric Charge Extraction (SECE). (**i**) Synchronized Switch Harvesting on Inductor Magnetic Rectifier (MR-SSHI). (**l**) Hybrid SSHI, made of MR-SSHI and P-SSHI. (**m**) Double Synchronized Switch Harvesting (DSSH). (**n**) Energy Injection (EI) technique.

5.2. Circuits for Triboelectricity

There are several issues related to the power management of TNGs. The first is that their high internal impedance (>10 MΩ) does not match with that of most standard electronic interfaces, thus the power transfer and the energy storage occurs with low efficiency [221,305]. The power management circuit plays a crucial role in the TNG-based energy harvesting, for efficiently storing the AC energy and overcome the huge impedance mismatch. The second issue is about the outputs of the TNG, i.e., high voltage and low current: this limits the practical applications of TNGs unless another system is used for the conversion to high currents. This could in principles be performed by a transformer but this has a high working frequency and a low-input-load resistance, which are the opposite of the TNG characteristics (low frequency and high-input-load resistance). The third issue regards the need of maximizing the extracted energy per cycle: generally, a switch approach between open-circuit and short-circuit conditions is needed [115,116,306]. The fourth aspect is the networking of several TNGs for distributed arrays of devices.

In order to reduce the TNG efficiency loss due to the impedance unmatching, Hu et al. [307] proposed an adaptable interface conditioning circuit, composed of an impedance matching circuit, a synchronous rectifier bridge, a control circuit and an energy storage device (Figure 10a). In particular, a novel bi-directional switch control mechanism is adopted to increase the frequency and reduce the energy loss of coupling impedance. Effectively, a TNG exhibits an increase of efficiency by 50% with the proposed interface.

The switch approach is usually adopted to maximize the extracted energy from the TNG. The common technique is to combine an electric switch and an inductance transducer and efficiencies up to 80% were reached in previous works [308,309], although plenty of energy is absorbed by the electric switch. Bao et al. [310] presented a new power management circuit for TNGs, that includes a rectification storage circuit and a DC-DC management circuit (Figure 10b). The first part (with a diode rectifier bridge and an optimal intermediate capacitor) serves to maximize the energy storage efficiency. The second circuit includes an automatic switch (transistor controlled by a low-power logic control circuit), an inductor and a diode in a buck-boost static converter; it works to obtain impedance match with the storage device or load. A rotating TNG equipped with the proposed circuit exhibits a storage efficiency of 50%.

Wang et al. [305] designed an SCPU for an arch-shaped TNG by integrating it with a flexible Li-ion battery (Figure 10c). It was employed to power a ZnO-nanowire-based UV sensor: the hybridization of the mechanical energy harvesting and energy storage in the SPCU allows the sensor to be self-powered continuously and sustainably, without any drop in the output current and voltage. Xi et al. [311,312] designed and patented a universal, efficient and autonomous power management module (PMM) made of a tribotronic energy extractor and a DC-DC buck converter (Figure 10d). The first serves to transfer energy efficiently from the TNG, and the second generates the DC output on the load. With the implemented PMM, about 85% energy can be autonomously extracted from the TNG as DC output voltage, and the matched impedance is reduced from 35 MΩ to 1 MΩ at 80% efficiency. Liang et al. [313] employed the PMM with a hexagonal TNG network consisting of spherical TNG units with spring-assisted multi-layered structure for water wave energy harvesting (Figure 10e): the units connected in series can produce a steady and continuous DC voltage on the load resistance and the PMM helps improving the energy storing by a factor 96.
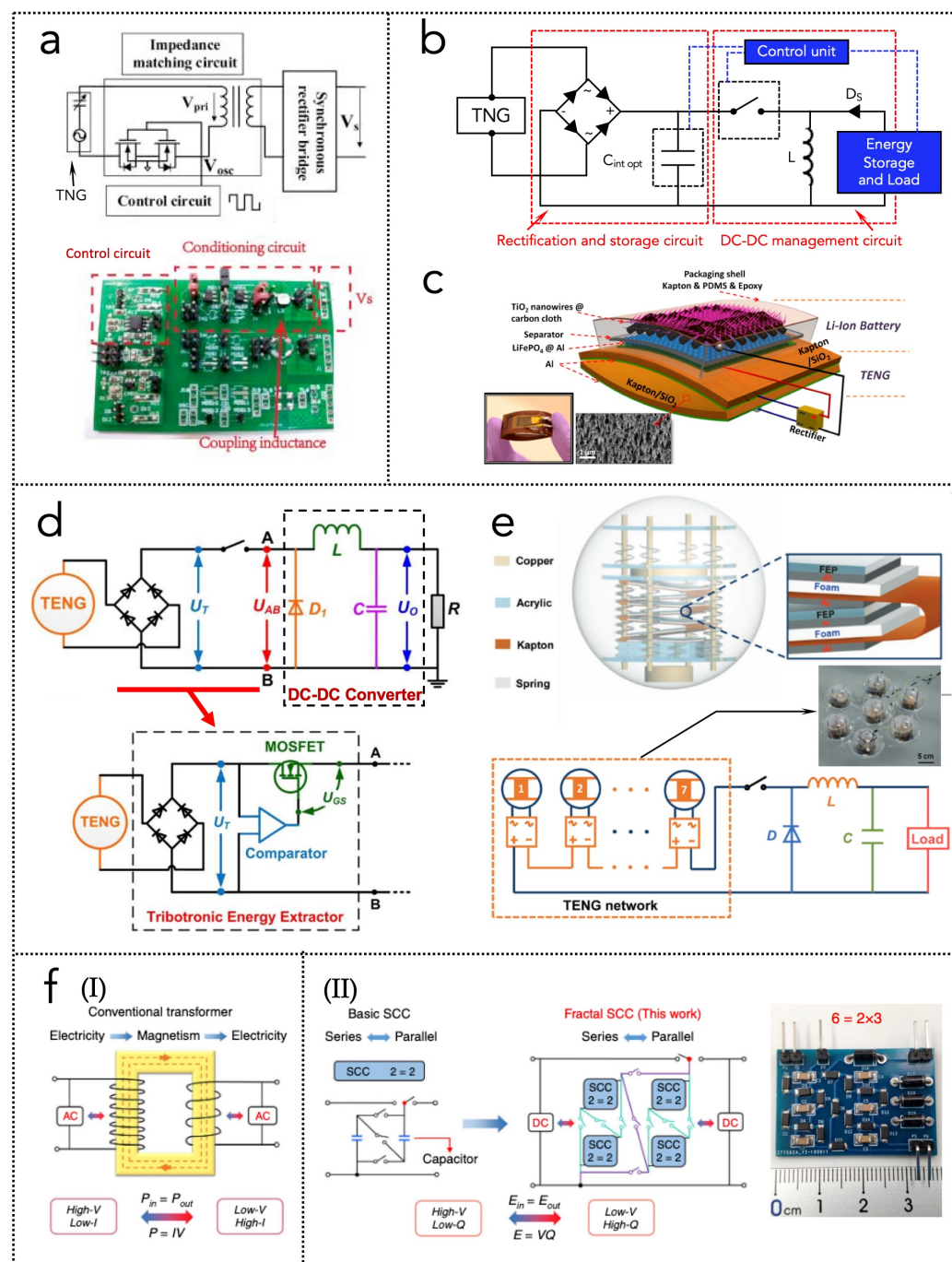
Figure 10. Electronic interfaces and power management circuits for TNGs. (**a**) Diagram and real photo of a power management circuit based on an impedance matching circuit and a synchronous rectifier bridge. Reprinted from ref. [307]. (**b**) Diagram of a power management circuit made of a rectification circuit and a DC-DC management circuit with an automatic switch. (**c**) Self-charging power unit (SCPU) of a TNG integrated with a Li-ion battery. Reprinted with permission from ref. [305], 2013, Copyright America Chemical Society. (**d**) Circuit diagram of PMM made of tribotronic energy extractor and DC-DC buck converter. Reprinted with permission from refs. [311,312], Copyright 2017, Elsevier. (**e**) PMM implemented with a hexagonal network of TNGs. Reprinted with permission from ref. [313], 2019, Copyright, WILEY-VCH Verlag GmbH and Co. KGaA. (**f**(**I,II**)) Fractal-design-based switched-capacitor-convertor compared to a conventional transformer. Reprinted with permission from ref. [314], 2020 Copyright Springer Nature, Creative Commons CC BY.

To avoid the energy loss due to the electric switches, another strategy has been proposed, based on an inductor-free mechanical switch between serial and parallel connections of capacitors [315,316]. Liu et al. [314] report on a fractal-design-based switched-capacitor-convertor with high conversion efficiency, minimum output impedance and electrostatic voltage applicability (Figure 10f(I,II)). The convertor is magnet-free, light-weight, easily integrated on printed circuit boards and if coupled to a TNG, it can enhance the charge transfer with a 67-fold factor, reaching a power density of 954 Wm^{-2} in pulse mode at 1 Hz, with a >94% total energy transfer efficiency. Xu et al. [188] proposed a multilayered-electrode-based TNG with the aim of lowering the output voltage and preserving the total power (to overcome the problem of high-voltage/low-current). With this design, the current flow is controlled by a mechanical switch, yielding an increasing total charge transport. The concept of multilayer design is also adopted by Xu et al. [317] who fabricated the switches by attaching Al foils on the air chambers of a TNG: the switches close when the corresponding foils acquire contact and current flow by the drive of the established voltage due to charge separation. The switch circuit reduces the duration of the charge transfer thus enhancing the output current and power.
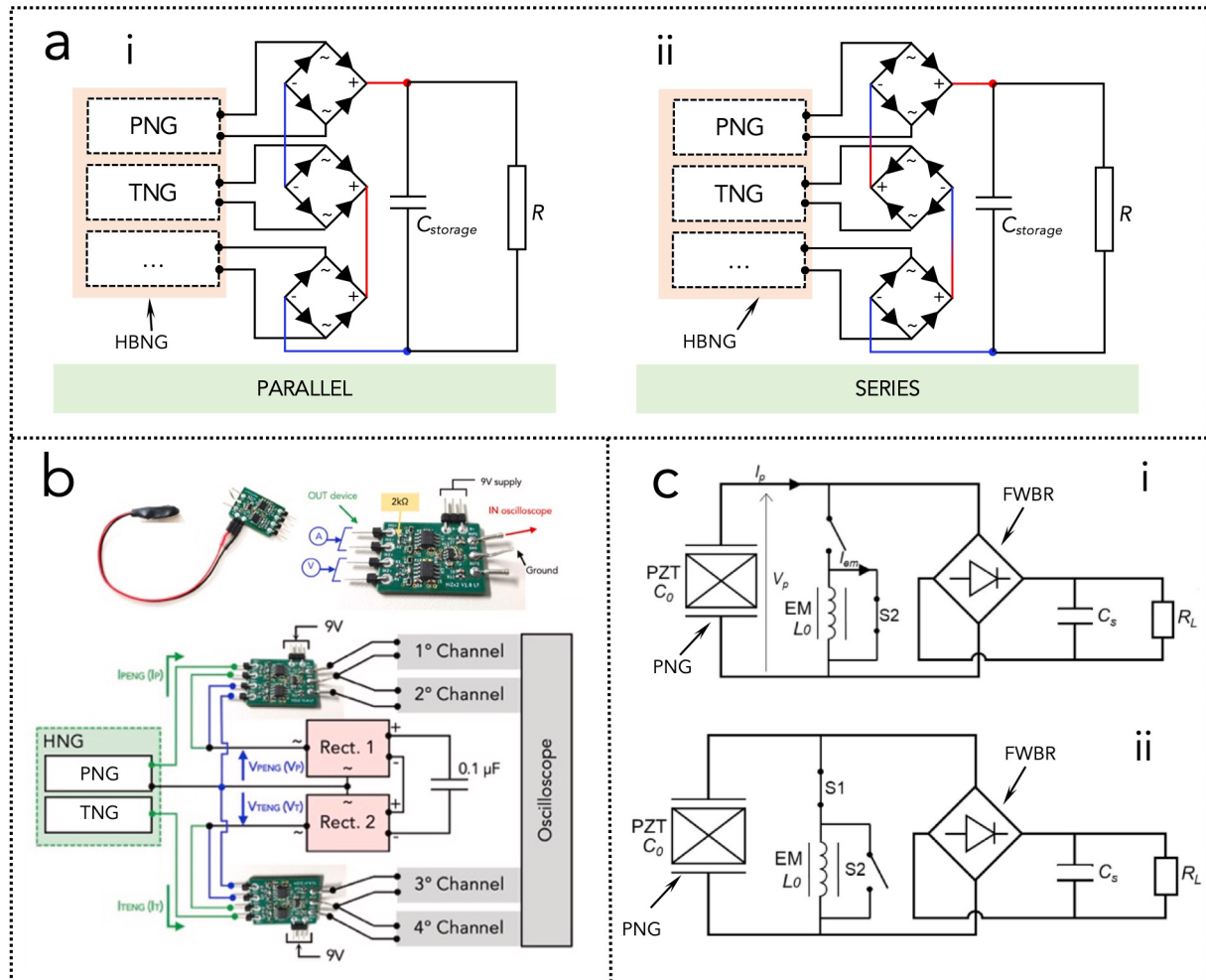
5.3. Circuits for HBNGs

Since an optimal universal solution for power management of PNGs and TNGs is still lacking due to the wide range of operating conditions and of technical issues to overcome, it is even harder and more challenging to provide an established approach for the electronic interfaces of HBNGs. In fact, the hybridization occurring inside the system is not necessarily additive in terms of voltages and currents, since this depends basically on the electrodes' configuration and the polarization direction of the piezoelectric material, as discussed in Section 3. In the simplest case, each elemental device (PNG or TNG) inside a HBNG needs a rectifying circuit to extract the signal, unless the HBNG is based on a 2-terminal hybridization with physical integration. Therefore, the most common electronic interfaces for a HBNG consists of some full-wave bridge rectifiers (FWBRs) connected in parallel (Figure 11a(i)) or in series (Figure 11a(ii)) and a storage capacitor [318]. Li et al. [319] reported on a HBNG to harvest energy from low-frequency ambient vibrations, made of a PNG patch, a TNG patch, a spring-mass system and an amplitude limiter, introduced to achieve the desired frequency up-conversion effect. The circuit for signal extraction and power management contains two rectifiers to invert the negative current signals into positive ones and they are connected independently to the PNG and TNG in parallel to a storage capacitor. A similar type of connection is used for the HBNGs presented by Wang et al. [150], whereas only one full-wave rectifier is adopted by Li et al. [320]. Mariello et al. [13,76] employed an electronic interface with two full-wave rectifiers in series or in parallel to extract the hybrid signal from the 3-electrode HBNGs, whereas to achieve the single voltage and current waveforms they used two differential high-impedance (~200 MΩ–1 GΩ) buffer circuits, supplied by 9 V batteries, to decouple the internal impedance of the measuring oscilloscope and separate the different signals (two for PNG, two for TNG) (Figure 11b). Singh and Khare [185] fabricated a piezoelectric-triboelectric-electromagnetic HBNG, based on ZnO-PVDF, to harvest mechanical vibrations. The electrical connections used to extract simultaneously the power outputs from the three transducing mechanisms include five terminals connected to three full-wave low-leakage bridge rectifier ICs (DF10M): all of the outputs from the rectifiers are connected in parallel. Intermediate transformers are often used between the nanogenerator and the bridge rectifier, in order to match the impedance between the different parts, reduce the power consumption in the power source and enhance the power transfer capability [175,177].

Different approaches can also be adopted and they can consist of exploiting a transducing component of the HBNG as an active part of the power management circuit. For instance, Lallart and Lombardi [321] presented a hybrid nonlinear interface combining piezoelectric and electromagnetic effects for energy harvesting purposes (Figure 11c(i,ii)). Inspired to the SSHI interface mentioned in Section 5.1, the new approach relies on the

replacement of the passive inductance with an electromagnetic transducer, thus it can be ascribed in the power management circuits for HBNGs. It is called synchronized switch harvesting on electromagnetic system (SSH-EM) and provides an increase of the output voltage and harvested power, compared to the SSHI or the standard DET approaches.

Figure 11. Power management circuits for HBNGs. (**a**) Electrical interfaces for HBNGs with full-wave bridge rectifiers connected in parallel (**i**) or in series (**ii**). (**b**) Differential high-impedance buffer circuit used to measure simultaneously voltage and current signals for the PNG and TNG, functioning as a voltmeter and an ammeter. In the bottom, circuit employed to obtain synchronized voltage/current waveforms for PNG and TNG. Two buffer circuits are used and each of them provides two pairs of outputs, detected as four separate channels by the oscilloscope. Reprinted with permission from ref. [13], Copyright 2021, Elsevier. (**c**) SSH-EM circuit configuration at default state (**i**) and switching state (**ii**). Reprinted with permission from ref. [321], Copyright 2019, Elsevier.

In conclusion, a unified solution for the power management of HBNGs with more than two terminals is still lacking and needs further investigation and analysis.

6. Conclusions and Future Challenges

Nowadays, the global energy problem implies a high demand of novel environmentally friendly, efficient and cost-effective technologies to scavenge energy from the environment and from humans. Nanogenerators represent a valid complementary option to the standard bulky systems such as power plants or turbines. On the other hand, in the context of the spreading Internet of Things revolution, there is a high demand of easy-to-use, rapid, biocompatible and non-invasive method for monitoring human life parameters, for sensing human body motion, for stimulating chemical reactions or for implantable ap-

plications. Nanogenerators have also emerged as powerful tools for these human-centered applications and many research efforts have been made for designing new architectures, for developing and using novel materials, for increasing the device's performances. Against most current devices based on single-mechanism transducers (nanogenerators or sensors), the future direction of these technologies is to exploit multi mechanisms simultaneously. Hybridization brings some key advantages such as a further miniaturization of the devices and enhanced signal generation. The technology of the hybrid bio-nanogenerators (HBNGs) is promising and in continuous growth.

In this paper, the recent advances of hybrid nanogenerators and sensors based on piezoelectric and triboelectric transduction mechanisms are reviewed. These two mechanisms are the most widely adopted and their advantages to other systems are discussed: when combined together, both mechanical deformation and contact friction of materials can be exploited in the same hybrid device to scavenge or convert mechanical energy.

Different possibilities for the design of hybridized devices are described, based on the physical domains involved in the energy conversion. In this respect, intra-domain or inter-domain hybridization can be exploited. The piezoelectric and triboelectric transducers can be used individually or together, in combination with other transducing principles (electromagnetic, solar, photovoltaic, etc.). Regarding the relative position and physical interpenetration of the piezoelectric and triboelectric components the hybridization can occur with physical separation or with physical integration.

Power management of piezoelectric, triboelectric and hybrid nanogenerators is also discussed, highlighting the higher complexity that hybrid devices bring for signal extraction. The three main applications of HBNGs are presented: energy harvesting, wearable bioelectronics and implantable bioelectronics. The first category is so far the most widely explored with plenty of examples of nanogenerators that scavenge energy from environmental clean-energy sources (wind, water etc.). The last two categories are less investigated and robust commercializable solutions are still lacking because of additional challenges regarding the skin adhesion, conformality, adaptability, miniaturization and implantation.

As similarly described in [294,322] for piezoelectric energy harvesting systems, there are many criteria to evaluate the performances of a HBNG: (1) efficiency, (2) standalone operation, (3) circuit complexity, (4) adaptivity to the environment, (5) micro-scale compatibility, (6) start-up operation, (7) minimum operating voltage, (8) internal impedance, (9) flexibility and conformality. Future research work is urgently needed for several key aspects and challenges, that are pointed out below and illustrated in Figure 12.

The first aspect to focus on is the *output generation performances* of the HBNGs, which depends on the performances of the single components and also the mutual combination and interaction. To enhance the performances, novel materials with higher capability of generation of piezo-potentials or surface charges are needed, in particular polymers with lower dielectric permittivity, electrostatic breakdown rigidity and mechanical robustness [221,323]. On the other hand, acting on the design and architecture of the hybridized device plays an important role in enhancing the overall performances. This holds true both for increasing the power density (for energy harvesting applications) and for increasing the sensitivity of sensing devices (for biomedical applications). The optimization of the design can be performed on two sides, i.e., the structural design or the electronic circuitry. General principles for the enhancement of triboelectrification are (i) multilayer structures, (ii) grating structures, (iii) softness to increase contact areas, (iv) charge pumping or surface treatments/functionalization strategies to increase surface charge densities [212,221].

The second aspect that needs further investigation and urgent solutions regards the *reliability* of HBNGs. This includes the durability of the materials involved in the fabrication of the devices: since they are supposed to undergo mechanical deformations or friction/contact, the stability of all the interfaces is necessary for a long-term operation. A second factor that affects the reliability, especially for devices aimed at being employed in water or implanted in the human body, is the package and external embodiment of the HBNGs. Hermetic packages or ultra-high barrier encapsulations are necessary for protect-

ing the devices against biofouling, humidity or water permeation that can induce internal short-circuits, corrosion or delaminations. Water affects negatively both triboelectricity, by forming thin layers on the tribo-surfaces, and piezoelectricity, by reducing the dielectric strength of the active material. Acting on the wettability (hydrophobicity) of the involved layered materials in HBNGs can be a solution for impeding the water absorption [137]. Other harsh agents of device failure are dryness, high temperatures (which cause the loss of piezoelectricity beyond the Curie temperature and a reduction of triboelectricity through electron thermion emission), UV radiations (which cause the desorption of oxygen molecules and formation of free radicals that influence the charge generation), the presence of chemical substances, contaminants, interstitial atomic hydrogen and oxygen vacancies in ceramic materials [209].
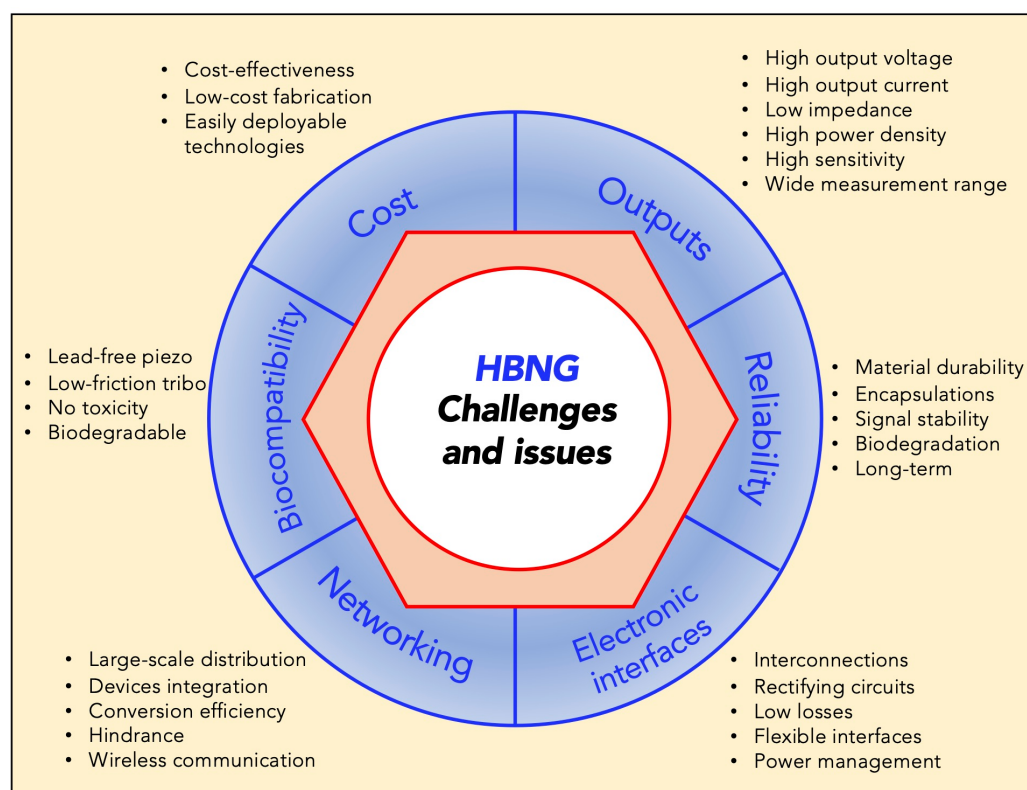
Figure 12. Illustrations of challenges and issues to be solved for the future employment of HBNGs.

The third aspect concerns the power management circuits and *electronic interfaces* used to extract signals from the HBNGs. They need to be optimized to minimize the losses, maximize the signal-to-noise ratio, increase the efficiency, especially for energy harvesting applications, or lower the sensitivity limit of the devices, for sensing applications. The sensitivity, as well as linearity, is crucial for physiological monitoring of heartbeat, intestinal movement or respiratory rate and hybrid devices can improve it to provide broad sensing ranges.

In case of implantable or wearable bioelectronic devices, the electronic interfaces can be incorporated in the package and they need to be carried by flexible or even stretchable substrates. This means that new methods of fabricating the electronic circuitry are required, based on soft substrates and reliable deposition of the metal interconnections. Additionally, piezoelectricity produces a low output voltage and higher output current while triboelectricity produces a high output voltage but with low output current. Leakage due to arc between the triboelectric materials can occur in the same device leading to degraded performances. Hence, proper circuits for handling the high triboelectric impedance must be designed.

The fourth aspect is the *networking*, i.e., the possibility to have distributed arrays of HBNGs for specific applications. An example is related to the blue energy harvesting for which coupling together different units of HBNGs can be exploited to enhance the overall efficiency of power scavenging. Distributed electrodes or devices are increasingly demanded for implantable applications, especially for stimulating simultaneously different regions of the human brain or other organs. This poses further challenges for the electronic systems that need to handle the signal of multiple devices simultaneously, thus multiplexing instrumentations are required. In addition, infrastructures for big data, artificial intelligence (AI) and deep learning are growingly required to connect large arrays of distributed self-powered sensors and to improve the systems for intelligent signal acquisition [323].

The fifth aspect is related to the *biocompatibility* of the materials used for the realization of HBNGs. The demand of environmentally friendly or biodegradable materials is of utmost important in order to develop green technologies both for power generation and for wearable/implantable sensing/actuation.

The sixth aspect is the *cost* of these novel technologies. Although they are really more cost-effective than the standard counterparts (power plants, turbines, etc.), the deposition techniques and the fabrication are still based on processes and equipment that are not affordable at very low price. These machines and processes typically are performed with cleanroom facilities and need frequent maintenance, thus lowering the price of these technologies can favor the spread and wide utilization of HBNGs, even on a large scale.

References

1. Wang, Z.L.; Song, J. Piezoelectric Nanogenerators Based on Zinc Oxide Nanowire Arrays. *Science* **2006**, *312*, 242–246. [CrossRef] [PubMed]
2. Zhang, Z.; Li, X.; Yin, J.; Xu, Y.; Fei, W.; Xue, M.; Wang, Q.; Zhou, J.; Guo, W. Emerging Hydrovoltaic Technology. *Nat. Nanotechnol.* **2018**, *13*, 1109–1119. [CrossRef] [PubMed]
3. Helseth, L.E.; Guo, X.D. Contact Electrification and Energy Harvesting Using Periodically Contacted and Squeezed Water Droplets. *Langmuir* **2015**, *31*, 3269–3276. [CrossRef] [PubMed]
4. Mariello, M.; Guido, F.; Mastronardi, V.M.; Todaro, M.T.; Desmaële, D.; De Vittorio, M. Nanogenerators for Harvesting Mechanical Energy Conveyed by Liquids. *Nano Energy* **2019**, *57*, 141–156. [CrossRef]
5. Mariello, M.; Guido, F.; Mastronardi, V.M.; Madaro, F.; Mehdipour, I.; Todaro, M.T.; Rizzi, F.; De Vittorio, M. Chapter 13—Micro- and nanodevices for wind energy harvesting. In *Nano Tools and Devices for Enhanced Renewable Energy*; Devasahayam, S., Hussain, C.M., Eds.; Micro and Nano Technologies; Elsevier: Amsterdam, The Netherlands, 2021; pp. 291–374. ISBN 978-0-12-821709-2.
6. Wang, Z.L. Catch Wave Power in Floating Nets. *Nat. News* **2017**, *542*, 159. [CrossRef] [PubMed]
7. Qin, Y.; Wang, X.; Wang, Z.L. Microfibre–Nanowire Hybrid Structure for Energy Scavenging. *Nature* **2008**, *451*, 809–813. [CrossRef] [PubMed]
8. Lai, Y.-C.; Hsiao, Y.-C.; Wu, H.-M.; Wang, Z.L. Waterproof Fabric-Based Multifunctional Triboelectric Nanogenerator for Universally Harvesting Energy from Raindrops, Wind, and Human Motions and as Self-Powered Sensors. *Adv. Sci.* **2019**, *6*, 1801883. [CrossRef]
9. Ippili, S.; Jella, V.; Thomas, A.M.; Yoon, S.-G. The Recent Progress on Halide Perovskite-Based Self-Powered Sensors Enabled by Piezoelectric and Triboelectric Effects. *Nanoenergy Adv.* **2021**, *1*, 3–31. [CrossRef]
10. Chen, J.; Huang, Y.; Zhang, N.; Zou, H.; Liu, R.; Tao, C.; Fan, X.; Wang, Z.L. Micro-Cable Structured Textile for Simultaneously Harvesting Solar and Mechanical Energy. *Nat. Energy* **2016**, *1*, 16138. [CrossRef]
11. Ren, Z.; Zheng, Q.; Wang, H.; Guo, H.; Miao, L.; Wan, J.; Xu, C.; Cheng, S.; Zhang, H. Wearable and Self-Cleaning Hybrid Energy Harvesting System Based on Micro/Nanostructured Haze Film. *Nano Energy* **2020**, *67*, 104243. [CrossRef]
12. Cho, Y.; Lee, S.; Hong, J.; Pak, S.; Hou, B.; Lee, Y.-W.; Jang, J.E.; Im, H.; Sohn, J.I.; Cha, S.; et al. Sustainable Hybrid Energy Harvester Based on Air Stable Quantum Dot Solar Cells and Triboelectric Nanogenerator. *J. Mater. Chem. A* **2018**, *6*, 12440–12446. [CrossRef]

13. Mariello, M.; Fachechi, L.; Guido, F.; De Vittorio, M. Multifunctional Sub-100 µm Thickness Flexible Piezo/Triboelectric Hybrid Water Energy Harvester Based on Biocompatible AlN and Soft Parylene C-PDMS-EcoflexTM. *Nano Energy* **2021**, *83*, 105811. [CrossRef]

14. Khan, U.; Kim, S.-W. Triboelectric Nanogenerators for Blue Energy Harvesting. *ACS Nano* **2016**, *10*, 6429–6432. [CrossRef] [PubMed]

15. Viet, N.V.; Wu, N.; Wang, Q. A Review on Energy Harvesting from Ocean Waves by Piezoelectric Technology. *J. Model. Mech. Mater.* **2017**, *1*. [CrossRef]

16. Wang, Z.L. Self-Powered Nanosensors and Nanosystems. *Adv. Mater.* **2012**, *24*, 280–285. [CrossRef]

17. Wu, Z.; Cheng, T.; Wang, Z.L. Self-Powered Sensors and Systems Based on Nanogenerators. *Sensors* **2020**, *20*, 2925. [CrossRef]

18. Wang, Z.L. Energy Harvesting for Self-Powered Nanosystems. *Nano Res.* **2008**, *1*, 1–8. [CrossRef]

19. Pu, X.; Li, L.; Liu, M.; Jiang, C.; Du, C.; Zhao, Z.; Hu, W.; Wang, Z.L. Wearable Self-Charging Power Textile Based on Flexible Yarn Supercapacitors and Fabric Nanogenerators. *Adv. Mater.* **2016**, *28*, 98–105. [CrossRef]

20. Sim, H.J.; Choi, C.; Kim, S.H.; Kim, K.M.; Lee, C.J.; Kim, Y.T.; Lepró, X.; Baughman, R.H.; Kim, S.J. Stretchable Triboelectric Fiber for Self-Powered Kinematic Sensing Textile. *Sci. Rep.* **2016**, *6*, 35153. [CrossRef]

21. Chen, X.; Shao, J.; An, N.; Li, X.; Tian, H.; Xu, C.; Ding, Y. Self-Powered Flexible Pressure Sensors with Vertically Well-Aligned Piezoelectric Nanowire Arrays for Monitoring Vital Signs. *J. Mater. Chem. C* **2015**, *3*, 11806–11814. [CrossRef]

22. Zheng, Q.; Zhang, H.; Shi, B.; Xue, X.; Liu, Z.; Jin, Y.; Ma, Y.; Zou, Y.; Wang, X.; An, Z.; et al. In Vivo Self-Powered Wireless Cardiac Monitoring via Implantable Triboelectric Nanogenerator. *ACS Nano* **2016**, *10*, 6510–6518. [CrossRef] [PubMed]

23. Gu, Y.; Zhang, T.; Chen, H.; Wang, F.; Pu, Y.; Gao, C.; Li, S. Mini Review on Flexible and Wearable Electronics for Monitoring Human Health Information. *Nanoscale Res. Lett.* **2019**, *14*, 263. [CrossRef] [PubMed]

24. Zhang, Z.; Du, K.; Chen, X.; Xue, C.; Wang, K. An Air-Cushion Triboelectric Nanogenerator Integrated with Stretchable Electrode for Human-Motion Energy Harvesting and Monitoring. *Nano Energy* **2018**, *53*, 108–115. [CrossRef]

25. Mitcheson, P.D.; Yeatman, E.M.; Rao, G.K.; Holmes, A.S.; Green, T.C. Energy Harvesting from Human and Machine Motion for Wireless Electronic Devices. *Proc. IEEE* **2008**, *96*, 1457–1486. [CrossRef]

26. Guido, F.; Qualtieri, A.; Algieri, L.; Lemma, E.D.; De Vittorio, M.; Todaro, M.T. AlN-Based Flexible Piezoelectric Skin for Energy Harvesting from Human Motion. *Microelectron. Eng.* **2016**, *159*, 174–178. [CrossRef]

27. Yang, Y.; Zhang, H.; Lin, Z.-H.; Zhou, Y.S.; Jing, Q.; Su, Y.; Yang, J.; Chen, J.; Hu, C.; Wang, Z.L. Human Skin Based Triboelectric Nanogenerators for Harvesting Biomechanical Energy and as Self-Powered Active Tactile Sensor System. *ACS Nano* **2013**, *7*, 9213–9222. [CrossRef]

28. Shi, Q.; Wang, H.; Wu, H.; Lee, C. Self-Powered Triboelectric Nanogenerator Buoy Ball for Applications Ranging from Environment Monitoring to Water Wave Energy Farm. *Nano Energy* **2017**, *40*, 203–213. [CrossRef]

29. Olsen, M.; Zhang, R.; Örtegren, J.; Andersson, H.; Yang, Y.; Olin, H. Frequency and Voltage Response of a Wind-Driven Fluttering Triboelectric Nanogenerator. *Sci. Rep.* **2019**, *9*, 5543. [CrossRef]

30. Shi, Q.; Zhang, Z.; Chen, T.; Lee, C. Minimalist and Multi-Functional Human Machine Interface (HMI) Using a Flexible Wearable Triboelectric Patch. *Nano Energy* **2019**, *62*, 355–366. [CrossRef]

31. O'Flynn, B.; Sanchez-Torres, J.; Tedesco, S.; Walsh, M. Challenges in the development of wearable human machine interface systems. In Proceedings of the 2019 IEEE International Electron Devices Meeting (IEDM), San Francisco, CA, USA, 7–11 December 2019; pp. 10.4.1–10.4.4.

32. Sun, Z.; Zhu, M.; Lee, C. Progress in the Triboelectric Human–Machine Interfaces (HMIs)-Moving from Smart Gloves to AI/Haptic Enabled HMI in the 5G/IoT Era. *Nanoenergy Adv.* **2021**, *1*, 81–120. [CrossRef]

33. Gerratt, A.P.; Michaud, H.O.; Lacour, S.P. Elastomeric Electronic Skin for Prosthetic Tactile Sensation. *Adv. Funct. Mater.* **2015**, *25*, 2287–2295. [CrossRef]

34. Brunelli, D.; Tadesse, A.M.; Vodermayer, B.; Nowak, M.; Castellini, C. Low-cost wearable multichannel surface EMG acquisition for prosthetic hand control. In Proceedings of the 6th International Workshop on Advances in Sensors and Interfaces (IWASI), Gallipoli, Italy, 18–19 June 2015; pp. 94–99.

35. Kim, B.-Y.; Lee, W.-H.; Hwang, H.-G.; Kim, D.-H.; Kim, J.-H.; Lee, S.-H.; Nahm, S. Resistive Switching Memory Integrated with Nanogenerator for Self-Powered Bioimplantable Devices. *Adv. Funct. Mater.* **2016**, *26*, 5211–5221. [CrossRef]

36. Zhang, X.-S.; Han, M.-D.; Wang, R.-X.; Zhu, F.-Y.; Li, Z.-H.; Wang, W.; Zhang, H.-X. Frequency-Multiplication High-Output Triboelectric Nanogenerator for Sustainably Powering Biomedical Microsystems. *Nano Lett.* **2013**, *13*, 1168–1172. [CrossRef] [PubMed]

37. Mukhopadhyay, S.C.; Suryadevara, N.K. *Internet of Things: Challenges and Opportunities*; Mukhopadhyay, S.C., Ed.; Smart Sensors, Measurement and Instrumentation; Springer International Publishing: Cham, Switzerland, 2014; pp. 1–17. ISBN 978-3-319-04223-7.

38. Yin, Y.; Zeng, Y.; Chen, X.; Fan, Y. The Internet of Things in Healthcare: An Overview. *J. Ind. Inf. Integr.* **2016**, *1*, 3–13. [CrossRef]

39. Lee, M.; Boudreaux, B.; Chaturvedi, R.; Romanosky, S.; Downing, B. *The Internet of Bodies: Opportunities, Risks, and Governance*; RAND Corporation: Santa Monica, CA, USA, 2020.

40. Fan, F.R.; Tang, W.; Wang, Z.L. Flexible Nanogenerators for Energy Harvesting and Self-Powered Electronics. *Adv. Mater.* **2016**, *28*, 4283–4305. [CrossRef]

99

41. Lee, J.-H.; Lee, K.Y.; Kumar, B.; Tien, N.T.; Lee, N.-E.; Kim, S.-W. Highly Sensitive Stretchable Transparent Piezoelectric Nanogenerators. *Energy Environ. Sci.* **2012**, *6*, 169–175. [CrossRef]

42. Akaydin, H.D.; Elvin, N.; Andreopoulos, Y. Energy Harvesting from Highly Unsteady Fluid Flows Using Piezoelectric Materials. *J. Intell. Mater. Syst. Struct.* **2010**, *21*, 1263–1278. [CrossRef]

43. Dagdeviren, C.; Joe, P.; Tuzman, O.L.; Park, K.-I.; Lee, K.J.; Shi, Y.; Huang, Y.; Rogers, J.A. Recent Progress in Flexible and Stretchable Piezoelectric Devices for Mechanical Energy Harvesting, Sensing and Actuation. *Extreme Mech. Lett.* **2016**, *9*, 269–281. [CrossRef]

44. Choi, A.Y.; Lee, C.J.; Park, J.; Kim, D.; Kim, Y.T. Corrugated Textile Based Triboelectric Generator for Wearable Energy Harvesting. *Sci. Rep.* **2017**, *7*, 45583. [CrossRef]

45. Wang, A.C.; Wu, C.; Pisignano, D.; Wang, Z.L.; Persano, L. Polymer Nanogenerators: Opportunities and Challenges for Large-Scale Applications. *J. Appl. Polym. Sci.* **2018**, *135*, 45674. [CrossRef]

46. Todaro, M.T.; Guido, F.; Mastronardi, V.; Desmaele, D.; Epifani, G.; Algieri, L.; De Vittorio, M. Piezoelectric MEMS Vibrational Energy Harvesters: Advances and Outlook. *Microelectron. Eng.* **2017**, *183–184*, 23–36. [CrossRef]

47. Todaro, M.T.; Guido, F.; Algieri, L.; Mastronardi, V.M.; Desmaële, D.; Epifani, G.; Vittorio, M.D. Biocompatible, Flexible, and Compliant Energy Harvesters Based on Piezoelectric Thin Films. *IEEE Trans. Nanotechnol.* **2018**, *17*, 220–230. [CrossRef]

48. Lu, N.; Lu, C.; Yang, S.; Rogers, J. Highly Sensitive Skin-Mountable Strain Gauges Based Entirely on Elastomers. *Adv. Funct. Mater.* **2012**, *22*, 4044–4050. [CrossRef]

49. Zheng, Y.-N.; Yu, Z.; Mao, G.; Li, Y.; Pravarthana, D.; Asghar, W.; Liu, Y.; Qu, S.; Shang, J.; Li, R.-W. A Wearable Capacitive Sensor Based on Ring/Disk-Shaped Electrode and Porous Dielectric for Noncontact Healthcare Monitoring. *Glob. Chall.* **2020**, *4*, 1900079. [CrossRef] [PubMed]

50. Lei, Z.; Wu, P. A Supramolecular Biomimetic Skin Combining a Wide Spectrum of Mechanical Properties and Multiple Sensory Capabilities. *Nat. Commun.* **2018**, *9*, 1134. [CrossRef] [PubMed]

51. Zhang, X.; Sheng, N.; Wang, L.; Tan, Y.; Liu, C.; Xia, Y.; Nie, Z.; Sui, K. Supramolecular Nanofibrillar Hydrogels as Highly Stretchable, Elastic and Sensitive Ionic Sensors. *Mater. Horiz.* **2019**, *6*, 326–333. [CrossRef]

52. Ryu, H.; Yoon, H.-J.; Kim, S.-W. Hybrid Energy Harvesters: Toward Sustainable Energy Harvesting. *Adv. Mater.* **2019**, *31*, 1802898. [CrossRef] [PubMed]

53. Kim, S.-G.; Priya, S.; Kanno, I. Piezoelectric MEMS for Energy Harvesting. *MRS Bull.* **2012**, *37*, 1039–1050. [CrossRef]

54. Li, P.; Ryu, J.; Hong, S. *Piezoelectric/Triboelectric Nanogenerators for Biomedical Applications*; IntechOpen: London, UK, 2019; ISBN 978-1-83881-060-3.

55. Fang, J.; Wang, X.; Lin, T. Electrical Power Generator from Randomly Oriented Electrospun Poly(Vinylidene Fluoride) Nanofibre Membranes. *J. Mater. Chem.* **2011**, *21*, 11088–11091. [CrossRef]

56. Chen, X.; Xu, S.; Yao, N.; Shi, Y. 1.6 V Nanogenerator for Mechanical Energy Harvesting Using PZT Nanofibers. *Nano Lett.* **2010**, *10*, 2133–2137. [CrossRef]

57. Bai, S.; Xu, Q.; Gu, L.; Ma, F.; Qin, Y.; Wang, Z.L. Single Crystalline Lead Zirconate Titanate (PZT) Nano/Micro-Wire Based Self-Powered UV Sensor. *Nano Energy* **2012**, *1*, 789–795. [CrossRef]

58. Wang, P.; Du, H. ZnO Thin Film Piezoelectric MEMS Vibration Energy Harvesters with Two Piezoelectric Elements for Higher Output Performance. *Rev. Sci. Instrum.* **2015**, *86*, 075002. [CrossRef] [PubMed]

59. Algieri, L.; Todaro, M.T.; Guido, F.; Mastronardi, V.; Desmaële, D.; Qualtieri, A.; Giannini, C.; Sibillano, T.; De Vittorio, M. Flexible Piezoelectric Energy-Harvesting Exploiting Biocompatible AlN Thin Films Grown onto Spin-Coated Polyimide Layers. *ACS Appl. Energy Mater.* **2018**, *1*, 5203–5210. [CrossRef]

60. Eom, C.-B.; Trolier-McKinstry, S. Thin-Film Piezoelectric MEMS. *MRS Bull.* **2012**, *37*, 1007–1017. [CrossRef]

61. Wasa, K.; Matsushima, T.; Adachi, H.; Kanno, I.; Kotera, H. Thin-Film Piezoelectric Materials for a Better Energy Harvesting MEMS. *J. Microelectromech. Syst.* **2012**, *21*, 451–457. [CrossRef]

62. Won, S.S.; Sheldon, M.; Mostovych, N.; Kwak, J.; Chang, B.-S.; Ahn, C.; Kingon, A.; Won Kim, I.; Kim, S.-H. Piezoelectric Poly(Vinylidene Fluoride Trifluoroethylene) Thin Film-Based Power Generators Using Paper Substrates for Wearable Device Applications. *Appl. Phys. Lett.* **2015**, *107*, 202901. [CrossRef]

63. Curie, J.; Curie, P. Phénomènes Électriques Des Cristaux Hémièdres à Faces Inclinées. *J. Phys. Theor. Appl.* **1882**, *1*, 245–251. [CrossRef]

64. Kim, H.S.; Kim, J.-H.; Kim, J. A Review of Piezoelectric Energy Harvesting Based on Vibration. *Int. J. Precis. Eng. Manuf.* **2011**, *12*, 1129–1141. [CrossRef]

65. Wang, Z.J.; Narita, F. Corona Poling Conditions for Barium Titanate/Epoxy Composites and Their Unsteady Wind Energy Harvesting Potential. *Adv. Eng. Mater.* **2019**, *21*, 1900169. [CrossRef]

66. Kosec, M.; Malič, B.; Benčan, A.; Rojac, T. KNN-based piezoelectric ceramics. In *Piezoelectric and Acoustic Materials for Transducer Applications*; Safari, A., Akdoğan, E.K., Eds.; Springer: Boston, MA, USA, 2008; pp. 81–102. ISBN 978-0-387-76540-2.

67. Clementi, G.; Lombardi, G.; Margueron, S.; Suarez, M.A.; Lebrasseur, E.; Ballandras, S.; Imbaud, J.; Lardet-Vieudrin, F.; Gauthier-Manuel, L.; Dulmet, B.; et al. LiNbO3 Films—A Low-Cost Alternative Lead-Free Piezoelectric Material for Vibrational Energy Harvesters. *Mech. Syst. Signal Process. MSSP* **2021**, *149*, 107171. [CrossRef]

68. Singh, H.H.; Khare, N. Flexible ZnO-PVDF/PTFE Based Piezo-Tribo Hybrid Nanogenerator. *Nano Energy* **2018**, *51*, 216–222. [CrossRef]

69. Qualtieri, A.; Rizzi, F.; Todaro, M.T.; Passaseo, A.; Cingolani, R.; De Vittorio, M. Stress-Driven AlN Cantilever-Based Flow Sensor for Fish Lateral Line System. *Microelectron. Eng.* **2011**, *88*, 2376–2378. [CrossRef]

70. Caro, M.A.; Zhang, S.; Riekkinen, T.; Ylilammi, M.; Moram, M.A.; Lopez-Acevedo, O.; Molarius, J.; Laurila, T. Piezoelectric Coefficients and Spontaneous Polarization of ScAlN. *J. Phys. Condens. Matter* **2015**, *27*, 245901. [CrossRef]

71. Koblmueller, G.; Averbeck, R.; Geelhaar, L.; Riechert, H.; Hösler, W.; Pongratz, P. Growth Diagram and Morphologies of AlN Thin Films Grown by Molecular Beam Epitaxy. *J. Appl. Phys.* **2003**, *93*, 9591–9596. [CrossRef]

72. Chen, D.; Colas, J.; Mercier, F.; Boichot, R.; Charpentier, L.; Escape, C.; Balat-Pichelin, M.; Pons, M. High Temperature Properties of AlN Coatings Deposited by Chemical Vapor Deposition for Solar Central Receivers. *Surf. Coat. Technol.* **2019**, *377*, 124872. [CrossRef]

73. Mariello, M.; Blad, T.W.A.; Mastronardi, V.M.; Madaro, F.; Guido, F.; Staufer, U.; Tolou, N.; De Vittorio, M. Flexible Piezoelectric AlN Transducers Buckled through Package-Induced Preloading for Mechanical Energy Harvesting. *Nano Energy* **2021**, *85*, 105986. [CrossRef]

74. Mariello, M.; Guido, F.; Algieri, L.; Mastronardi, V.M.; Qualtieri, A.; Pisanello, F.; De Vittorio, M. Microstructure and Electrical Properties of Novel Piezo-Optrodes Based on Thin-Film Piezoelectric Aluminium Nitride for Sensing. *IEEE Trans. Nanotechnol.* **2021**, *20*, 10–19. [CrossRef]

75. Akiyama, M.; Morofuji, Y.; Kamohara, T.; Nishikubo, K.; Tsubai, M.; Fukuda, O.; Ueno, N. Flexible Piezoelectric Pressure Sensors Using Oriented Aluminum Nitride Thin Films Prepared on Polyethylene Terephthalate Films. *J. Appl. Phys.* **2006**, *100*, 114318. [CrossRef]

76. Mariello, M.; Fachechi, L.; Guido, F.; Vittorio, M.D. Conformal, Ultra-Thin Skin-Contact-Actuated Hybrid Piezo/Triboelectric Wearable Sensor Based on AlN and Parylene-Encapsulated Elastomeric Blend. *Adv. Funct. Mater.* **2021**, *31*, 2101047. [CrossRef]

77. Signore, M.A.; Rescio, G.; De Pascali, C.; Iacovacci, V.; Dario, P.; Leone, A.; Quaranta, F.; Taurino, A.; Siciliano, P.; Francioso, L. Fabrication and Characterization of AlN-Based Flexible Piezoelectric Pressure Sensor Integrated into an Implantable Artificial Pancreas. *Sci. Rep.* **2019**, *9*, 17130. [CrossRef]

78. Jackson, N.; Keeney, L.; Mathewson, A. Flexible-CMOS and Biocompatible Piezoelectric AlN Material for MEMS Applications. *Smart Mater. Struct.* **2013**, *22*, 115033. [CrossRef]

79. Hu, X.; Yang, F.; Guo, M.; Pei, J.; Zhao, H.; Wang, Y. Fabrication of Polyimide Microfluidic Devices by Laser Ablation Based Additive Manufacturing. *Microsyst. Technol.* **2020**, *26*, 1573–1583. [CrossRef]

80. Sun, Y.; Lacour, S.; Brooks, R.; Rushton, N.; Fawcett, J.; Cameron, R.E. Assessment of the Biocompatibility of Photosensitive Polyimide for Implantable Medical Device Use. *J. Biomed. Mater. Res. A* **2009**, *90*, 648–655. [CrossRef]

81. Bartasyte, A.; Margueron, S.; Baron, T.; Oliveri, S.; Boulet, P. Toward High-Quality Epitaxial LiNbO3 and LiTaO3 Thin Films for Acoustic and Optical Applications. *Adv. Mater. Interfaces* **2017**, *4*, 1600998. [CrossRef]

82. Kovacs, G.; Anhorn, M.; Engan, H.E.; Visintini, G.; Ruppel, C.C.W. Improved material constants for LiNbO/Sub 3/and LiTaO/Sub 3/. In Proceedings of the IEEE Symposium on Ultrasonics, Honolulu, HI, USA, 4–7 December 1990; Volume 1, pp. 435–438.

83. Pi, Z.; Zhang, J.; Wen, C.; Zhang, Z.; Wu, D. Flexible Piezoelectric Nanogenerator Made of Poly(Vinylidenefluoride-Co-Trifluoroethylene) (PVDF-TrFE) Thin Film. *Nano Energy* **2014**, *7*, 33–41. [CrossRef]

84. Mariello, M.; Qualtieri, A.; Mele, G.; De Vittorio, M. Metal-Free Multilayer Hybrid PENG Based on Soft Electrospun/-Sprayed Membranes with Cardanol Additive for Harvesting Energy from Surgical Face Masks. *ACS Appl. Mater. Interfaces* **2021**, *13*, 20606–20621. [CrossRef]

85. Liu, J.; Yu, D.; Zheng, Z.; Huangfu, G.; Guo, Y. Lead-Free BiFeO3 Film on Glass Fiber Fabric: Wearable Hybrid Piezoelectric-Triboelectric Nanogenerator. *Ceram. Int.* **2021**, *47*, 3573–3579. [CrossRef]

86. Chiu, Y.-Y.; Lin, W.-Y.; Wang, H.-Y.; Huang, S.-B.; Wu, M.-H. Development of a Piezoelectric Polyvinylidene Fluoride (PVDF) Polymer-Based Sensor Patch for Simultaneous Heartbeat and Respiration Monitoring. *Sens. Actuators Phys.* **2013**, *189*, 328–334. [CrossRef]

87. Bae, J.-H.; Chang, S.-H. PVDF-Based Ferroelectric Polymers and Dielectric Elastomers for Sensor and Actuator Applications: A Review. *Funct. Compos. Struct.* **2019**, *1*, 012003. [CrossRef]

88. Hutson, A.R.; White, D.L. Elastic Wave Propagation in Piezoelectric Semiconductors. *J. Appl. Phys.* **1962**, *33*, 40–47. [CrossRef]

89. Auld, B.A. *Acoustic Fields and Waves in Solids*; John Wiley & Sons: New York, NY, USA, 1973; Volume 1, ISBN 978-0-471-03700-2.

90. Pierret, R. *Semiconductor Fundamentals: Volume I*; Pearson: Reading, MA, USA, 1988; ISBN 978-0-201-12295-4.

91. Asthana, A.; Asayesh-Ardakani, H.; Yap, Y.K.; Yassar, R. Real Time Observation of Mechanically Triggered Piezoelectric Current in Individual ZnO Nanobelts. *J. Mater. Chem. C* **2014**, *2*, 3995–4004. [CrossRef]

92. Yang, G.; Du, J.; Wang, J.; Yang, J. Electromechanical Fields in a Nonuniform Piezoelectric Semiconductor Rod. *J. Mech. Mater. Struct.* **2018**, *13*, 103–120. [CrossRef]

93. Luo, Y.; Zhang, C.; Chen, W.; Yang, J. An Analysis of PN Junctions in Piezoelectric Semiconductors. *J. Appl. Phys.* **2017**, *122*, 204502. [CrossRef]

94. Huang, H.; Qian, Z.; Yang, J. I-V Characteristics of a Piezoelectric Semiconductor Nanofiber under Local Tensile/Compressive Stress. *J. Appl. Phys.* **2019**, *126*, 164902. [CrossRef]

95. Wang, Z. Piezopotential Gated Nanowire Devices: Piezotronics and Piezo-Phototronics. *Nano Today* **2010**, *5*, 540–552. [CrossRef]

96. Liu, Y.; Zhang, Y.; Yang, Q.; Niu, S.; Wang, Z.L. Fundamental Theories of Piezotronics and Piezo-Phototronics. *Nano Energy* **2015**, *14*, 257–275. [CrossRef]

97.   Zhang, Y.; Leng, Y.; Willatzen, M.; Huang, B. Theory of Piezotronics and Piezo-Phototronics. *MRS Bull.* **2018**, *43*, 928–935. [CrossRef]
98.   Zhang, Y.; Liu, Y.; Wang, Z.L. Fundamental Theory of Piezotronics. *Adv. Mater.* **2011**, *23*, 3004–3013. [CrossRef] [PubMed]
99.   Wang, Z.L.; Wu, W. Piezotronics and Piezo-Phototronics: Fundamentals and Applications. *Natl. Sci. Rev.* **2014**, *1*, 62–90. [CrossRef]
100. Yang, Y.; Tang, L. Equivalent Circuit Modeling of Piezoelectric Energy Harvesters. *J. Intell. Mater. Syst. Struct.* **2009**, *20*, 2223–2235. [CrossRef]
101. Kuang, Y.; Chew, Z.J.; Zhu, M. Strongly Coupled Piezoelectric Energy Harvesters: Finite Element Modelling and Experimental Validation. *Energy Convers. Manag.* **2020**, *213*, 112855. [CrossRef]
102. Liang, J.; Liao, W.-H. Impedance Modeling and Analysis for Piezoelectric Energy Harvesting Systems. *IEEE/ASME Trans. Mechatron.* **2012**, *17*, 1145–1157. [CrossRef]
103. Erturk, A.; Inman, D.J. Issues in Mathematical Modeling of Piezoelectric Energy Harvesters. *Smart Mater. Struct.* **2008**, *17*, 065016. [CrossRef]
104. Kuang, Y.; Ruan, T.; Chew, Z.J.; Zhu, M. Energy Harvesting during Human Walking to Power a Wireless Sensor Node. *Sens. Actuators Phys.* **2017**, *254*, 69–77. [CrossRef]
105. Elvin, N.G.; Elvin, A.A.; Spector, M. A Self-Powered Mechanical Strain Energy Sensor. *Smart Mater. Struct.* **2001**, *10*, 293–299. [CrossRef]
106. Elvin, N.G.; Elvin, A.A. A General Equivalent Circuit Model for Piezoelectric Generators. *J. Intell. Mater. Syst. Struct.* **2008**, *20*, 3–9. [CrossRef]
107. Pozo, B.; Garate, J.I.; Araujo, J.Á.; Ferreiro, S. Energy Harvesting Technologies and Equivalent Electronic Structural Models—Review. *Electronics* **2019**, *8*, 486. [CrossRef]
108. Kong, N.; Ha, D.S.; Erturk, A.; Inman, D.J. Resistive Impedance Matching Circuit for Piezoelectric Energy Harvesting. *J. Intell. Mater. Syst. Struct.* **2010**, *21*, 1293–1302. [CrossRef]
109. Qi, Y.; Jafferis, N.T.; Lyons, K.; Lee, C.M.; Ahmad, H.; McAlpine, M.C. Piezoelectric Ribbons Printed onto Rubber for Flexible Energy Conversion. *Nano Lett.* **2010**, *10*, 524–528. [CrossRef] [PubMed]
110. Cheng, C.; Chen, Z.; Shi, H.; Liu, Z.; Xiong, Y. System-Level Coupled Modeling of Piezoelectric Vibration Energy Harvesting Systems by Joint Finite Element and Circuit Analysis. Available online: https://www.hindawi.com/journals/sv/2016/2413578/ (accessed on 12 October 2020).
111. Lei, A.; Xu, R.; Borregaard, L.; Guizzetti, M.; Hansen, O.; Thomsen, E. Impedance Based Characterization of a High-Coupled Screen Printed PZT Thick Film Unimorph Energy Harvester. *J. Microelectromech. Syst.* **2014**, *23*, 842–854. [CrossRef]
112. Fan, F.-R.; Tian, Z.-Q.; Lin Wang, Z. Flexible Triboelectric Generator. *Nano Energy* **2012**, *1*, 328–334. [CrossRef]
113. Wang, Z.; Lin, L.; Chen, J.; Niu, S.; Zi, Y. *Triboelectric Nanogenerators*; Green Energy and Technology; Springer International Publishing: Berlin/Heidelberg, Germany, 2016; ISBN 978-3-319-40038-9.
114. Luo, J.; Wang, Z.L. Recent Progress of Triboelectric Nanogenerators: From Fundamental Theory to Practical Applications. *EcoMat* **2020**, *2*, e12059. [CrossRef]
115. Niu, S.; Wang, Z.L. Theoretical Systems of Triboelectric Nanogenerators. *Nano Energy* **2015**, *14*, 161–192. [CrossRef]
116. Niu, S.; Liu, Y.; Wang, S.; Lin, L.; Zhou, Y.S.; Hu, Y.; Wang, Z.L. Theoretical Investigation and Structural Optimization of Single-Electrode Triboelectric Nanogenerators. *Adv. Funct. Mater.* **2014**, *24*, 3332–3340. [CrossRef]
117. Henniker, J. Triboelectricity in Polymers. *Nature* **1962**, *196*, 474. [CrossRef]
118. Zou, H.; Zhang, Y.; Guo, L.; Wang, P.; He, X.; Dai, G.; Zheng, H.; Chen, C.; Wang, A.; Xu, C.; et al. Quantifying the Triboelectric Series. *Nat. Commun.* **2019**, *10*, 1427. [CrossRef] [PubMed]
119. Ibrahim, M.; Jiang, J.; Wen, Z.; Sun, X. Surface Engineering for Enhanced Triboelectric Nanogenerator. *Nanoenergy Adv.* **2021**, *1*, 58–80. [CrossRef]
120. Arcot Narasimulu, A.; Zhao, P.; Soin, N.; Kovur, P.; Ding, P.; Chen, J.; Dong, S.; Chen, L.; Zhou, E.; Montemagno, C.; et al. Significant Triboelectric Enhancement Using Interfacial Piezoelectric ZnO Nanosheet Layer. *Nano Energy* **2017**, *40*, 471–480. [CrossRef]
121. Ravichandran, A.N.; Ramuz, M.; Blayac, S. Increasing Surface Charge Density by Effective Charge Accumulation Layer Inclusion for High-Performance Triboelectric Nanogenerators. *MRS Commun.* **2019**, *9*, 682–689. [CrossRef]
122. Kim, H.-J.; Yim, E.-C.; Kim, J.-H.; Kim, S.-J.; Park, J.-Y.; Oh, I.-K. Bacterial Nano-Cellulose Triboelectric Nanogenerator. *Nano Energy* **2017**, *33*, 130–137. [CrossRef]
123. Wen, R.; Guo, J.; Yu, A.; Zhang, K.; Kou, J.; Zhu, Y.; Zhang, Y.; Li, B.-W.; Zhai, J. Remarkably Enhanced Triboelectric Nanogenerator Based on Flexible and Transparent Monolayer Titania Nanocomposite. *Nano Energy* **2018**, *50*, 140–147. [CrossRef]
124. Kil Yun, B.; Soo Kim, H.; Joon Ko, Y.; Murillo, G.; Hoon Jung, J. Interdigital Electrode Based Triboelectric Nanogenerator for Effective Energy Harvesting from Water. *Nano Energy* **2017**, *36*, 233–240. [CrossRef]
125. Mariello, M.; Scarpa, E.; Algieri, L.; Guido, F.; Mastronardi, V.M.; Qualtieri, A.; De Vittorio, M. Novel Flexible Triboelectric Nanogenerator Based on Metallized Porous PDMS and Parylene C. *Energies* **2020**, *13*, 1625. [CrossRef]
126. Qian, Y.; Lyu, Z.; Kim, D.-H.; Kang, D.J. Enhancing the Output Power Density of Polydimethylsiloxane-Based Flexible Triboelectric Nanogenerators with Ultrathin Nickel Telluride Nanobelts as a Co-Triboelectric Layer. *Nano Energy* **2021**, *90*, 106536. [CrossRef]

127. Qian, Y.; Kang, D.J. Large-Area High-Quality AB-Stacked Bilayer Graphene on h-BN/Pt Foil by Chemical Vapor Deposition. *ACS Appl. Mater. Interfaces* **2018**, *10*, 29069–29075. [CrossRef]

128. Harnchana, V.; Ngoc, H.V.; He, W.; Rasheed, A.; Park, H.; Amornkitbamrung, V.; Kang, D.J. Enhanced Power Output of a Triboelectric Nanogenerator Using Poly(Dimethylsiloxane) Modified with Graphene Oxide and Sodium Dodecyl Sulfate. *ACS Appl. Mater. Interfaces* **2018**, *10*, 25263–25272. [CrossRef]

129. Kim, D.Y.; Kim, H.S.; Kong, D.S.; Choi, M.; Kim, H.B.; Lee, J.-H.; Murillo, G.; Lee, M.; Kim, S.S.; Jung, J.H. Floating Buoy-Based Triboelectric Nanogenerator for an Effective Vibrational Energy Harvesting from Irregular and Random Water Waves in Wild Sea. *Nano Energy* **2018**, *45*, 247–254. [CrossRef]

130. Chen, J.; Yang, J.; Li, Z.; Fan, X.; Zi, Y.; Jing, Q.; Guo, H.; Wen, Z.; Pradel, K.C.; Niu, S.; et al. Networks of Triboelectric Nanogenerators for Harvesting Water Wave Energy: A Potential Approach toward Blue Energy. *ACS Nano* **2015**, *9*, 3324–3331. [CrossRef]

131. Wang, Z.L.; Jiang, T.; Xu, L. Toward the Blue Energy Dream by Triboelectric Nanogenerator Networks. *Nano Energy* **2017**, *39*, 9–23. [CrossRef]

132. Xiong, J.; Lin, M.-F.; Wang, J.; Gaw, S.L.; Parida, K.; Lee, P.S. Wearable All-Fabric-Based Triboelectric Generator for Water Energy Harvesting. *Adv. Energy Mater.* **2017**, *7*, 1701243. [CrossRef]

133. Luo, J.; Tang, W.; Fan, F.R.; Liu, C.; Pang, Y.; Cao, G.; Wang, Z.L. Transparent and Flexible Self-Charging Power Film and Its Application in a Sliding Unlock System in Touchpad Technology. *ACS Nano* **2016**, *10*, 8078–8086. [CrossRef] [PubMed]

134. Luo, J.; Wang, Z.; Xu, L.; Wang, A.C.; Han, K.; Jiang, T.; Lai, Q.; Bai, Y.; Tang, W.; Fan, F.R.; et al. Flexible and Durable Wood-Based Triboelectric Nanogenerators for Self-Powered Sensing in Athletic Big Data Analytics. *Nat. Commun.* **2019**, *10*, 5147. [CrossRef] [PubMed]

135. Genter, S.; Langhof, T.; Paul, O. Electret-Based Out-Of-Plane Micro Energy Harvester with Parylene-C Serving as the Electret and Spring Material. *Procedia Eng.* **2015**, *120*, 341–344. [CrossRef]

136. Lo, H.; Tai, Y.-C. Parylene-Based Electret Power Generators. *J. Micromech. Microeng.* **2008**, *18*, 104006. [CrossRef]

137. Mariello, M.; Guido, F.; Mastronardi, V.M.; De Donato, F.; Salbini, M.; Brunetti, V.; Qualtieri, A.; Rizzi, F.; De Vittorio, M. Captive-Air-Bubble Aerophobicity Measurements of Antibiofouling Coatings for Underwater MEMS Devices. *Nanomater. Nanotechnol.* **2019**, *9*, 1847980419862075. [CrossRef]

138. Mariello, M.; Guido, F.; Mastronardi, V.M.; Giannuzzi, R.; Algieri, L.; Qualtieri, A.; Maffezzoli, A.; De Vittorio, M. Reliability of Protective Coatings for Flexible Piezoelectric Transducers in Aqueous Environments. *Micromachines* **2019**, *10*, 739. [CrossRef]

139. Golda-Cepa, M.; Brzychczy-Wloch, M.; Engvall, K.; Aminlashgari, N.; Hakkarainen, M.; Kotarba, A. Microbiological Investigations of Oxygen Plasma Treated Parylene C Surfaces for Metal Implant Coating. *Mater. Sci. Eng. C* **2015**, *52*, 273–281. [CrossRef]

140. Chen, T.-N.; Wuu, D.-S.; Wu, C.-C.; Chiang, C.-C.; Chen, Y.-P.; Horng, R.-H. Improvements of Permeation Barrier Coatings Using Encapsulated Parylene Interlayers for Flexible Electronic Applications. *Plasma Process. Polym.* **2007**, *4*, 180–185. [CrossRef]

141. Applerot, G.; Abu-Mukh, R.; Irzh, A.; Charmet, J.; Keppner, H.; Laux, E.; Guibert, G.; Gedanken, A. Decorating Parylene-Coated Glass with ZnO Nanoparticles for Antibacterial Applications: A Comparative Study of Sonochemical, Microwave, and Microwave-Plasma Coating Routes. *ACS Appl. Mater. Interfaces* **2010**, *2*, 1052–1059. [CrossRef]

142. Cieślik, M.; Engvall, K.; Pan, J.; Kotarba, A. Silane–Parylene Coating for Improving Corrosion Resistance of Stainless Steel 316L Implant Material. *Corros. Sci.* **2011**, *53*, 296–301. [CrossRef]

143. Gorham, W.F. A New, General Synthetic Method for the Preparation of Linear Poly-p-Xylylenes. *J. Polym. Sci. A1* **1966**, *4*, 3027–3039. [CrossRef]

144. Calcagnile, P.; Blasi, L.; Rizzi, F.; Qualtieri, A.; Athanassiou, A.; Gogolides, E.; De Vittorio, M. Parylene C Surface Functionalization and Patterning with PH-Responsive Microgels. ACS Appl. Mater. *Interfaces* **2014**, *6*, 15708–15715. [CrossRef]

145. Scarpa, E.; Dattoma, T.; Calcagnile, P.; Blasi, L.; Qualtieri, A.; Rizzi, F.; Vittorio, M.D. Surface-tension-confined fluidics on Parylene C coated paper substrate. In Proceedings of the IEEE 17th International Conference on Nanotechnology, Pittsburgh, PA, USA, 25–27 July 2017; pp. 259–262.

146. Wu, C.; Wang, A.C.; Ding, W.; Guo, H.; Wang, Z.L. Triboelectric Nanogenerator: A Foundation of the Energy for the New Era. *Adv. Energy Mater.* **2019**, *9*, 1802906. [CrossRef]

147. Gauntt, S.; Batt, G.; Gibert, J. Dynamic modeling of triboelectric generators using lagrange's equation. In *Smart Materials, Adaptive Structures and Intelligent Systems*; American Society of Mechanical Engineers Digital Collection: New York, NY, USA, 2017.

148. Fang, C.; Tong, T.; Bu, T.; Cao, Y.; Xu, S.; Qi, Y.; Zhang, C. Overview of Power Management for Triboelectric Nanogenerators. *Adv. Intell. Syst.* **2020**, *2*, 1900129. [CrossRef]

149. Shao, J.; Willatzen, M.; Wang, Z.L. Theoretical Modeling of Triboelectric Nanogenerators (TENGs). *J. Appl. Phys.* **2020**, *128*, 111101. [CrossRef]

150. Wang, X.; Yang, B.; Liu, J.; Zhu, Y.; Yang, C.; He, Q. A Flexible Triboelectric-Piezoelectric Hybrid Nanogenerator Based on P(VDF-TrFE) Nanofibers and PDMS/MWCNT for Wearable Devices. *Sci. Rep.* **2016**, *6*, 36409. [CrossRef]

151. Nguyen, V.; Kelly, S.; Yang, R. Piezoelectric Peptide-Based Nanogenerator Enhanced by Single-Electrode Triboelectric Nanogenerator. *APL Mater.* **2017**, *5*, 074108. [CrossRef]

152. He, J.; Wen, T.; Qian, S.; Zhang, Z.; Tian, Z.; Zhu, J.; Mu, J.; Hou, X.; Geng, W.; Cho, J.; et al. Triboelectric-Piezoelectric-Electromagnetic Hybrid Nanogenerator for High-Efficient Vibration Energy Harvesting and Self-Powered Wireless Monitoring System. *Nano Energy* **2017**, *43*, 326–339. [CrossRef]

153. Yu, J.; Hou, X.; Cui, M.; Zhang, S.; He, J.; Geng, W.; Mu, J.; Chou, X. Highly Skin-Conformal Wearable Tactile Sensor Based on Piezoelectric-Enhanced Triboelectric Nanogenerator. *Nano Energy* **2019**, *64*, 103923. [CrossRef]

154. Han, Z.; Jiao, P.; Zhu, Z. Combination of Piezoelectric and Triboelectric Devices for Robotic Self-Powered Sensors. *Micromachines* **2021**, *12*, 813. [CrossRef]

155. Han, M.; Chen, X.; Yu, B.; Zhang, H. Coupling of Piezoelectric and Triboelectric Effects: From Theoretical Analysis to Experimental Verification. *Adv. Electron. Mater.* **2015**, *1*, 1500187. [CrossRef]

156. Wang, Z.L. On Maxwell's Displacement Current for Energy and Sensors: The Origin of Nanogenerators. *Mater. Today* **2017**, *20*, 74–82. [CrossRef]

157. Chen, S.; Tao, X.; Zeng, W.; Yang, B.; Shang, S. Quantifying Energy Harvested from Contact-Mode Hybrid Nanogenerators with Cascaded Piezoelectric and Triboelectric Units. *Adv. Energy Mater.* **2017**, *7*, 1601569. [CrossRef]

158. Chen, C.Y.; Tsai, C.Y.; Xu, M.H.; Wu, C.T.; Huang, C.Y.; Lee, T.H.; Fuh, Y.K. A Fully Encapsulated Piezoelectric–Triboelectric Hybrid Nanogenerator for Energy Harvesting from Biomechanical and Environmental Sources. *Express Polym. Lett.* **2019**, *13*, 533–542. [CrossRef]

159. Chen, X.; Han, M.; Chen, H.; Cheng, X.; Song, Y.; Su, Z.; Jiang, Y.; Zhang, H. A Wave-Shaped Hybrid Piezoelectric and Triboelectric Nanogenerator Based on P(VDF-TrFE) Nanofibers. *Nanoscale* **2017**, *9*, 1263–1270. [CrossRef] [PubMed]

160. Zhao, C.; Zhang, Q.; Zhang, W.; Du, X.; Zhang, Y.; Gong, S.; Ren, K.; Sun, Q.; Wang, Z.L. Hybrid Piezo/Triboelectric Nanogenerator for Highly Efficient and Stable Rotation Energy Harvesting. *Nano Energy* **2019**, *57*, 440–449. [CrossRef]

161. Xia, Y.; Zhou, J.; Chen, T.; Liu, H.; Liu, W.; Yang, Z.; Wang, P.; Sun, L. A hybrid flapping-leaf microgenerator for harvesting wind-flow energy. In Proceedings of the 29th International Conference on Micro Electro Mechanical Systems (MEMS), Shanghai, China, 24–28 January 2016; pp. 1224–1227.

162. Suo, G.; Yu, Y.; Zhang, Z.; Wang, S.; Zhao, P.; Li, J.; Wang, X. Piezoelectric and Triboelectric Dual Effects in Mechanical-Energy Harvesting Using BaTiO3/Polydimethylsiloxane Composite Film. *ACS Appl. Mater. Interfaces* **2016**, *8*, 34335–34341. [CrossRef] [PubMed]

163. Guo, Y.; Zhang, X.-S.; Wang, Y.; Gong, W.; Zhang, Q.; Wang, H.; Brugger, J. All-Fiber Hybrid Piezoelectric-Enhanced Triboelectric Nanogenerator for Wearable Gesture Monitoring. *Nano Energy* **2018**, *48*, 152–160. [CrossRef]

164. Wang, X.; Yang, B.; Liu, J.; Yang, C. A Transparent and Biocompatible Single-Friction-Surface Triboelectric and Piezoelectric Generator and Body Movement Sensor. *J. Mater. Chem. A* **2017**, *5*, 1176–1183. [CrossRef]

165. Huang, T.; Wang, C.; Yu, H.; Wang, H.; Zhang, Q.; Zhu, M. Human Walking-Driven Wearable All-Fiber Triboelectric Nanogenerator Containing Electrospun Polyvinylidene Fluoride Piezoelectric Nanofibers. *Nano Energy* **2015**, *14*, 226–235. [CrossRef]

166. Chen, X.; Song, Y.; Su, Z.; Chen, H.; Cheng, X.; Zhang, J.; Han, M.; Zhang, H. Flexible Fiber-Based Hybrid Nanogenerator for Biomechanical Energy Harvesting and Physiological Monitoring. *Nano Energy* **2017**, *38*, 43–50. [CrossRef]

167. Jung, W.-S.; Kang, M.-G.; Moon, H.G.; Baek, S.-H.; Yoon, S.-J.; Wang, Z.-L.; Kim, S.-W.; Kang, C.-Y. High Output Piezo/Triboelectric Hybrid Generator. *Sci. Rep.* **2015**, *5*, 9309. [CrossRef] [PubMed]

168. Li, X.; Lin, Z.-H.; Cheng, G.; Wen, X.; Liu, Y.; Niu, S.; Wang, Z.L. 3D Fiber-Based Hybrid Nanogenerator for Energy Harvesting and as a Self-Powered Pressure Sensor. *ACS Nano* **2014**, *8*, 10674–10681. [CrossRef]

169. Zhu, J.; Hou, X.; Niu, X.; Guo, X.; Zhang, J.; He, J.; Guo, T.; Chou, X.; Xue, C.; Zhang, W. The D-Arched Piezoelectric-Triboelectric Hybrid Nanogenerator as a Self-Powered Vibration Sensor. *Sens. Actuators Phys.* **2017**, *263*, 317–325. [CrossRef]

170. Wang, L.; He, T.; Zhang, Z.; Zhao, L.; Lee, C.; Luo, G.; Mao, Q.; Yang, P.; Lin, Q.; Li, X.; et al. Self-Sustained Autonomous Wireless Sensing Based on a Hybridized TENG and PEG Vibration Mechanism. *Nano Energy* **2021**, *80*, 105555. [CrossRef]

171. Yang, X.; Li, P.; Wu, B.; Li, H.; Zhou, G. A Flexible Piezoelectric-Triboelectric Hybrid Nanogenerator in One Structure with Dual Doping Enhancement Effects. *Curr. Appl. Phys.* **2021**, *32*, 50–58. [CrossRef]

172. Wang, X.; Wang, S.; Yang, Y.; Wang, Z.L. Hybridized Electromagnetic–Triboelectric Nanogenerator for Scavenging Air-Flow Energy to Sustainably Power Temperature Sensors. *ACS Nano* **2015**, *9*, 4553–4562. [CrossRef]

173. Yang, H.; Yang, H.; Lai, M.; Xi, Y.; Guan, Y.; Liu, W.; Zeng, Q.; Lu, J.; Hu, C.; Wang, Z.L. Triboelectric and Electromagnetic Hybrid Nanogenerator Based on a Crankshaft Piston System as a Multifunctional Energy Harvesting Device. *Adv. Mater. Technol.* **2020**, *4*, 1800278. [CrossRef]

174. Wang, P.; Pan, L.; Wang, J.; Xu, M.; Dai, G.; Zou, H.; Dong, K.; Wang, Z.L. An Ultra-Low-Friction Triboelectric–Electromagnetic Hybrid Nanogenerator for Rotation Energy Harvesting and Self-Powered Wind Speed Sensor. *ACS Nano* **2018**, *12*, 9433–9440. [CrossRef]

175. Hu, Y.; Yang, J.; Niu, S.; Wu, W.; Wang, Z.L. Hybridizing Triboelectrification and Electromagnetic Induction Effects for High-Efficient Mechanical Energy Harvesting. *ACS Nano* **2014**, *8*, 7442–7450. [CrossRef]

176. Quan, T.; Wang, X.; Wang, Z.L.; Yang, Y. Hybridized Electromagnetic–Triboelectric Nanogenerator for a Self-Powered Electronic Watch. *ACS Nano* **2015**, *9*, 12301–12310. [CrossRef] [PubMed]

177. Zhang, B.; Chen, J.; Jin, L.; Deng, W.; Zhang, L.; Zhang, H.; Zhu, M.; Yang, W.; Wang, Z.L. Rotating-Disk-Based Hybridized Electromagnetic-Triboelectric Nanogenerator for Sustainably Powering Wireless Traffic Volume Sensors. *ACS Nano* **2016**, *10*, 6241–6247. [CrossRef]

178. Cao, R.; Zhou, T.; Wang, B.; Yin, Y.; Yuan, Z.; Li, C.; Wang, Z.L. Rotating-Sleeve Triboelectric–Electromagnetic Hybrid Nanogenerator for High Efficiency of Harvesting Mechanical Energy. *ACS Nano* **2017**, *11*, 8370–8378. [CrossRef]

179. Zhao, L.-C.; Zou, H.-X.; Yan, G.; Liu, F.-R.; Tan, T.; Zhang, W.-M.; Peng, Z.-K.; Meng, G. A Water-Proof Magnetically Coupled Piezoelectric-Electromagnetic Hybrid Wind Energy Harvester. *Appl. Energy* **2019**, *239*, 735–746. [CrossRef]

180. Hamid, R.; Yuce, M.R. A Wearable Energy Harvester Unit Using Piezoelectric–Electromagnetic Hybrid Technique. *Sens. Actuators Phys.* **2017**, *257*, 198–207. [CrossRef]

181. Fan, K.; Tan, Q.; Liu, H.; Zhu, Y.; Wang, W.; Zhang, D. Hybrid Piezoelectric-Electromagnetic Energy Harvester for Scavenging Energy from Low-Frequency Excitations. *Smart Mater. Struct.* **2018**, *27*, 085001. [CrossRef]

182. Toyabur, R.M.; Salauddin, M.; Cho, H.; Park, J.Y. A Multimodal Hybrid Energy Harvester Based on Piezoelectric-Electromagnetic Mechanisms for Low-Frequency Ambient Vibrations. *Energy Convers. Manag.* **2018**, *168*, 454–466. [CrossRef]

183. He, X.; Wen, Q.; Sun, Y.; Wen, Z. A Low-Frequency Piezoelectric-Electromagnetic-Triboelectric Hybrid Broadband Vibration Energy Harvester. *Nano Energy* **2017**, *40*, 300–307. [CrossRef]

184. Rodrigues, C.; Gomes, A.; Ghosh, A.; Pereira, A.; Ventura, J. Power-Generating Footwear Based on a Triboelectric-Electromagnetic-Piezoelectric Hybrid Nanogenerator. *Nano Energy* **2019**, *62*, 660–666. [CrossRef]

185. Hemojit Singh, H.; Kumar, D.; Khare, N. A Synchronous Piezoelectric–Triboelectric–Electromagnetic Hybrid Generator for Harvesting Vibration Energy. Sustain. *Energy Fuels* **2021**, *5*, 212–218. [CrossRef]

186. Wang, S.; Wang, Z.L.; Yang, Y. A One-Structure-Based Hybridized Nanogenerator for Scavenging Mechanical and Thermal Energies by Triboelectric-Piezoelectric-Pyroelectric Effects. *Adv. Mater. Deerfield Beach Fla* **2016**, *28*, 2881–2887. [CrossRef]

187. Zheng, H.; Zi, Y.; He, X.; Guo, H.; Lai, Y.-C.; Wang, J.; Zhang, S.L.; Wu, C.; Cheng, G.; Wang, Z.L. Concurrent Harvesting of Ambient Energy by Hybrid Nanogenerators for Wearable Self-Powered Systems and Active Remote Sensing. *ACS Appl. Mater. Interfaces* **2018**, *10*, 14708–14715. [CrossRef]

188. Xu, C.; Wang, X.; Wang, Z.L. Nanowire Structured Hybrid Cell for Concurrently Scavenging Solar and Mechanical Energies. *J. Am. Chem. Soc.* **2009**, *131*, 5866–5872. [CrossRef]

189. Xu, C.; Wang, Z.L. Compact Hybrid Cell Based on a Convoluted Nanowire Structure for Harvesting Solar and Mechanical Energy. *Adv. Mater.* **2011**, *23*, 873–877. [CrossRef]

190. Yoon, G.C.; Shin, K.-S.; Gupta, M.K.; Lee, K.Y.; Lee, J.-H.; Wang, Z.L.; Kim, S.-W. High-Performance Hybrid Cell Based on an Organic Photovoltaic Device and a Direct Current Piezoelectric Nanogenerator. *Nano Energy* **2015**, *12*, 547–555. [CrossRef]

191. Liu, G.; Mrad, N.; Abdel-Rahman, E.; Ban, D. Cascade-Type Hybrid Energy Cells for Driving Wireless Sensors. *Nano Energy* **2016**, *26*, 641–647. [CrossRef]

192. Yang, Y.; Zhang, H.; Zhu, G.; Lee, S.; Lin, Z.-H.; Wang, Z.L. Flexible Hybrid Energy Cell for Simultaneously Harvesting Thermal, Mechanical, and Solar Energies. *ACS Nano* **2013**, *7*, 785–790. [CrossRef] [PubMed]

193. Pan, C.; Li, Z.; Guo, W.; Zhu, J.; Wang, Z.L. Fiber-Based Hybrid Nanogenerators for/as Self-Powered Systems in Biological Liquid. *Angew. Chem. Int. Ed. Engl.* **2011**, *50*, 11192–11196. [CrossRef] [PubMed]

194. Hansen, B.J.; Liu, Y.; Yang, R.; Wang, Z.L. Hybrid Nanogenerator for Concurrently Harvesting Biomechanical and Biochemical Energy. *ACS Nano* **2010**, *4*, 3647–3652. [CrossRef] [PubMed]

195. Wu, Y.; Zhong, X.; Wang, X.; Yang, Y.; Wang, Z.L. Hybrid Energy Cell for Simultaneously Harvesting Wind, Solar, and Chemical Energies. *Nano Res.* **2014**, *7*, 1631–1639. [CrossRef]

196. Zheng, L.; Lin, Z.-H.; Cheng, G.; Wu, W.; Wen, X.; Lee, S.; Wang, Z. Silicon-Based Hybrid Cell for Harvesting Solar Energy and Raindrop Electrostatic Energy. *Nano Energy* **2014**, *9*, 291–300. [CrossRef]

197. Yang, Y.; Zhang, H.; Liu, Y.; Lin, Z.-H.; Lee, S.; Lin, Z.; Wong, C.P.; Wang, Z.L. Silicon-Based Hybrid Energy Cell for Self-Powered Electrodegradation and Personal Electronics. *ACS Nano* **2013**, *7*, 2808–2813. [CrossRef] [PubMed]

198. Dudem, B.; Ko, Y.H.; Leem, J.W.; Lim, J.H.; Yu, J.S. Hybrid Energy Cell with Hierarchical Nano/Micro-Architectured Polymer Film to Harvest Mechanical, Solar, and Wind Energies Individually/Simultaneously. *ACS Appl. Mater. Interfaces* **2016**, *8*, 30165–30175. [CrossRef] [PubMed]

199. Wang, S.; Wang, X.; Wang, Z.L.; Yang, Y. Efficient Scavenging of Solar and Wind Energies in a Smart City. *ACS Nano* **2016**, *10*, 5696–5700. [CrossRef] [PubMed]

200. Wang, X.; Wang, Z.L.; Yang, Y. Hybridized Nanogenerator for Simultaneously Scavenging Mechanical and Thermal Energies by Electromagnetic-Triboelectric-Thermoelectric Effects. *Nano Energy* **2016**, *26*, 164–171. [CrossRef]

201. Kim, M.-K.; Kim, M.-S.; Jo, S.-E.; Kim, Y.-J. Triboelectric–Thermoelectric Hybrid Nanogenerator for Harvesting Frictional Energy. *Smart Mater. Struct.* **2016**, *25*, 125007. [CrossRef]

202. Kim, H.; Sohn, C.; Hwang, G.-T.; Park, K.-I.; Jeong, C.K. (K,Na)NbO3-LiNbO3 Nanocube-Based Flexible and Lead-Free Piezoelectric Nanocomposite Energy Harvesters. *J. Korean Ceram. Soc.* **2020**, *57*, 401–408. [CrossRef]

203. Mimura, K.; Liu, Z.; Itasaka, H.; Lin, Y.-C.; Suenaga, K.; Kato, K. One-Step Synthesis of BaTiO3/CaTiO3 Core-Shell Nanocubes by Hydrothermal Reaction. *J. Asian Ceram. Soc.* **2021**, *9*, 359–365. [CrossRef]

204. Mimura, K.; Kato, K.; Imai, H.; Wada, S.; Haneda, H.; Kuwabara, M. Piezoresponse Properties of Orderly Assemblies of BaTiO3 and SrTiO3 Nanocube Single Crystals. *Appl. Phys. Lett.* **2012**, *101*, 012901. [CrossRef]

205. Rovisco, A.; dos Santos, A.; Cramer, T.; Martins, J.; Branquinho, R.; Águas, H.; Fraboni, B.; Fortunato, E.; Martins, R.; Igreja, R.; et al. Piezoelectricity Enhancement of Nanogenerators Based on PDMS and ZnSnO3 Nanowires through Microstructuration. *ACS Appl. Mater. Interfaces* **2020**, *12*, 18421–18430. [CrossRef]

206. Qin, W.; Zhou, P.; Qi, Y.; Zhang, T. Lead-Free Bi3.15Nd0.85Ti3O12 Nanoplates Filler-Elastomeric Polymer Composite Films for Flexible Piezoelectric Energy Harvesting. *Micromachines* **2020**, *11*, 966. [CrossRef] [PubMed]

207. Ma, S.W.; Fan, Y.J.; Li, H.Y.; Su, L.; Wang, Z.L.; Zhu, G. Flexible Porous Polydimethylsiloxane/Lead Zirconate Titanate-Based Nanogenerator Enabled by the Dual Effect of Ferroelectricity and Piezoelectricity. *ACS Appl. Mater. Interfaces* **2018**, *10*, 33105–33111. [CrossRef]

208. Jeronimo, K.; Koutsos, V.; Cheung, R.; Mastropaolo, E. PDMS-ZnO Piezoelectric Nanocomposites for Pressure Sensors. *Sensors* **2021**, *21*, 5873. [CrossRef] [PubMed]

209. Zhang, J.; He, Y.; Boyer, C.; Kalantar-Zadeh, K.; Peng, S.; Chu, D.; Wang, C.H. Recent Developments of Hybrid Piezo–Triboelectric Nanogenerators for Flexible Sensors and Energy Harvesters. *Nanoscale Adv.* **2021**, *3*, 5465–5486. [CrossRef]

210. Hajra, S.; Padhan, A.M.; Sahu, M.; Alagarsamy, P.; Lee, K.; Kim, H.J. Lead-Free Flexible Bismuth Titanate-PDMS Composites: A Multifunctional Colossal Dielectric Material for Hybrid Piezo-Triboelectric Nanogenerator to Sustainably Power Portable Electronics. *Nano Energy* **2021**, *89*, 106316. [CrossRef]

211. He, W.; Qian, Y.; Lee, B.S.; Zhang, F.; Rasheed, A.; Jung, J.-E.; Kang, D.J. Ultrahigh Output Piezoelectric and Triboelectric Hybrid Nanogenerators Based on ZnO Nanoflakes/Polydimethylsiloxane Composite Films. *ACS Appl. Mater. Interfaces* **2018**, *10*, 44415–44420. [CrossRef] [PubMed]

212. Pongampai, S.; Charoonsuk, T.; Pinpru, N.; Pulphol, P.; Vittayakorn, W.; Pakawanit, P.; Vittayakorn, N. Triboelectric-Piezoelectric Hybrid Nanogenerator Based on BaTiO3-Nanorods/Chitosan Enhanced Output Performance with Self-Charge-Pumping System. *Compos. Part B Eng.* **2021**, *208*, 108602. [CrossRef]

213. Zi, Y.; Lin, L.; Wang, J.; Wang, S.; Chen, J.; Fan, X.; Yang, P.-K.; Yi, F.; Wang, Z.L. Triboelectric–Pyroelectric–Piezoelectric Hybrid Cell for High-Efficiency Energy-Harvesting and Self-Powered Sensing. *Adv. Mater.* **2020**, *27*, 2340–2347. [CrossRef] [PubMed]

214. Minhas, J.Z.; Hasan, M.A.M.; Yang, Y. Ferroelectric Materials Based Coupled Nanogenerators. *Nanoenergy Adv.* **2021**, *1*, 131–180. [CrossRef]

215. Wang, H.; Ma, Y.; Yang, H.; Jiang, H.; Ding, Y.; Xie, H. MEMS Ultrasound Transducers for Endoscopic Photoacoustic Imaging Applications. *Micromachines* **2020**, *11*, 928. [CrossRef] [PubMed]

216. Dangi, A.; Agrawal, S.; Kothapalli, S.-R. Lithium Niobate-Based Transparent Ultrasound Transducers for Photoacoustic Imaging. *Opt. Lett.* **2019**, *44*, 5326–5329. [CrossRef] [PubMed]

217. Qiu, Y.; Gigliotti, J.V.; Wallace, M.; Griggio, F.; Demore, C.E.M.; Cochran, S.; Trolier-McKinstry, S. Piezoelectric Micromachined Ultrasound Transducer (PMUT) Arrays for Integrated Sensing, Actuation and Imaging. *Sensors* **2015**, *15*, 8020–8041. [CrossRef] [PubMed]

218. Dangi, A.; Cheng, C.Y.; Agrawal, S.; Tiwari, S.; Datta, G.R.; Benoit, R.R.; Pratap, R.; Trolier-Mckinstry, S.; Kothapalli, S.-R. A Photoacoustic Imaging Device Using Piezoelectric Micromachined Ultrasound Transducers (PMUTs). *IEEE Trans. Ultrason. Ferroelectr. Freq. Control* **2020**, *67*, 801–809. [CrossRef] [PubMed]

219. WindEurope Homepage. Available online: https://windeurope.org/ (accessed on 12 December 2021).

220. Energy Harvesting: Solar, Wind, and Ocean Energy Conversion Systems. Available online: https://www.routledge.com/Energy-Harvesting-Solar-Wind-and-Ocean-Energy-Conversion-Systems/Khaligh-Onar/p/book/9781439815083 (accessed on 4 December 2021).

221. Wang, H.; Xu, L.; Wang, Z. Advances of High-Performance Triboelectric Nanogenerators for Blue Energy Harvesting. *Nanoenergy Adv.* **2021**, *1*, 32–57. [CrossRef]

222. Zhao, L.; Yang, Y. Toward Small-Scale Wind Energy Harvesting: Design, Enhancement, Performance Comparison, and Applicability. Available online: https://www.hindawi.com/journals/sv/2017/3585972/ (accessed on 23 May 2020).

223. Xu, C.; Pan, C.; Liu, Y.; Wang, Z.L. Hybrid Cells for Simultaneously Harvesting Multi-Type Energies for Self-Powered Micro/Nanosystems. *Nano Energy* **2012**, *1*, 259–272. [CrossRef]

224. Lai, Z.H.; Wang, J.L.; Zhang, C.L.; Zhang, G.Q.; Yurchenko, D. Harvest Wind Energy from a Vibro-Impact DEG Embedded into a Bluff Body. *Energy Convers. Manag.* **2019**, *199*, 111993. [CrossRef]

225. Zhao, L.-C.; Zou, H.-X.; Yan, G.; Liu, F.-R.; Tan, T.; Wei, K.-X.; Zhang, W.-M. Magnetic Coupling and Flextensional Amplification Mechanisms for High-Robustness Ambient Wind Energy Harvesting. *Energy Convers. Manag.* **2019**, *201*, 112166. [CrossRef]

226. Wang, X.; Pan, C.L.; Liu, Y.B.; Feng, Z.H. Electromagnetic Resonant Cavity Wind Energy Harvester with Optimized Reed Design and Effective Magnetic Loop. *Sens. Actuators Phys.* **2014**, *205*, 63–71. [CrossRef]

227. Emirates Aviation University; Aljadiri, R.T.; Taha, L.Y.; Windsor University; Ivey, P. Birmingham City University Electrostatic Energy Harvesting Systems: A Better Understanding of Their SustainabilityElectrostatic Energy Harvesting Systems: A Better Understanding of Their Sustainability. *J. Clean Energy Technol.* **2017**, *5*, 409–416. [CrossRef]

228. Bryant, M.; Garcia, E. Modeling and Testing of a Novel Aeroelastic Flutter Energy Harvester. *J. Vib. Acoust.* **2011**, *133*, 011010. [CrossRef]

229. Dai, H.L.; Abdelmoula, H.; Abdelkefi, A.; Wang, L. Towards Control of Cross-Flow-Induced Vibrations Based on Energy Harvesting. *Nonlinear Dyn.* **2017**, *88*, 2329–2346. [CrossRef]

230. Hu, G.; Tse, K.T.; Wei, M.; Naseer, R.; Abdelkefi, A.; Kwok, K.C.S. Experimental Investigation on the Efficiency of Circular Cylinder-Based Wind Energy Harvester with Different Rod-Shaped Attachments. *Appl. Energy* **2018**, *226*, 682–689. [CrossRef]

231. Usman, M.; Hanif, A.; Kim, I.-H.; Jung, H.-J. Experimental Validation of a Novel Piezoelectric Energy Harvesting System Employing Wake Galloping Phenomenon for a Broad Wind Spectrum. *Energy* **2018**, *153*, 882–889. [CrossRef]

232. Wang, J.; Tang, L.; Zhao, L.; Zhang, Z. Efficiency Investigation on Energy Harvesting from Airflows in HVAC System Based on Galloping of Isosceles Triangle Sectioned Bluff Bodies. *Energy* **2019**, *172*, 1066–1078. [CrossRef]

233. Wang, J.; Zhou, S.; Zhang, Z.; Yurchenko, D. High-Performance Piezoelectric Wind Energy Harvester with Y-Shaped At-tachments. *Energy Convers. Manag.* **2019**, *181*, 645–652. [CrossRef]

234. Zhou, S.; Wang, J. Erratum: "Dual Serial Vortex-Induced Energy Harvesting System for Enhanced Energy Harvesting". *AIP Adv.* **2018**, *8*, 089901. [CrossRef]

235. Jirayupat, C.; Wongwiriyapan, W.; Kasamechonchung, P.; Wutikhun, T.; Tantisantisom, K.; Rayanasukha, Y.; Jiemsakul, T.; Tansarawiput, C.; Liangruksa, M.; Khanchaitit, P.; et al. Piezoelectric-Induced Triboelectric Hybrid Nanogenerators Based on the ZnO Nanowire Layer Decorated on the Au/Polydimethylsiloxane–Al Structure for Enhanced Triboelectric Performance. *ACS Appl. Mater. Interfaces* **2018**, *10*, 6433–6440. [CrossRef]

236. Han, M.; Zhang, X.-S.; Meng, B.; Liu, W.; Tang, W.; Sun, X.; Wang, W.; Zhang, H. R-Shaped Hybrid Nanogenerator with Enhanced Piezoelectricity. *ACS Nano* **2013**, *7*, 8554–8560. [CrossRef]

237. Dai, H.L.; Abdelkefi, A.; Wang, L. Theoretical Modeling and Nonlinear Analysis of Piezoelectric Energy Harvesting from Vortex-Induced Vibrations. *J. Intell. Mater. Syst. Struct.* **2020**, *25*, 1861–1874. [CrossRef]

238. Abdelkefi, A. Aeroelastic Energy Harvesting: A Review. *Int. J. Eng. Sci.* **2016**, *100*, 112–135. [CrossRef]

239. Yang, K.; Wang, J.; Yurchenko, D. A Double-Beam Piezo-Magneto-Elastic Wind Energy Harvester for Improving the Galloping-Based Energy Harvesting. *Appl. Phys. Lett.* **2020**, *115*, 193901. [CrossRef]

240. Challa, V.R.; Prasad, M.G.; Fisher, F.T. A Coupled Piezoelectric–Electromagnetic Energy Harvesting Technique for Achieving Increased Power Output through Damping Matching. *Smart Mater. Struct.* **2009**, *18*, 095029. [CrossRef]

241. Naseer, R.; Dai, H.L.; Abdelkefi, A.; Wang, L. Piezomagnetoelastic Energy Harvesting from Vortex-Induced Vibrations Using Monostable Characteristics. *Appl. Energy* **2017**, *203*, 142–153. [CrossRef]

242. Huang, L.; Xu, W.; Bai, G.; Wong, M.-C.; Yang, Z.; Hao, J. Wind Energy and Blue Energy Harvesting Based on Magnetic-Assisted Noncontact Triboelectric Nanogenerator. *Nano Energy* **2016**, *30*, 36–42. [CrossRef]

243. Su, Y.; Wen, X.; Zhu, G.; Yang, J.; Bai, P.; Wu, Z.; Jiang, Y.; Wang, Z. Hybrid Triboelectric Nanogenerator for Harvesting Water Wave Energy and as a Self-Powered Distress Signal Emitter. *Nano Energy* **2014**, *9*, 186–195. [CrossRef]

244. Wang, X.; Wen, Z.; Guo, H.; Wu, C.; He, X.; Lin, L.; Cao, X.; Wang, Z.L. Fully Packaged Blue Energy Harvester by Hybridizing a Rolling Triboelectric Nanogenerator and an Electromagnetic Generator. *ACS Nano* **2016**, *10*, 11369–11376. [CrossRef]

245. Wen, Z.; Guo, H.; Zi, Y.; Yeh, M.-H.; Wang, X.; Deng, J.; Wang, J.; Li, S.; Hu, C.; Zhu, L.; et al. Harvesting Broad Frequency Band Blue Energy by a Triboelectric–Electromagnetic Hybrid Nanogenerator. *ACS Nano* **2016**, *10*, 6526–6534. [CrossRef]

246. Shao, H.; Wen, Z.; Cheng, P.; Sun, N.; Shen, Q.; Zhou, C.; Peng, M.; Yang, Y.; Xie, X.; Sun, X. Multifunctional Power Unit by Hybridizing Contact-Separate Triboelectric Nanogenerator, Electromagnetic Generator and Solar Cell for Harvesting Blue Energy. *Nano Energy* **2017**, *39*, 608–615. [CrossRef]

247. Zhu, J.; Wang, A.; Hu, H.; Zhu, H. Hybrid Electromagnetic and Triboelectric Nanogenerators with Multi-Impact for Wideband Frequency Energy Harvesting. *Energies* **2017**, *10*, 2024. [CrossRef]

248. Shao, H.; Cheng, P.; Chen, R.; Xie, L.; Sun, N.; Shen, Q.; Chen, X.; Zhu, Q.; Zhang, Y.; Liu, Y.; et al. Triboelectric–Electromagnetic Hybrid Generator for Harvesting Blue Energy. *Nano Micro Lett.* **2018**, *10*, 54. [CrossRef]

249. Wang, H.; Zhu, Q.; Ding, Z.; Li, Z.; Zheng, H.; Fu, J.; Diao, C.; Zhang, X.; Tian, J.; Zi, Y. A Fully-Packaged Ship-Shaped Hybrid Nanogenerator for Blue Energy Harvesting toward Seawater Self-Desalination and Self-Powered Positioning. *Nano Energy* **2019**, *57*, 616–624. [CrossRef]

250. Guo, H.; Wen, Z.; Zi, Y.; Yeh, M.-H.; Wang, J.; Zhu, L.; Hu, C.; Wang, Z.L. A Water-Proof Triboelectric–Electromagnetic Hybrid Generator for Energy Harvesting in Harsh Environments. *Adv. Energy Mater.* **2020**, *6*, 1501593. [CrossRef]

251. Sun, T.; Tasnim, F.; McIntosh, R.T.; Amiri, N.; Solav, D.; Anbarani, M.T.; Sadat, D.; Zhang, L.; Gu, Y.; Karami, M.A.; et al. Decoding of Facial Strains via Conformable Piezoelectric Interfaces. *Nat. Biomed. Eng.* **2020**, *4*, 954–972. [CrossRef] [PubMed]

252. Fernandez, S.V.; Cai, F.; Chen, S.; Suh, E.; Tiepelt, J.; McIntosh, R.; Marcus, C.; Acosta, D.; Mejorado, D.; Dagdeviren, C. On-Body Piezoelectric Energy Harvesters through Innovative Designs and Conformable Structures. *ACS Biomater. Sci. Eng.* 2021; *in press*. [CrossRef] [PubMed]

253. Dhakar, L.; Pitchappa, P.; Tay, F.E.H.; Lee, C. An Intelligent Skin Based Self-Powered Finger Motion Sensor Integrated with Triboelectric Nanogenerator. *Nano Energy* **2016**, *19*, 532–540. [CrossRef]

254. Zhang, N.; Tao, C.; Fan, X.; Chen, J. Progress in Triboelectric Nanogenerators as Self-Powered Smart Sensors. *J. Mater. Res.* **2017**, *32*, 1628–1646. [CrossRef]

255. Zhang, H.; Yang, Y.; Hou, T.-C.; Su, Y.; Hu, C.; Wang, Z.L. Triboelectric Nanogenerator Built inside Clothes for Self-Powered Glucose Biosensors. *Nano Energy* **2013**, *2*, 1019–1024. [CrossRef]

256. Shawon, S.M.A.Z.; Sun, A.X.; Vega, V.S.; Chowdhury, B.D.; Tran, P.; Carballo, Z.D.; Tolentino, J.A.; Li, J.; Rafaqut, M.S.; Danti, S.; et al. Piezo-Tribo Dual Effect Hybrid Nanogenerators for Health Monitoring. *Nano Energy* **2021**, *82*, 105691. [CrossRef]

257. Tang, G.; Shi, Q.; Zhang, Z.; He, T.; Sun, Z.; Lee, C. Hybridized Wearable Patch as a Multi-Parameter and Multi-Functional Human-Machine Interface. *Nano Energy* **2021**, *81*, 105582. [CrossRef]

258. Fang, H.; Zhao, J.; Yu, K.J.; Song, E.; Farimani, A.B.; Chiang, C.-H.; Jin, X.; Xue, Y.; Xu, D.; Du, W.; et al. Ultrathin, Transferred Layers of Thermally Grown Silicon Dioxide as Biofluid Barriers for Biointegrated Flexible Electronic Systems. *Proc. Natl. Acad. Sci. USA* **2016**, *113*, 11682–11687. [CrossRef]

259. Wu, C.-Y.; Liao, R.-M.; Lai, L.-W.; Jeng, M.-S.; Liu, D.-S. Organosilicon/Silicon Oxide Gas Barrier Structure Encapsulated Flexible Plastic Substrate by Using Plasma-Enhanced Chemical Vapor Deposition. *Surf. Coat. Technol.* **2012**, *206*, 4685–4691. [CrossRef]

260. Song, E.; Fang, H.; Jin, X.; Zhao, J.; Jiang, C.; Yu, K.J.; Zhong, Y.; Xu, D.; Li, J.; Fang, G.; et al. Thin, Transferred Layers of Silicon Dioxide and Silicon Nitride as Water and Ion Barriers for Implantable Flexible Electronic Systems. *Adv. Electron. Mater.* **2017**, *3*, 1700077. [CrossRef]

261. Carcia, P.F.; McLean, R.S.; Reilly, M.H.; Groner, M.D.; George, S.M. Ca Test of Al2O3 Gas Diffusion Barriers Grown by Atomic Layer Deposition on Polymers. *Appl. Phys. Lett.* **2006**, *89*, 031915. [CrossRef]

262. Li, J.; Li, R.; Du, H.; Zhong, Y.; Chen, Y.; Nan, K.; Won, S.M.; Zhang, J.; Huang, Y.; Rogers, J.A. Ultrathin, Transferred Layers of Metal Silicide as Faradaic Electrical Interfaces and Biofluid Barriers for Flexible Bioelectronic Implants. *ACS Nano* **2019**, *13*, 660–670. [CrossRef] [PubMed]

263. Behrendt, A.; Friedenberger, C.; Gahlmann, T.; Trost, S.; Becker, T.; Zilberberg, K.; Polywka, A.; Görrn, P.; Riedl, T. Highly Robust Transparent and Conductive Gas Diffusion Barriers Based on Tin Oxide. *Adv. Mater.* **2015**, *27*, 5961–5967. [CrossRef]

264. Zheng, Q.; Shi, B.; Li, Z.; Wang, Z.L. Recent Progress on Piezoelectric and Triboelectric Energy Harvesters in Biomedical Systems. *Adv. Sci.* **2017**, *4*, 1700029. [CrossRef] [PubMed]

265. Shi, B.; Li, Z.; Fan, Y. Implantable Energy-Harvesting Devices. *Adv. Mater.* **2018**, *30*, 1801511. [CrossRef] [PubMed]

266. Han, S.A.; Lee, J.-H.; Seung, W.; Lee, J.; Kim, S.-W.; Kim, J.H. Patchable and Implantable 2D Nanogenerator. *Small* **2021**, *17*, 1903519. [CrossRef] [PubMed]

267. Dong, L.; Jin, C.; Closson, A.B.; Trase, I.; Richards, H.C.; Chen, Z.; Zhang, J.X.J. Cardiac Energy Harvesting and Sensing Based on Piezoelectric and Triboelectric Designs. *Nano Energy* **2020**, *76*, 105076. [CrossRef]

268. Zhang, G.; Li, M.; Li, H.; Wang, Q.; Jiang, S. Harvesting Energy from Human Activity: Ferroelectric Energy Harvesters for Portable, Implantable, and Biomedical Electronics. *Energy Technol.* **2018**, *6*, 791–812. [CrossRef]

269. Dagdeviren, C.; Yang, B.D.; Su, Y.; Tran, P.L.; Joe, P.; Anderson, E.; Xia, J.; Doraiswamy, V.; Dehdashti, B.; Feng, X.; et al. Conformal Piezoelectric Energy Harvesting and Storage from Motions of the Heart, Lung, and Diaphragm. *Proc. Natl. Acad. Sci. USA* **2014**, *111*, 1927–1932. [CrossRef] [PubMed]

270. Dagdeviren, C.; Shi, Y.; Joe, P.; Ghaffari, R.; Balooch, G.; Usgaonkar, K.; Gur, O.; Tran, P.L.; Crosby, J.R.; Meyer, M.; et al. Conformal Piezoelectric Systems for Clinical and Experimental Characterization of Soft Tissue Biomechanics. *Nat. Mater.* **2015**, *14*, 728–736. [CrossRef] [PubMed]

271. Zhang, H.; Zhang, X.-S.; Cheng, X.; Liu, Y.; Han, M.; Xue, X.; Wang, S.; Yang, F.; Smitha, S.A.; Zhang, H.; et al. A Flexible and Implantable Piezoelectric Generator Harvesting Energy from the Pulsation of Ascending Aorta: In Vitro and In Vivo Studies. *Nano Energy* **2015**, *12*, 296–304. [CrossRef]

272. Yang, R.; Qin, Y.; Li, C.; Zhu, G.; Wang, Z.L. Converting Biomechanical Energy into Electricity by a Muscle-Movement-Driven Nanogenerator. *Nano Lett.* **2009**, *9*, 1201–1205. [CrossRef] [PubMed]

273. Li, Z.; Zhu, G.; Yang, R.; Wang, A.C.; Wang, Z.L. Muscle-Driven in Vivo Nanogenerator. *Adv. Mater. Deerfield Beach Fla* **2010**, *22*, 2534–2537. [CrossRef] [PubMed]

274. Hwang, G.-T.; Park, H.; Lee, J.-H.; Oh, S.; Park, K.-I.; Byun, M.; Park, H.; Ahn, G.; Jeong, C.K.; No, K.; et al. Self-Powered Cardiac Pacemaker Enabled by Flexible Single Crystalline PMN-PT Piezoelectric Energy Harvester. *Adv. Mater.* **2014**, *26*, 4880–4887. [CrossRef]

275. Liu, Z.; Li, H.; Shi, B.; Fan, Y.; Wang, Z.L.; Li, Z. Wearable and Implantable Triboelectric Nanogenerators. *Adv. Funct. Mater.* **2019**, *29*, 1808820. [CrossRef]

276. Ouyang, H.; Liu, Z.; Li, N.; Shi, B.; Zou, Y.; Xie, F.; Ma, Y.; Li, Z.; Li, H.; Zheng, Q.; et al. Symbiotic Cardiac Pacemaker. *Nat. Commun.* **2019**, *10*, 1821. [CrossRef] [PubMed]

277. Shi, Q.; He, T.; Lee, C. More than Energy Harvesting—Combining Triboelectric Nanogenerator and Flexible Electronics Technology for Enabling Novel Micro-/Nano-Systems. *Nano Energy* **2019**, *57*, 851–871. [CrossRef]

278. Maiti, S.; Karan, S.K.; Kim, J.K.; Khatua, B.B. Nature Driven Bio-Piezoelectric/Triboelectric Nanogenerator as Next-Generation Green Energy Harvester for Smart and Pollution Free Society. *Adv. Energy Mater.* **2019**, *9*, 1803027. [CrossRef]

279. Ryu, H.; Park, H.-M.; Kim, M.-K.; Kim, B.; Myoung, H.S.; Kim, T.Y.; Yoon, H.-J.; Kwak, S.S.; Kim, J.; Hwang, T.H.; et al. Self-Rechargeable Cardiac Pacemaker System with Triboelectric Nanogenerators. *Nat. Commun.* **2021**, *12*, 4374. [CrossRef] [PubMed]

280. Zheng, Q.; Shi, B.; Fan, F.; Wang, X.; Yan, L.; Yuan, W.; Wang, S.; Liu, H.; Li, Z.; Wang, Z.L. In Vivo Powering of Pacemaker by Breathing-Driven Implanted Triboelectric Nanogenerator. *Adv. Mater.* **2014**, *26*, 5851–5856. [CrossRef] [PubMed]

281. Dagdeviren, C.; Li, Z.; Wang, Z.L. Energy Harvesting from the Animal/Human Body for Self-Powered Electronics. *Annu. Rev. Biomed. Eng.* **2017**, *19*, 85–108. [CrossRef] [PubMed]

282. Falconi, C.; Mandal, S. Interface Electronics: State-of-the-Art, Opportunities and Needs. *Sens. Actuators Phys.* **2019**, *296*, 24–30. [CrossRef]

283. Falconi, C.; Martinelli, E.; Di Natale, C.; D'Amico, A.; Maloberti, F.; Malcovati, P.; Baschirotto, A.; Stornelli, V.; Ferri, G. Electronic Interfaces. *Sens. Actuators B Chem.* **2007**, *121*, 295–329. [CrossRef]

284. Ponmozhi, J.; Frias, C.; Marques, T.; Frazão, O. Smart Sensors/Actuators for Biomedical Applications: Review. *Measurement* **2012**, *45*, 1675–1688. [CrossRef]

285. Schiavone, G.; Fallegger, F.; Kang, X.; Barra, B.; Vachicouras, N.; Roussinova, E.; Furfaro, I.; Jiguet, S.; Seáñez, I.; Borgognon, S.; et al. Soft, Implantable Bioelectronic Interfaces for Translational Research. *Adv. Mater.* **2020**, *32*, 1906512. [CrossRef]

286. Fallegger, F.; Schiavone, G.; Lacour, S. Conformable Hybrid Systems for Implantable Bioelectronic Interfaces. *Adv. Mater.* **2019**, *32*, 1903904. [CrossRef]

287. Liang, J.; Liao, W.-H. Energy Flow in Piezoelectric Energy Harvesting Systems. *Smart Mater. Struct.* **2010**, *20*, 015005. [CrossRef]

288. Li, P.; Wen, Y.; Jia, C.; Li, X. A Magnetoelectric Composite Energy Harvester and Power Management Circuit. *IEEE Trans. Ind. Electron.* **2011**, *58*, 2944–2951. [CrossRef]

289. Li, P.; Wen, Y.; Yin, W.; Wu, H. An Upconversion Management Circuit for Low-Frequency Vibrating Energy Harvesting. *IEEE Trans. Ind. Electron.* **2014**, *61*, 3349–3358. [CrossRef]

290. Guyomar, D.; Lallart, M. Recent Progress in Piezoelectric Conversion and Energy Harvesting Using Nonlinear Electronic Interfaces and Issues in Small Scale Implementation. *Micromachines* **2011**, *2*, 274–294. [CrossRef]

291. Szarka, G.D.; Stark, B.H.; Burrow, S.G. Review of Power Conditioning for Kinetic Energy Harvesting Systems. *IEEE Trans. Power Electron.* **2012**, *27*, 803–815. [CrossRef]

292. Dicken, J.; Mitcheson, P.D.; Stoianov, I.; Yeatman, E.M. Power-Extraction Circuits for Piezoelectric Energy Harvesters in Miniature and Low-Power Applications. *IEEE Trans. Power Electron.* **2012**, *27*, 4514–4529. [CrossRef]

293. Dell'Anna, F.; Dong, T.; Li, P.; Wen, Y.; Yang, Z.; Casu, M.R.; Azadmehr, M.; Berg, Y. State-of-the-Art Power Management Circuits for Piezoelectric Energy Harvesters. *IEEE Circuits Syst. Mag.* **2018**, *18*, 27–48. [CrossRef]

294. Lefeuvre, E.; Badel, A.; Richard, C.; Petit, L.; Guyomar, D. A Comparison between Several Vibration-Powered Piezoelectric Generators for Standalone Systems. *Sens. Actuators Phys.* **2006**, *126*, 405–416. [CrossRef]

295. Krihely, N.; Ben-Yaakov, S. Self-Contained Resonant Rectifier for Piezoelectric Sources Under Variable Mechanical Excitation. *IEEE Trans. Power Electron.* **2011**, *26*, 612–621. [CrossRef]

296. Long, Z.; Wang, X.; Li, P.; Wang, B.; Zhang, X.; Chung, H.S.-H.; Yang, Z. Self-Powered SSDCI Array Interface for Multiple Piezoelectric Energy Harvesters. *IEEE Trans. Power Electron.* **2021**, *36*, 9093–9104. [CrossRef]

297. Tang, L.; Yang, Y. Analysis of Synchronized Charge Extraction for Piezoelectric Energy Harvesting. *Smart Mater. Struct.* **2011**, *20*, 085022. [CrossRef]

298. Lefeuvre, E.; Badel, A.; Brenes, A.; Seok, S.; Yoo, C.-S. Power and Frequency Bandwidth Improvement of Piezoelectric Energy Harvesting Devices Using Phase-Shifted Synchronous Electric Charge Extraction Interface Circuit. *J. Intell. Mater. Syst. Struct.* **2017**, *28*, 2988–2995. [CrossRef]

299. Garbuio, L.; Lallart, M.; Guyomar, D.; Richard, C.; Audigier, D. Mechanical Energy Harvester with Ultralow Threshold Rectification Based on SSHI Nonlinear Technique. *IEEE Trans. Ind. Electron.* **2009**, *56*, 1048–1056. [CrossRef]

300. Lallart, M.; Garbuio, L.; Petit, L.; Richard, C.; Guyomar, D. Double Synchronized Switch Harvesting (DSSH): A New Energy Harvesting Scheme for Efficient Energy Extraction. *IEEE Trans. Ultrason. Ferroelectr. Freq. Control* **2008**, *55*, 2119–2130. [CrossRef]

301. Shen, H.; Qiu, J.; Ji, H.; Zhu, K.; Balsi, M. Enhanced Synchronized Switch Harvesting: A New Energy Harvesting Scheme for Efficient Energy Extraction. *Smart Mater. Struct.* **2010**, *19*, 115017. [CrossRef]

302. Lallart, M.; Guyomar, D. Piezoelectric Conversion and Energy Harvesting Enhancement by Initial Energy Injection. *Appl. Phys. Lett.* **2010**, *97*, 014104. [CrossRef]

303. Sankman, J.; Ma, D. A 12-MW to 1.1-MW AIM Piezoelectric Energy Harvester for Time-Varying Vibrations With 450-NA\bm Q. IEEE Trans. *Power Electron.* **2015**, *30*, 632–643. [CrossRef]

304. Wang, S.; Lin, Z.-H.; Niu, S.; Lin, L.; Xie, Y.; Pradel, K.C.; Wang, Z.L. Motion Charged Battery as Sustainable Flexible-Power-Unit. *ACS Nano* **2013**, *7*, 11263–11271. [CrossRef] [PubMed]

305. Zi, Y.; Niu, S.; Wang, J.; Wen, Z.; Tang, W.; Wang, Z.L. Standards and Figure-of-Merits for Quantifying the Performance of Triboelectric Nanogenerators. *Nat. Commun.* **2015**, *6*, 8376. [CrossRef] [PubMed]

306. Hu, Y.; Yue, Q.; Lu, S.; Yang, D.; Shi, S.; Zhang, X.; Yu, H. An Adaptable Interface Conditioning Circuit Based on Triboelectric Nanogenerators for Self-Powered Sensors. *Micromachines* **2018**, *9*, 105. [CrossRef] [PubMed]

307. Cheng, X.; Miao, L.; Song, Y.; Su, Z.; Chen, H.; Chen, X.; Zhang, J.; Zhang, H. High Efficiency Power Management and Charge Boosting Strategy for a Triboelectric Nanogenerator. *Nano Energy* **2017**, *38*, 438–446. [CrossRef]

308. Niu, S.; Wang, X.; Yi, F.; Zhou, Y.S.; Wang, Z.L. A Universal Self-Charging System Driven by Random Biomechanical Energy for Sustainable Operation of Mobile Electronics. *Nat. Commun.* **2015**, *6*, 8975. [CrossRef]

309. Bao, D.; Luo, L.; Zhang, Z.; Ren, T. A Power Management Circuit with 50% Efficiency and Large Load Capacity for Triboelectric Nanogenerator. *J. Semicond.* **2017**, *38*, 095001. [CrossRef]

310. Xi, F.; Pang, Y.; Li, W.; Jiang, T.; Zhang, L.; Guo, T.; Liu, G.; Zhang, C.; Wang, Z.L. Universal Power Management Strategy for Triboelectric Nanogenerator. *Nano Energy* **2017**, *37*, 168–176. [CrossRef]

311. Zhang, C.; LI, W.; Wang, Z.; Fengben, X.I.; Pang, Y. Power Management Circuit and Power Management Method for Triboelectric Nanogenerator, and Energy System. U.S. Patent 20200099316A1, 26 March 2020.

312. Liang, X.; Jiang, T.; Liu, G.; Xiao, T.; Xu, L.; Li, W.; Xi, F.; Zhang, C.; Wang, Z.L. Triboelectric Nanogenerator Networks Integrated with Power Management Module for Water Wave Energy Harvesting. *Adv. Funct. Mater.* **2019**, *29*, 1807241. [CrossRef]

313. Liu, W.; Wang, Z.; Wang, G.; Zeng, Q.; He, W.; Liu, L.; Wang, X.; Xi, Y.; Guo, H.; Hu, C.; et al. Switched-Capacitor-Convertors Based on Fractal Design for Output Power Management of Triboelectric Nanogenerator. *Nat. Commun.* **2020**, *11*, 1883. [CrossRef] [PubMed]

314. Zi, Y.; Guo, H.; Wang, J.; Wen, Z.; Li, S.; Hu, C.; Wang, Z.L. An Inductor-Free Auto-Power-Management Design Built-in Triboelectric Nanogenerators. *Nano Energy* **2017**, *31*, 302–310. [CrossRef]

315. Tang, W.; Zhou, T.; Zhang, C.; Fan, F.R.; Han, C.B.; Wang, Z.L. A Power-Transformed-and-Managed Triboelectric Nanogenerator and Its Applications in a Self-Powered Wireless Sensing Node. *Nanotechnology* **2014**, *25*, 225402. [CrossRef] [PubMed]

316. Xu, L.; Pang, Y.; Zhang, C.; Jiang, T.; Chen, X.; Luo, J.; Tang, W.; Cao, X.; Wang, Z.L. Integrated Triboelectric Nanogenerator Array Based on Air-Driven Membrane Structures for Water Wave Energy Harvesting. *Nano Energy* **2017**, *31*, 351–358. [CrossRef]

317. He, J.; Fan, X.; Zhao, D.; Cui, M.; Han, B.; Hou, X.; Chou, X. A High-Efficient Triboelectric-Electromagnetic Hybrid Nanogenerator for Vibration Energy Harvesting and Wireless Monitoring. *Sci. China Inf. Sci.* **2021**, *65*, 142401. [CrossRef]

318. Li, Z.; Saadatnia, Z.; Yang, Z.; Naguib, H. A Hybrid Piezoelectric-Triboelectric Generator for Low-Frequency and Broad-Bandwidth Energy Harvesting. *Energy Convers. Manag.* **2018**, *174*, 188–197. [CrossRef]

319. Li, X.; Yu, W.; Gao, X.; Liu, H.; Han, N.; Zhang, X. PVDF Microspheres ≅ PLLA Nanofibers-Based Hybrid Tribo/Piezoelectric Nanogenerator with Excellent Electrical Output Properties. *Mater. Adv.* **2021**, *2*, 6011–6019. [CrossRef]

320. Lallart, M.; Lombardi, G. Synchronized Switch Harvesting on ElectroMagnetic System: A Nonlinear Technique for Hybrid Energy Harvesting Based on Active Inductance. *Energy Convers. Manag.* **2020**, *203*, 112135. [CrossRef]

321. Tabesh, A.; Frechette, L.G. A Low-Power Stand-Alone Adaptive Circuit for Harvesting Energy from a Piezoelectric Micropower Generator. *IEEE Trans. Ind. Electron.* **2010**, *57*, 840–849. [CrossRef]

322. Yu, Y.; Li, Z.; Wang, Y.; Gong, S.; Wang, X. Sequential Infiltration Synthesis of Doped Polymer Films with Tunable Electrical Properties for Efficient Triboelectric Nanogenerator Development. *Adv. Mater. Deerfield Beach Fla* **2015**, *27*, 4938–4944. [CrossRef] [PubMed]

323. Jiang, M.; Li, B.; Jia, W.; Zhu, Z. Predicting Output Performance of Triboelectric Nanogenerators Using Deep Learning Model. *Nano Energy* **2022**, *93*, 106830. [CrossRef]